ALL-SEMICONDUCTOR HIGH POWER MODE-LOCKED LASER SYSTEM

by

KYUNGBUM KIM
B.Sc. Inha University, Republic of Korea, 1993
M.Sc. Inha University, Republic of Korea, 1999

A dissertation submitted in partial fulfillment of the requirements
for the degree of Doctor of Philosophy
in the College of Optics and Photonics/CREOL
at the University of Central Florida
Orlando, Florida

Spring Term
2006

Major Professor: Peter J. Delfyett, Jr.

To my mother, my father, my sister, and my wife, Sunah

ABSTRACT

The objective of this dissertation is to generate high power ultrashort optical pulses from an all-semiconductor mode-locked laser system.

The limitations of semiconductor optical amplifier in high energy, ultrashort pulse amplification are reviewed. A method to overcome the fundamental limit of small stored energy inside semiconductor optical amplifier called "eXtreme Chirped Pulse Amplification (X-CPA)" is proposed and studied theoretically and experimentally. The key benefits of the concept of X-CPA are addressed.

Based on theoretical and experimental study, an all-semiconductor mode-locked X-CPA system consisting of a mode-locked master oscillator, an optical pulse pre-stretcher, a semiconductor optical amplifier (SOA) pulse picker, an extreme pulse stretcher/compressor, cascaded optical amplifiers, and a bulk grating compressor is successfully demonstrated and generates >kW record peak power.

A potential candidate for generating high average power from an X-CPA system, novel grating coupled surface emitting semiconductor laser (GCSEL) devices, are studied experimentally. The first demonstration of mode-locking with GCSELs and associated amplification characteristics of grating coupled surface emitting SOAs will be presented.

In an effort to go beyond the record setting results of the X-CPA system, a passive optical cavity amplification technique in conjunction with the X-CPA system is constructed, and studied experimentally and theoretically.

ACKNOWLEDGMENTS

I would like to express my deepest gratitude to Professor Peter J. Delfyett, Jr. for his great support and thoughtful guidance. His enthusiasm toward research motivated me all the time.

I am sincerely grateful to committee members, Professor Eric Van Stryland, Professor Patrick LiKamWa, and Professor Robert Peale for their support to my accomplishment.

It was great experience to be part of College of Optics and Photonics / Center for Research and Education in Optics and Lasers (CREOL). I am proud to be in Ultrafast Photonics Group, lead by Prof. Peter Delfyett and I am thankful to current and former Ultrafast Photonics Group Members, Dr. Sangyoun Gee, Dr. Myoung-Teak Choi, Wangkuen Lee, Luis Archundia-Berra, Dr. Bojan Resan, Dr. Michael Mielke, Franklyn Quinlan, Sarper Ozharar, Ji-Myoung Kim, Leonard Kisimbi, Scott Rozzo, and especially Shinwook Lee for their help and many insightful discussions. Also I would like to thank Dr. Oleg Smolski for his sincere support.

I am deeply grateful to Professor Jaewoo Noh in Inha University, Republic of Korea, who have inspired and encouraged me to keep pursuing my dream.

This work is dedicated to my mother who lives in heaven, my father, my sister and my wife, Sunah Jung, who have shown their tremendous support and their greatest love to me.

TABLE OF CONTENTS

LIST OF FIGURES

x

LIST OF TABLES

LIST OF ACRONYMS/ABBREVIATIONS

AOM	Acousto-Optic Modulator
ASE	Amplified Spontaneous Emission
CFBG	Chirped Fiber Bragg Grating
COMD	Catastrophic Optical Mirror Damage
CPA	Chirped Pulse Amplification
CPMLL	Colliding Pulse Mode-Locked semiconductor Laser
EDFA	Erbium Doped Fiber Amplifier
EDWA	Erbium Doped Waveguide Amplifier
GCSEL	Grating Coupled Surface Emitting Laser
GCSOA	Grating Coupled surface emitting Semiconductor Optical Amplifier
GFMLL	Gain Flattened actively Mode-Locked semiconductor Laser
HWP	Half Wave Plate
IBTSOA	Inverse Bow-Tie Semiconductor Optical Amplifier
FA	Flared Amplifier
FR	Faraday Rotator
FWHM	Full Width Half Maximum
MM	Multi-spatial Mode
MOPA	Master Oscillator Power Amplifier
MQW SA	Multiple Quantum Well Saturable Absorber

OI	Optical Isolator
OSNR	Optical Signal to Noise Ratio
PBS	Polarizing Beam Splitter
POC	Passive Optical Cavity
QWP	Quarter Wave Plate
RF	Radio Frequency
ROC	Radius of Curvature
RWGSOA	Ridge Wave-Guide Semiconductor Optical Amplifier
SHG	Second Harmonic Generation
SOA	Semiconductor Optical Amplifier
SM	Single-spatial Mode
TA	Tapered Amplifier
X-CPA	eXtreme Chirped Pulse Amplification
YDFA	Ytterbium Doped Fiber Amplifier

CHAPTER 1: INTRODUCTION

1-1. Review of High Power Pulsed Semiconductor Laser System

Compact, ultrashort pulse, high energy sources are desirable for various applications such as free space optical communications, material processing [1] and bio-medical optics [2]. Semiconductor gain media have many superior characteristics compared to other laser gain media in terms of i) compactness, ii) high wall-plug efficiency [3,4], iii) simple current pumping, iv) broadband wavelength emission (GaN laser [5] to quantum cascaded laser [6]), v) cost-effectiveness, vi) robustness, etc.

Superior characteristics of semiconductor gain medium:

i) compactness: because of small size of semiconductor laser it is possible to make a simple packaged laser (fiber coupled butterfly package, TO can, etc)

ii) high wall plug efficiency: less electrical power consumption, semiconductor lasers with more than 70% wall plug efficiency have been demonstrated

iii) simple current pumping: instead of using optical pumping which increases complexity, a simple electrical current can excite semiconductor gain media

iv) broadband emission: GaN laser (UV radiation) to quantum cascade laser (Mid- and Far-IR).

Owing to such attractive characteristics, there have been extensive efforts focused on high power, ultrashort pulse generation with semiconductor gain media. Efforts can be

categorized into two main approaches. One approach is the development of a short pulse semiconductor laser utilizing optical pulse generation mechanisms such as mode-locking [7], gain switching [8], and Q-switching [9,10]. The other approach is the development of high power semiconductor optical amplifiers incorporating a large output aperture and diffraction-limited beam quality [11-13]. Typically, the development of both short pulse semiconductor lasers and power amplifiers has been done in parallel. Coherent and incoherent beam combining might be considered as a third approach [14, 15].

Electrically pumped mode-locked semiconductor MOPA systems

Delfyett *et al.* demonstrated 165W peak power of 205fs optical pulse combining a mode-locked semiconductor laser with a single spatial mode, angle-tilted SOA. The maximum output energy from the angle-tilted SOA was 32pJ after pulse compression [7]. Resan *et al.* improved the system performance by reducing a detrimental nonlinearity inside a mode-locked semiconductor laser. This "breathing mode mode-locked oscillator" combined with the angle-tilted SOA achieved 230W peak power [16]. But output energy from this system was limited to a maximum of 42.5pJ. In both experiments, the injected optical pulse was linearly chirped and compressible. This helped to reduce the detrimental nonlinearity during the amplification of the optical pulse. After amplification, the linearly chirped pulse was compressed by a dual bulk grating compressor. There have also been efforts to increase the output energy using multi-spatial mode, high power amplifiers such as inverse bowtie SOAs (IBTSOAs) [11], tapered amplifiers (TAs) [12, 13], etc. Higher saturation power in conjunction with the wide output aperture (typically, >100um) of multi-spatial mode SOAs make the output energy higher than single spatial mode SOAs. By implementing an IBTSOA as a power amplifier in a mode-locked

master oscillator power amplifier (MOPA) system, Gee *et al.* demonstrated 376pJ prior to pulse compression [11]. Using a tapered amplifier, pulses with 500pJ output energy and a 12ps pulse duration were obtained at 855nm [12]. Similarly, pulses with 118pJ output energy and a 4.2ps pulse duration were obtained at 940nm. [13].

As these results demonstrate, the output energy from mode-locked semiconductor laser systems incorporating edge emitting SOAs is limited by the low saturation energy: tens of pico-joules from single spatial mode SOAs and hundreds of pico-joules from multi-spatial mode SOAs. The characteristic of low saturation energy in an SOA can be understood by a short energy storage lifetime (<1ns) as well as a high gain cross section.

Optically pumped passively mode-locked lasers

Alternatively, optically pumped passively mode-locked lasers have been developed as a high average power source. Achwandan *et al.* achieved 2.1W of average power with 18.9W of optical pump [17]. The time duration of optical pulse was 4.7ps with a 4GHz repetition rate, which corresponds to 525pJ of output energy per pulse. In terms of short pulse generation, Garnache *et al.* demonstrated a 477fs soliton-like pulse train at 1.4GHz with output energy of 89pJ per pulse [18]. Even though this approach takes advantage of high saturation power by enlarging output aperture size via controlling the pumping beam size, optically pumped passive mode-locked semiconductor lasers have shown low wall-plug efficiency and the output energy has been limited to hundreds of pJ.

Gain-switched and Q-switched semiconductor laser MOPA systems

Short pulse generation with gain-switched [8] and Q-switched semiconductor lasers [9,10] is limited by the fundamental mechanism of pulse generation. Typically the pulse duration from gain-switched and Q-switched lasers is limited to >10ps. Given a similar output energy, a ~200fs optical pulse from a mode-locked semiconductor laser [7,16] gives ~50 times higher peak power than a 10ps optical pulse from gain-switched or Q-switched semiconductor laser.

1-2. Dissertation Statement and Overview

In high energy, ultrashort pulse amplification, semiconductor optical amplifiers (SOAs) as power amplifiers revealed the limitation of small energy storage. In addition, another limitation in high energy, ultrashort pulse amplification using SOAs is the distortion of the amplified optical pulse due to nonlinearities caused by carrier dynamics such as integrating self phase modulation, carrier heating, carrier cooling, etc.

In chapter 2, a proposed method called "eXtreme Chirped Pulse Amplification (X-CPA)" to overcome the limitations of small energy storage and nonlinearities is studied theoretically and experimentally. The concept of X-CPA reveals the key benefits; 1) the fundamental energy storage limit of an SOA is overcome, 2) detrimental nonlinearities during pulse amplification are reduced, 3) optical signal to noise ratio in pulse amplification is significantly improved.

In chapter 3, based on the theoretical and experimental study of X-CPA, an all-semiconductor X-CPA system consisting of a master oscillator, an optical pulse pre-stretcher, an SOA pulse picker, a free space polarization-dependent optical circulator, an extreme pulse

stretcher/compressor, cascaded amplifiers and a bulk grating pulse compressor is demonstrated successfully and generates >kW record peak power from a semiconductor mode-locked laser system. Also almost ~16,000 times extreme pulse compression using a chirped fiber Bragg grating (CFBG) which possesses the group delay of 1600 ps/nm with 6nm bandwidth at 974nm center wavelength is performed. Because the output comes out of single mode fiber CFBG, the beam profile is diffraction-limited. Nonlinearities generated at the extreme pulse compression stage is reduced by inserting an optical pulse pre-stretcher. Approximately 1.6uJ output energy per 20ns stretched optical pulse prior to the extreme pulse compression stage is extracted using a commercially available, high power optical amplifier. As one of applications of the X-CPA system, 488nm blue light via second harmonic generation is demonstrated.

In chapter 4, a potential candidate for generating high average power from an X-CPA system, novel grating coupled surface emitting semiconductor laser (GCSEL) devices are studied experimentally. The first demonstration of mode-locking with GCSELs and associated amplification characteristics of grating coupled surface emitting SOAs will be presented.

In chapter 5, in an effort to go beyond the record setting results of the X-CPA system, a passive optical cavity amplification technique in conjunction with the X-CPA system is constructed, and studied experimentally and theoretically.

CHAPTER 2: CONCEPT OF EXTREME CHIRPED PULSE AMPLIFICAITON

2-1. Fundamentals of Optical Amplifiers

In various laser applications such as laser radar ranging, nonlinear frequency conversion, material processing, etc, the laser system must meet the specified requirement. Typical requirements are power, quality of the optical spectrum, optical pulse width, and type of spatial beam. For many applications, the output power directly from the laser oscillator is not necessarily enough. Therefore, in order to boost the output power of the laser oscillator to meet requirements, a so called "optical amplifier" is implemented after the laser oscillator. A system which combines the laser oscillator with an optical amplifier is called a "Master Oscillator Power Amplifier (MOPA)" [19, 20]. In the MOPA system, optical pulse shape, beam divergence, and spectral width are primarily determined by the master oscillator, whereas pulse energy and power are determined by the power amplifier. Operating an oscillator at relatively low energy levels maintains the quality of the beam divergence and spectral width while also preserving the quality of the pulse profile. Therefore, by using an oscillator-amplifier combination one can obtain either a higher energy than is achievable from an oscillator alone, or same energy in a beam which a smaller beam divergence, narrower linewidth, etc.

Definitions of gain saturation characteristics inside an optical amplifier

In a bulk-type optical amplifier, the size of input beam is adjustable using a telescope and therefore it is more convenient to define the saturation effect of an optical amplifier by energy or power per unit area. "Saturation fluence [J/cm^2]" and "saturation intensity [W/cm^2]" are usually used for bulk-type optical amplifiers such as Nd:YAG, Yb:YAG and Ti:Sapphire. But in a waveguide-type optical amplifier, the mode field diameter is fixed inside the optical waveguide. Therefore it is preferable to use "saturation energy [J]" and "saturation power [W]" to describe the saturation effect. These words are being used for optical amplifiers such as EDFA, YDFA, SOA, EDWA, etc.

Table 1. Definition of saturation effects of optical amplifiers

type of optical amplifier	c.w. amplification	pulse amplification
bulk-type beam size is **scalable**	saturation **intensity** $$I_{sat} = \frac{h\nu}{\sigma\tau}\left[\frac{W}{area}\right]$$	saturation **fluence** $$J_{sat} = \frac{h\nu}{\sigma}\left[\frac{J}{area}\right]$$
waveguide-type beam size is **fixed**	saturation **power** $$P_{sat} = \frac{h\nu A}{\Gamma\sigma\tau}[W]$$	saturation **energy** $$E_{sat} = \frac{h\nu A}{\Gamma\sigma}[J]$$

* $h\nu$: photon energy, A : emission area, Γ : mode confinement factor, τ : lifetime, σ : emission cross section

Table 2. Basic parameters of different optical gain media

	type	fluorescence lifetime	emission cross section 10^{-20} cm^2	spectral bandwidth	center wavelength	saturation fluence J/cm^2
Er:glass *	bulk/WG	7.9ms	0.8	55nm	1535nm	16
Yb:glass *	"	2ms	0.4	56.5nm	1032nm	48
Nd:glass *	"	0.35ms	3.8	27.6nm	1054nm	5
Yb:YAG **	bulk	0.95ms	0.31	5.6nm	1.05um	30
Nd:YAG **	bulk	0.23ms	33	0.6nm	1.064um	0.57
Ti:Sapphire ***	bulk	3.2us	28	180nm	790nm	0.9
SOA ****	waveguide	~ns	10^6	30-100nm	0.5~1.55um	$2*10^{-4}$

* http://www.kigre.com

** C. Honninger *et al.*, "Ultrafast ytterbium-doped bulk lasers and laser amplifiers", Applied Physics B, 69, pp3-17 (1999)

*** W. Koechner, "Solid State Laser Engineering"

**** W. T. Silfvast, "Laser Fundamentals,' 1st edition (Cambridge University Press, 1996)

Optical amplifiers for continuous wave or pulse amplification

Table 2 lists basic parameters of different optical gain media. Based on fundamental characteristics, one can choose a proper amplifier for different applications. For example, in optical communication, to compensate signal loss from hundreds of km of optical fiber, EDFAs

have been successfully implemented [21]. The main reasons are that EDFAs are scalable in terms of length, which provides a high gain (20~30dB), demonstrate a relatively low noise characteristic and reduce the pattern effect which causes signal distortion, while being a simple fiberized device. In optical communications, for wavelength conversion, SOAs, which have a rapid saturation characteristic with small input power, are successfully used [22]. In high energy ultrashort pulse generation, a disk type optical amplifier made of Nd:glass is frequently used due to volume scalability and a high saturation fluence [23]. In a table-top terawatt system, a Ti:sapphire amplifier is implemented using a regeneration amplification scheme and/or multi-pass amplification scheme.

Detrimental temporal and spatial nonlinearities inside optical amplifiers

Semiconductor Optical Amplifier: In ultrashort amplification with SOAs, ultrafast dynamic behaviors have been observed such as integrating self phase modulation [24] due to gain saturation, carrier heating, spectral hole burning [25], and ultrafast refractive index change [26]. These dynamics cause a significant distortion of the optical pulse during amplification. As an example, because of the dynamics from the SOA it is hard to generate ultrashort pulses directly from a mode-locked semiconductor laser. Therefore typical optical pulses from the mode-locked semiconductor laser are chirped. By compensating the chirping of the optical pulses using an external bulk grating pulse compressor sub-picosecond optical pulses can be obtained [7, 16]. Also in ultrashort amplification, a pulse distortion due to the dynamics has been observed experimentally and theoretically [27].

In high power semiconductor optical amplifiers such as a tapered amplifier, flared amplifier, broad area amplifier, etc, a spatial beam distortion called "filamentation" [28, 29]

arises at high power operation. Natural multi-spatial mode characteristics, spatial gain saturation, and non-uniform carrier distribution are considered physical mechanisms of filament formation inside the semiconductor optical amplifier.

Rare earth doped fiber amplifier: As the energy of an ultrashort pulse is increased through an EDFA, an intensity dependent refractive index causes instantaneous self phase modulation [30]. As a result, significant distortion of the optical pulse occurs as output energy is increased. In a mode-locked fiber laser, this is one of the reasons that a high energy pulse can not be generated. There have been efforts to minimize this effect by stretching and compressing optical pulses inside a mode-locked fiber laser. It has been called a "stretched pulse", "wave breaking free", and "similariton" mode-locked fiber laser [31-33]. In ultrashort amplification, to reduce this detrimental effect, the chirped pulse amplification technique is applied successfully [34, 35].

Bulk optical amplifier: In pulse amplification, spatial beam distortion (as well as temporal pulse distortion) will arise as the result of a number of physical processes. If the spatial beam distribution is not uniform, at high intensities of light, the area inside the optical amplifier behaves like lens. It causes catastrophic damage to the optical amplifier. Well known physical processes are non-uniform pumping, non-uniformities in gain media, spatial gain saturation, diffraction effects, thermal distortions, and index nonlinearity [30].

2-2. Concept: X-CPA

As mentioned in Chapter 1, when a short pulse is injected into a semiconductor optical amplifier, the output energy is limited by tens of pico-joules with single spatial mode SOAs and hundreds of pico-joules with multiple spatial mode SOAs. It is a well known characteristic of optical amplifiers with a high gain, a short upper state lifetime and low saturation energy. One example is a semiconductor optical amplifier. Delfyett *et al.* proposes a novel method to overcome small saturation energy and calls it **"eXtreme Chirped Pulse Amplification (X-CPA)"** (Figure 1, patent pending). The concept of X-CPA is that extremely stretched optical
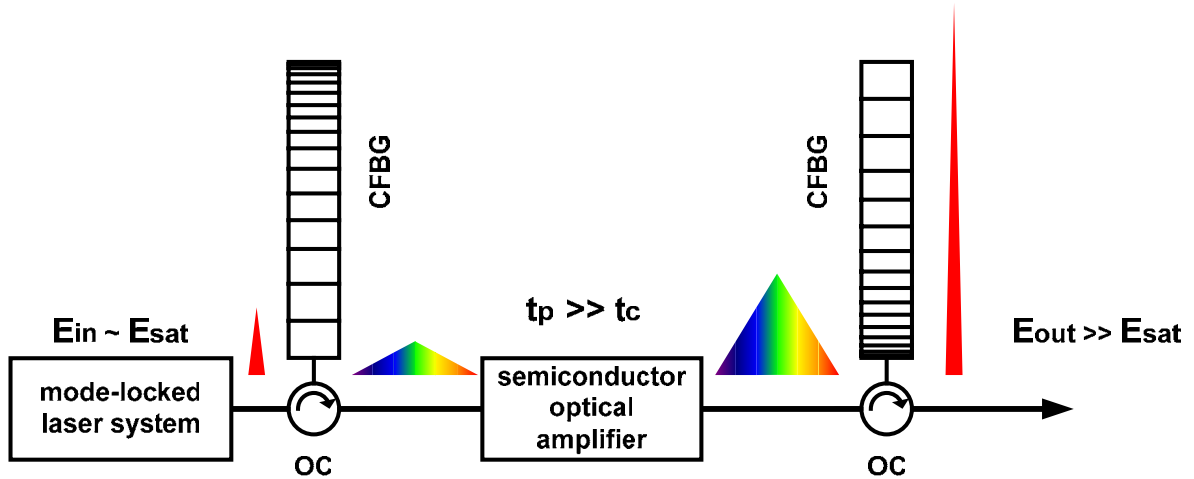
Figure 1. Simplified diagram of X-CPA system, E_{in} : input energy, E_{sat} : saturation energy of semiconductor optical amplifier (SOA), E_{out} : output energy, t_p : pulse width of extremely stretched pulse, t_c : carrier lifetime of SOA, CFBG: chirped fiber Bragg grating, OC: optical circulator

pulses from a mode-locked oscillator that have a time duration much longer than that of the energy storage upper state lifetime is injected into an optical amplifier. Even though there is gain saturation of the leading part of the extremely stretched pulse within the SOA, there is enough time to re-pump the SOA. As a result, the trailing part of the extremely stretched optical pulse is able to extract more energy from the SOA. After compression of the extremely stretched pulse, output energy of the recompressed pulse becomes larger than the stored energy of the SOA.

This "X-CPA" method is simply called **"temporal domain approach"** because temporal stretching of the optical pulse is required to overcome the fundamental limit of small saturation energy inside an SOA. As mentioned in Chapter 1, another approach to increase the saturation energy of an SOA is simply to increase the output emission area and use a **"spatial domain approach"**. Tapered amplifiers, flared amplifiers, and broad area amplifiers are devices that incorporate the spatial approach. Output power from these types of devices is scalable by increasing the emission aperture but it is difficult to keep the output beam close to diffraction limit as output power is increased. An optically pumped vertical external cavity surface emitting semiconductor laser (VECSEL) is considered as one candidate that has an output power scalable optical amplifier keeping beam close to diffraction limited [17,18].

Comparison of X-CPA with conventional CPA: In rare earth doped bulk- and fiber-based ultrashort pulse amplification systems, due to a longer upper state energy storage lifetime, the stored energy inside the gain medium is nearly six orders of magnitude larger than that inside an SOA (in the case of Er^{3+} doped or Yb^{3+} doped gain medium.). Therefore in a solid state or fiber based chirped pulse amplification (CPA) system, the purpose of optical pulse stretching is to reduce the optical damage due to nonlinear self focusing or pulse distortion due to self phase

modulation. But in an X-CPA system, the purpose of optical pulse stretching is to extract more energy from the amplifier. As an example, let's assume there are two amplifiers with the same output saturation power: one is an SOA and other is a rare earth doped fiber amplifier. If a 1ps optical pulse at 1GHz is close to the upper state lifetime of an SOA is injected into both amplifiers, the average output power and energy per pulse from both amplifiers will be more or less same. But as the repetition rate is decreased to 1 kHz, it is easily seen that a different output behavior from two different amplifiers, as shown in Figure 2, can be observed. With a 1 kHz repetition rate, the output energy from the SOA will be same as the 1GHz case. But the average output power will be dropped by a ratio of the two different repetition rates. However in the fiber amplifier case, output energy from the EDFA will be increased by the same ratio of the two different repetition rates and average output power will be equivalent to the 1GHz case. This can be summarized as in Figure 2. (It should be noted that this estimation is based on fundamental characteristics of amplifiers. Nonlinearities, damage, amplified spontaneous noise, losses etc. are not considered and also input energy is high enough to saturate both amplifiers.)

Input source	1GHz mode-locked laser	1kHz mode-locked laser
semiconductor gain ~1ns lifetime	$E_{out,1GHz} \sim E_{out,1kHz}$ $P_{ave,1GHz} \gg P_{ave,1kHz}$	
rare earth doped gain ~1ms lifetime	$E_{out,1GHz} \ll E_{out,1kHz}$ $P_{ave,1GHz} \sim P_{ave,1kHz}$	
semiconductor gain ~1ns lifetime with 1ms stretched pulse	$E_{out,1GHz} \ll E_{out,1kHz}$ $P_{ave,1GHz} \sim P_{ave,1kHz}$	

Figure 2. Comparison: semiconductor optical amplifier vs. rare-doped fiber amplifier

As shown in Figure 2, the output energy of the amplified pulse after the SOA becomes comparable with the fiber amplifier if the extremely stretched pulse is matched with a repetition rate that is injected into the SOA. Again it is the main purpose of X-CPA in ultrashort pulse amplification with an SOA. In the next two sections, the concept of X-CPA will be proven theoretically and experimentally.
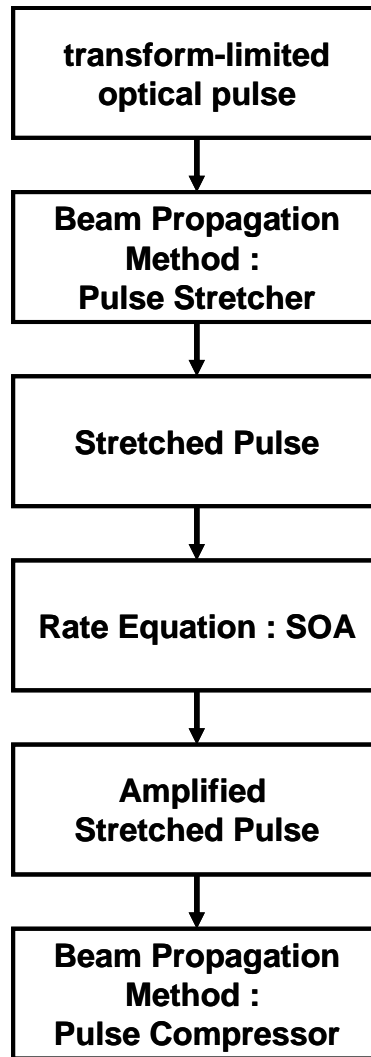
Figure 3. Simulation procedure of X-CPA

2-3. Theoretical Study of X-CPA

In order to quantify the efficiency of energy extraction in extreme chirped pulse amplification, the phenomenological semiconductor rate equations in reference 24 and 36 are solved numerically (Appendix A). The simulation sequence is explained in Figure 3. A transform-limited optical pulse from a mode-locked semiconductor laser is stretched by a chirped fiber Bragg grating. Pulse stretching with any dispersion value is simulated by a beam propagation method [37]. The amplification of the stretched pulse inside a semiconductor optical amplifier is simulated using the semiconductor rate equations which will be explained in detail. Again, the pulse compression of the amplified stretched pulse through the chirped fiber Bragg grating is simulated with the beam propagation method. From the simulation the output energy, spectral amplitude, spectral phase, temporal amplitude, and temporal phase of the optical pulse at each stage can be calculated.

Rate equations that describe a medium's response to the optical field and time domain amplitude and phase rate equations that describe pulse propagation are

$$P_{out}(\tau) = P_{in}(\tau) \cdot e^{h(\tau)}$$

$$\phi_{out}(\tau) = \phi_{in}(\tau) - \tfrac{1}{2} \cdot \alpha \cdot h(\tau)$$

$$h(\tau) = \int_0^L g(z,\tau)d\tau$$

$$\frac{dh}{d\tau} = \frac{g_0 L - h}{\tau_c} - \frac{P_{in}(\tau)}{E_{sat}}\left[e^{h(\tau)} - 1\right]$$

where $\tau(=t-\dfrac{z}{\upsilon_g})$ is a reduced time (υ_g is a group velocity), P is power, h represents the integrated gain at each point of the pulse profile, ϕ is phase, α is a linewidth enhancement factor, g is gain, τ_c is the carrier lifetime, $E_{sat}(=\dfrac{\hbar\omega_o\sigma}{a})$ is the saturation energy of the optical amplifier, σ is the mode cross section and a is the differential gain.

These semiconductor rate equations are solved in three different regimes; i) $\tau_i < \tau_p < \tau_c$,
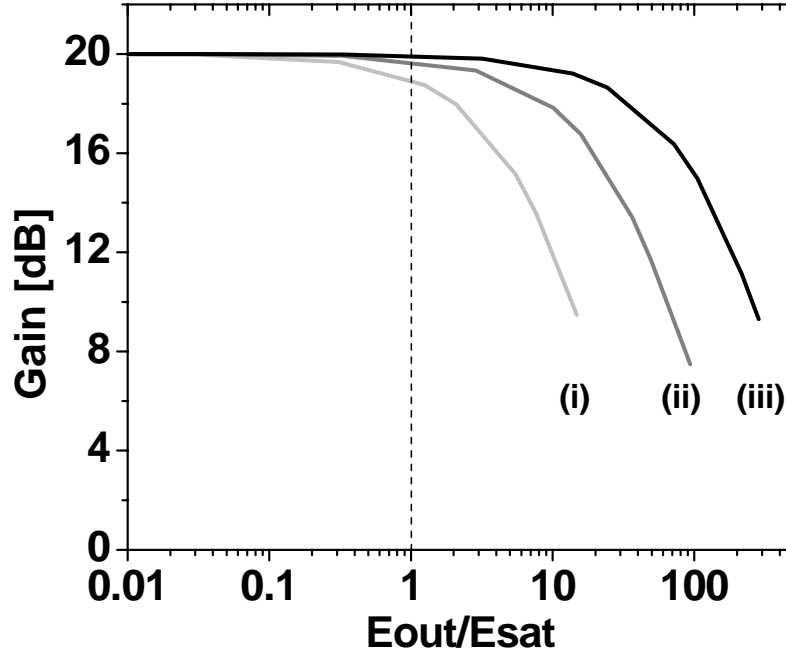
Figure 4. Simulation results of extreme chirped pulse amplification, gain [dB] with respect to E_{out}/E_{sat} (E_{out} : output energy, E_{sat} : saturation energy of the SOA), $t_p/t_c =$ (i)2.5, (ii)12, and (iii) 48, (t_p : pulse width of the stretched pulse, t_c :carrier lifetime of SOA)

ii) $\tau_p \sim \tau_c$, and iii) $\tau_p \gg \tau_c$, where τ_i is an intraband relaxation time (~ 0.1ps) and τ_p is the time duration of the optical pulse. In regime i) $\tau_i < \tau_p < \tau_c$, the rate equations can be solved analytically. In regime ii) $\tau_p \sim \tau_c$, the differential rate equations can be solved numerically using the Runge-Kutta algorithm. And in regime iii) $\tau_p \gg \tau_c$, the steady state rate equations can be solved with Newton's method.

In this simulation, the time duration of a stretched input pulse is varied from 200ps up to 10ns, and the input energy of each stretched pulse is increased until energy saturation occurs. The parameters of the SOA used in this simulation are as follows: a small signal gain of 20dB, a carrier lifetime of 200ps, and saturation energy of 30pJ. Figure 4 describes the energy gain with respect to the ratio of time duration of the stretched input pulse to the carrier lifetime of the SOA. As the time duration of the stretched input pulse is increased, the 3dB output saturation energy from the SOA is increased leading to an output energy that is greater than the saturation energy of the SOA. The result shows that in the case of the stretched pulse of 10ns and a carrier lifetime of 200ps, amplified output energy after the SOA is 100 times more than the saturation energy of the SOA. This simulation demonstrates that the fundamental limit of small saturation energy of the SOA is overcome utilizing the proposed concept of X-CPA. This is one of main advantages of extreme chirped pulse amplification.

In Figure 5, the 3dB output saturation energy from the SOA is calculated and plotted with respect to the time duration of the extremely stretched pulse. This result implies that the output energy is linearly increased as the time duration of the extremely stretched pulse is increased. In other words, the greater the stretching of the optical pulse the greater the output energy in the X-CPA system.

Figure 6 shows the energy extraction efficiency with respect to carrier lifetime. Given the same parameters except the carrier lifetime, the injection of a 10ns extremely stretched pulse into
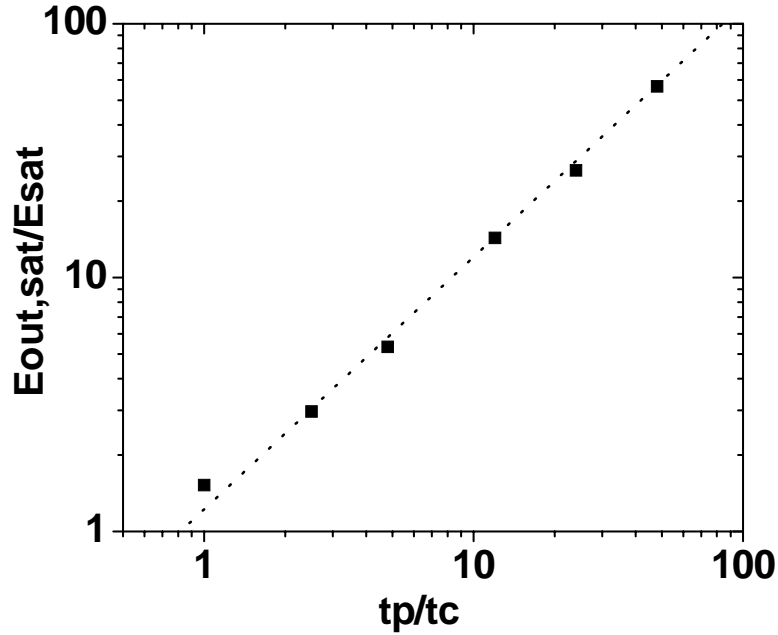
Figure 5. Simulation result of extreme chirped pulse amplification, $E_{out,sat}/E_{sat}$ w.r.t. t_p/t_c ($E_{out,sat}$: 3dB output saturation energy, E_{sat} : saturation energy of SOA, t_p : pulse width of the stretched pulse, t_c :carrier lifetime of the SOA)

two SOAs which possess a different carrier lifetime was simulated. In this case, the carrier time of each SOA was 200ps and 800ps respectively. As shown in Figure 6, given a 10ns stretched pulse as an input, the SOA which possesses a carrier lifetime of 200ps shows a better energy extraction than that with 800ps. This simulation can be applied to SOAs with different quantum structures such as quantum dots, quantum well, bulk, etc.
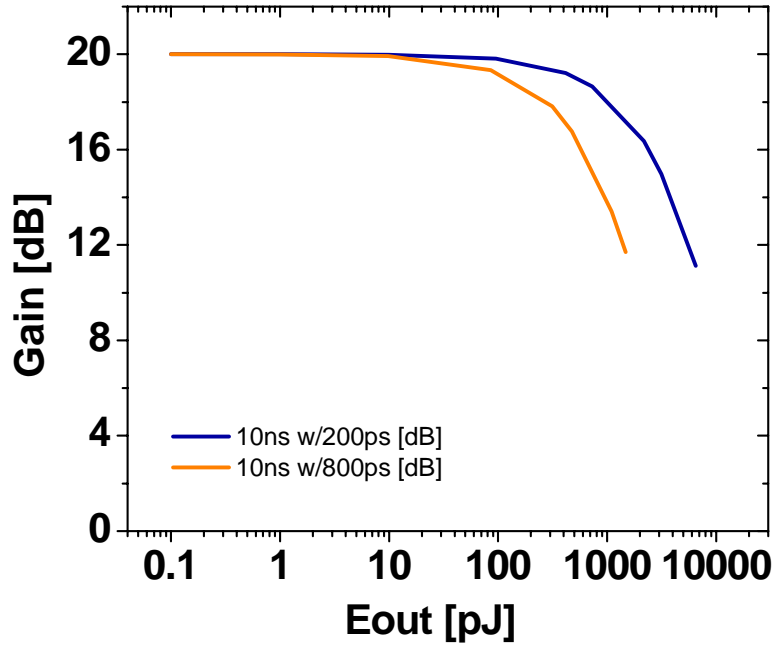
Figure 6. Simulation result, carrier lifetime dependent gain in X-CPA, carrier lifetime: 800ps (orange) and 200ps (blue)

2-4. Experimental Study of X-CPA

Simulation results show the advantage of extreme chirped pulse amplification in terms of energy extraction. The small saturation energy limit from the SOA is overcome by stretching and amplifying an optical pulse longer than the carrier lifetime. In order to see the advantages of X-CPA in practice, an energy extraction experiment is performed using a colliding pulse hybrid mode-locked semiconductor laser (CPMLL, Chapter 3-1), a chirped fiber Bragg grating (CFBG, Chapter 3-3), and a single spatial mode angle-tilted ridge waveguide SOA (RWGSOA, Chapter 3-6-2). In order to compare the energy extraction efficiency with and without pulse stretching, an energy amplification experiment is performed with two pulses that have two different pulse durations, ~1ps pulse and a ~9.6ns extremely stretched pulse, respectively. Figure 7 illustrates a simplified schematic diagram of the two cases.
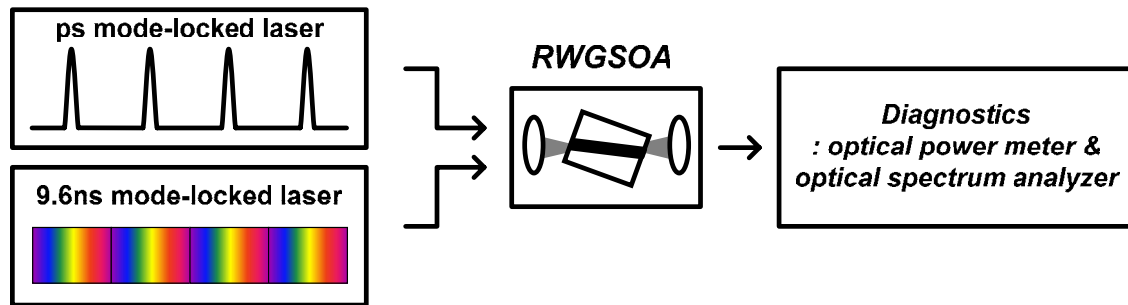
Figure 7. Simplified schematic diagram of extreme chirped pulse amplification, RWGSOA: ridge waveguide semiconductor optical amplifier

2-4-1. ~1ps pulse injection

The 285MHz repetition rate of the CPMLL is reduced to 95MHz after the SOA pulse picker in order to avoid temporal pulse overlapping (addressed in Chapter 3-5) caused by a mismatch between the repetition rate and the group delay of the CFBG. Pre-chirping directly from the CPMLL is compensated by a dual bulk grating compressor. After the SOA pulse picker and the grating compressor, the optical pulse with time duration of ~1ps is injected into the RWGSOA (Figure 8). In this experiment, a 1.5mm long, angle-tilted RWGSOA was used as an amplifier with a DC-bias of 150mA current. Also, by using an optical power meter and an optical spectrum analyzer, an optical signal to noise ratio is calculated in order to extract an amplified
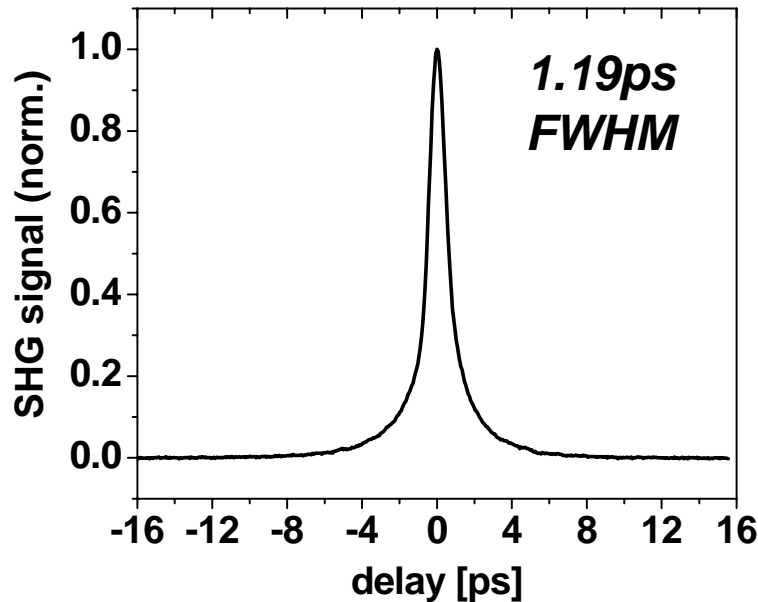
Figure 8. Autocorrelation trace of ~1ps input pulse at 95MHz

signal.

Optical spectra from the SOA were measured with and without the injection of ps pulses from the mode-locked laser, shown in Figure 10. From these spectra an optical signal to noise ratio (OSNR) was extracted (Figure 11). Based on the measurement of the output power after the RWGSOA with injection and extracted OSNR, the energy gain is plotted with respect to output energy in Figure 9. The optical signal to noise is 3.2 with 1mW injected average power and the 3dB output saturation energy is ~30pJ (Figure 9).
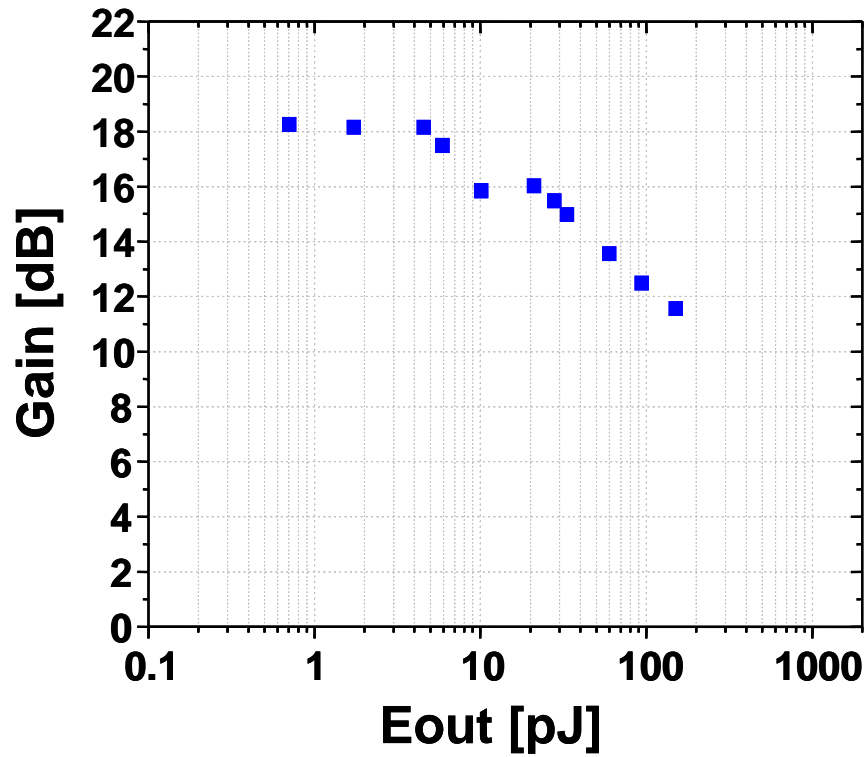
Figure 9. Energy gain vs. output energy in the case of ~1ps injection
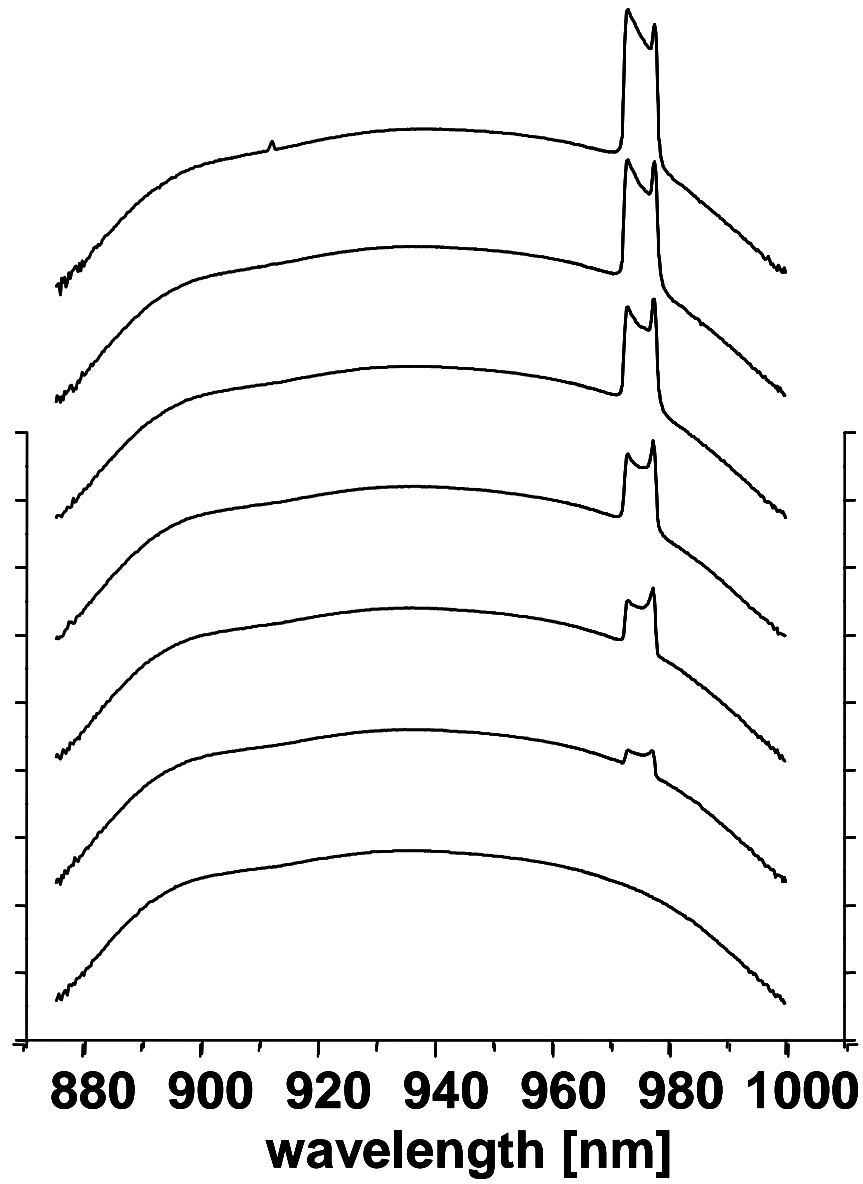
Figure 10. Experimental result, optical spectrum of amplified signal through RWGSOA in the

case of ~1ps injection, input average power is from 0mW to 1mW. vertical axis: 10dB/div.
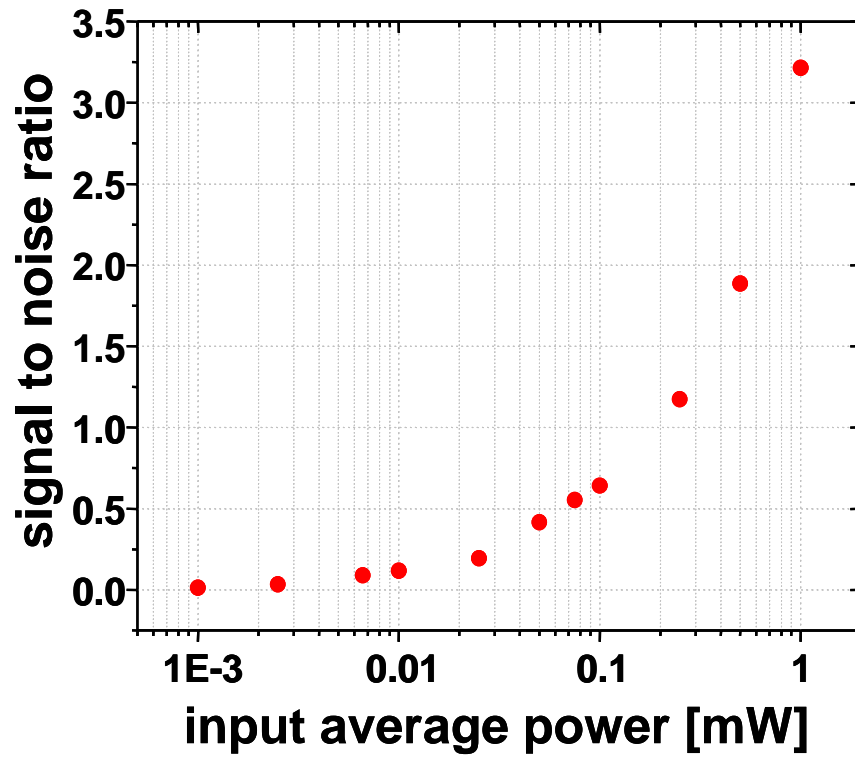
Figure 11. Optical signal to noise ratio with respect to input average power, in the case of ~1ps injection

2-4-2. ~10ns extremely stretched pulse injection

The 95MHz pulse train after the SOA pulse picker is stretched to 9.6ns using a CFBG with a group delay of 1600ps/nm and a spectral bandwidth of 6nm. Instead of a 1ps pulse, a 9.6ns extremely stretched pulse was injected into the RWGSOA (Figure 12). In the same way, the output power and the optical spectrum of the amplified signal though the RWGSOA (Figure 15) are measured to extract OSNR, energy gain, and output energy of the amplified signal (Figure 13 and 14). For 1mW injected average power, the optical signal to noise is 12.6 as compared to that of 3.2 in the 1ps pulse injection (Figure 14). The 3dB output saturation energy is 514pJ as compared to that of 30pJ in the 1ps pulse injection (Figure 13). Again in these experiments, the concept of X-CPA is clearly advantageous for overcoming the small storage limit of an SOA in terms of energy extraction and for improving the optical signal to noise ratio through an amplification process.
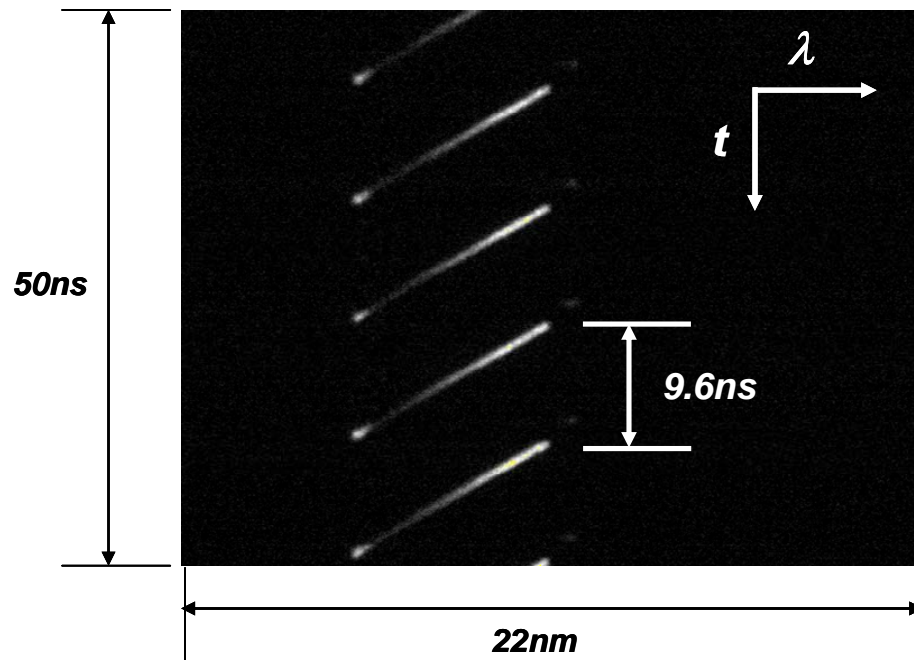
Figure 12. Streak camera image of ~9.6ns extremely stretched pulse at

95MHz, vertical axis: time, horizontal axis: wavelength
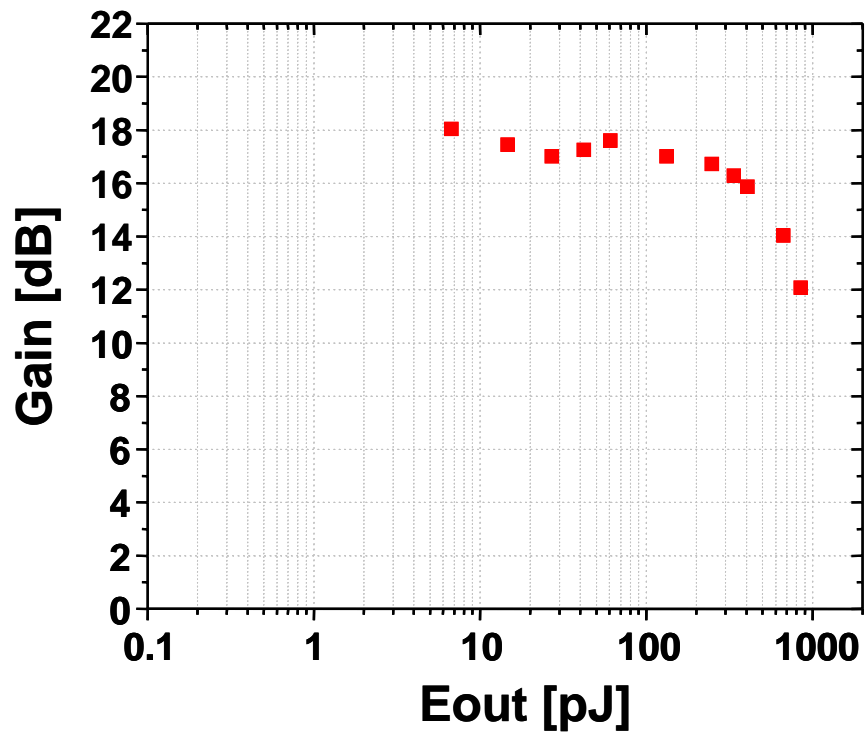
Figure 13. Energy gain vs. output energy in the case of ~9.6ns injection
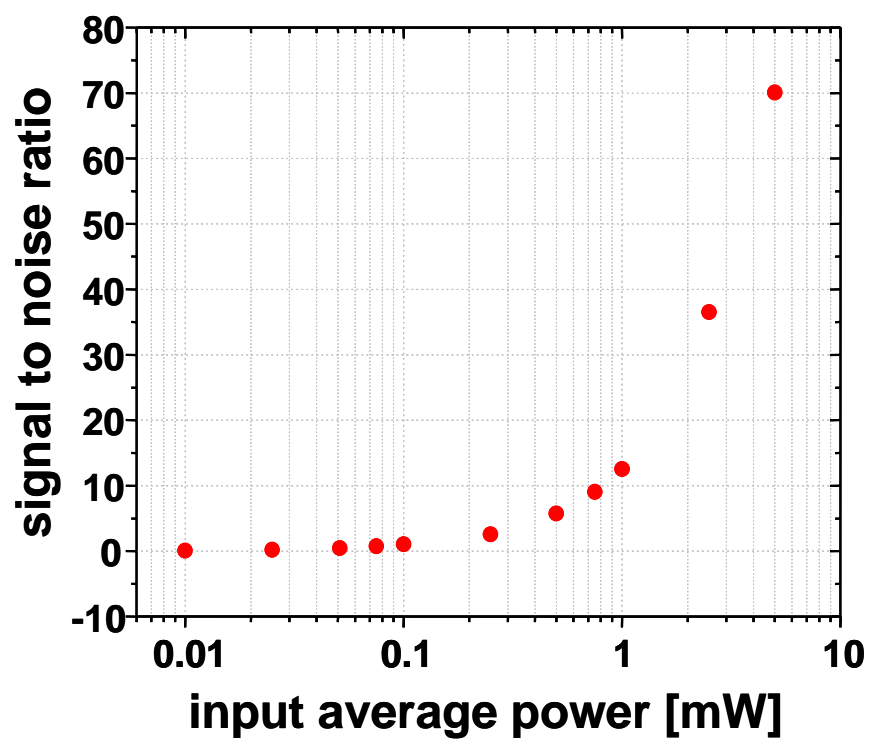
Figure 14. Optical signal to noise ratio vs. input average power. (in

the case of ~9.6ns injection)
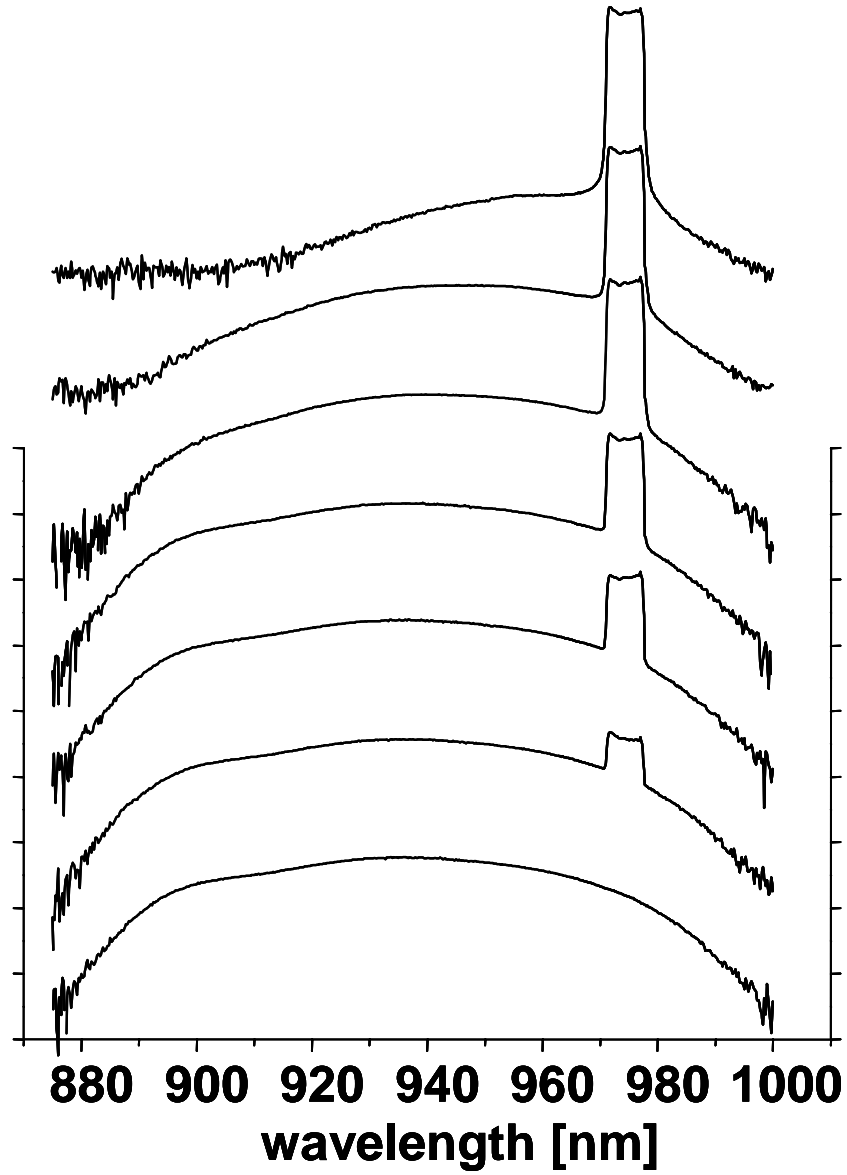
Figure 15. Experimental result, optical spectrum of amplified signal through RWGSOA, in the case of ~9.6ns injection, input average power is from 0mW to 1mW, vertical axis: 10dB/div.

Another salient feature of X-CPA in ultrashort pulse amplification is that detrimental nonlinearities which cause optical pulse distortion will be reduced by stretching the optical pulse

before an SOA. In the measured optical spectrum in Figure 10, carrier heating as well as an integrated self phase modulation due to gain saturation is inferred from the sharp peaks on the blue and red edges of the spectrum as the input average power is increased [27]. But in Figure 15, the nonlinearities are not observed even though the input average power is higher than the 1ps injection experiment. In reference [16] and [38], the advantage of pulse stretching before an SOA inside a semiconductor mode-locked laser is addressed. Given the same input average power, the optical signal to noise ratio of the two cases is calculated from the measured optical spectrum and plotted in Figure 16. Significant enhancement of the optical signal to noise ratio in X-CPA is observed as compared with the injection of a 1ps optical pulse.
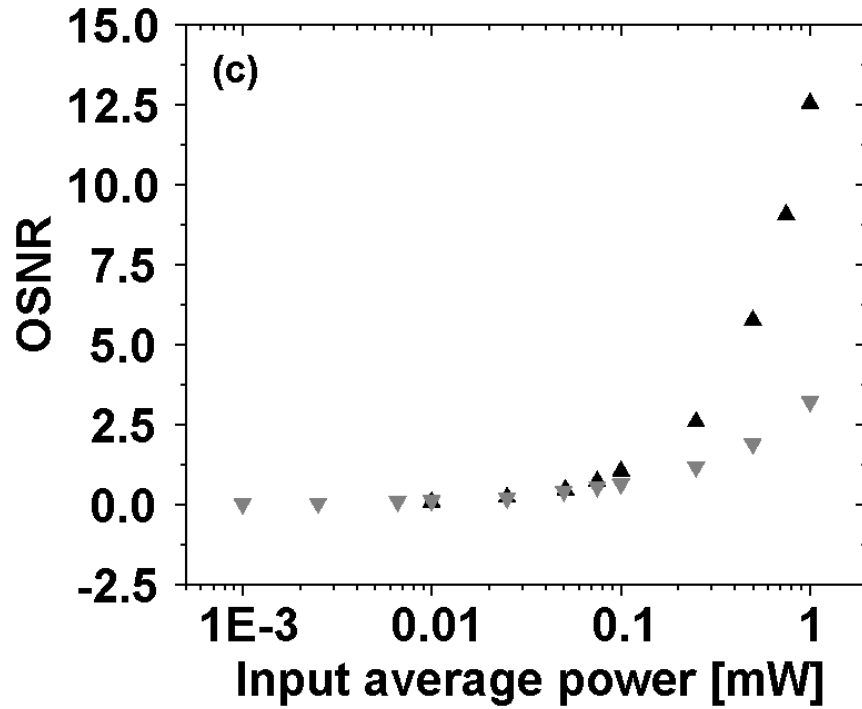
Figure 16. Optical signal to noise ratio vs. input average power, grey: ~1ps injection, black: ~9.6ns injection

Based on the semiconductor rate equations, a numerical simulation was performed to fit the measured output energy (Figure 9 and Figure 13). As shown in Figure 17, simulation results are in good agreement with the measured data. The parameters used in this simulation were as follows: saturation energy of 30pJ, a small signal gain of 18dB and a carrier lifetime of 600ps.
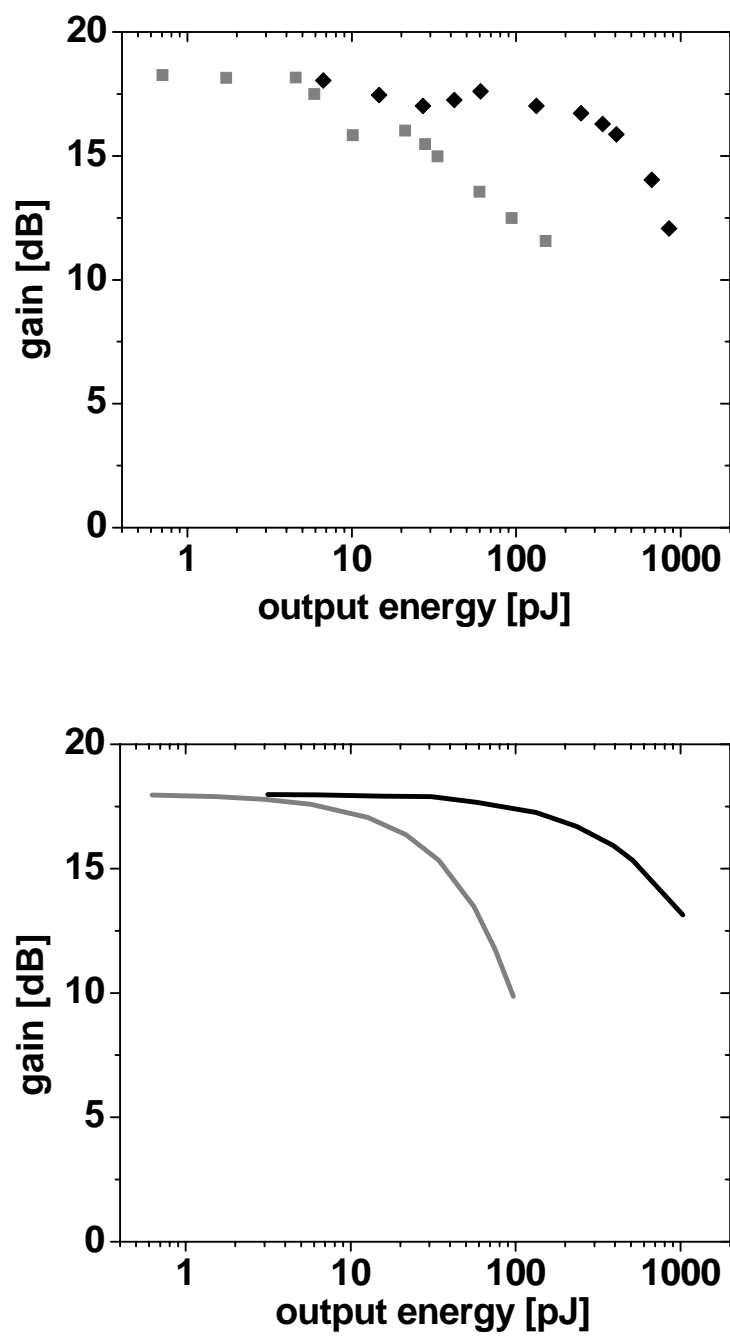
Figure 17. Comparison of the experiment (top) and simulation (bottom) results, grey: ~1ps injection, black: ~9.6ns injection

CHAPTER 3: ALL-SEMICONDUCTOR EXTREME CHIRPED PULSE AMPLIFICATION SYSTEM

3-1. Master Oscillator: Colliding Pulse Hybrid Mode-Locked Semiconductor Laser

As a master oscillator in the X-CPA system, a novel colliding-pulse, hybrid mode-locked semiconductor laser (CPMLL) was developed. The schematic diagram of the CPMLL is displayed in Figure 18.
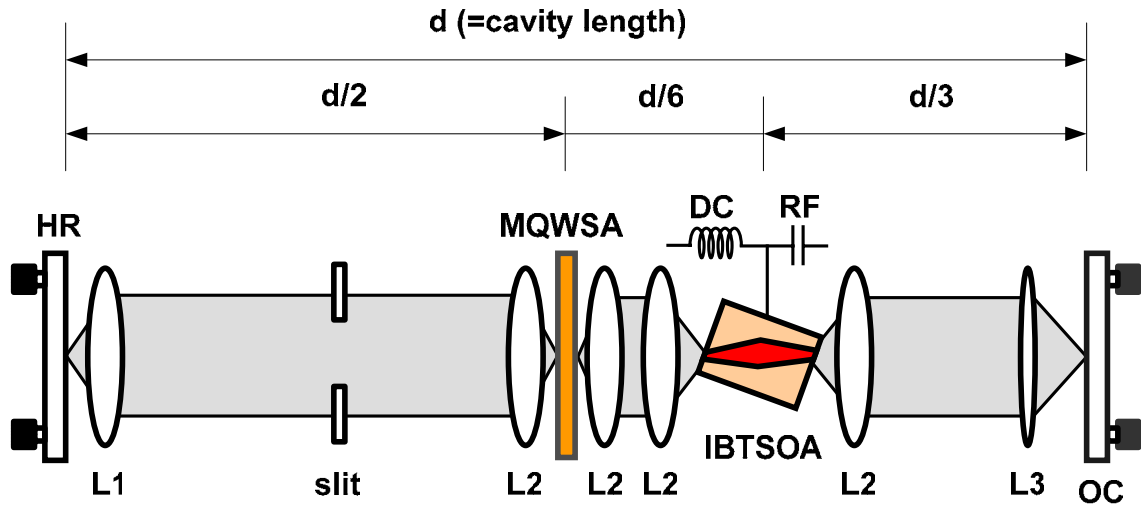
Figure 18. Schematic diagram of colliding pulse hybrid mode-locked semiconductor laser, HR: high reflector, slit: adjustable slit, L1: lens. L2: lens, L3: lens, MQWSA: multiple quantum well saturable absorber, IBTSOA: inverse bowtie semiconductor optical amplifier, OC: output coupler

A transmission-type **multiple quantum well saturable absorber** (MQW SA), used as a passive mode-locker, was placed at the half cavity position and an **inverse bowtie semiconductor optical amplifier** (IBTSOA) (addressed in chapter 3-6-1), used as a gain medium, was placed at the 1/3 cavity position. Four anti-reflection coated aspheric lenses with f=8mm (L2, Thorlabs C240, 0.50 numerical aperture) were both used for collimating light from IBTSOA and for focusing light into MQWSA. One plano-convex spherical lens (L1) with f=30mm and one achromat lens (L3) with f=50mm were used to create a stable cavity. The reflectance of the output coupler (OC) is 30%. IBTSOA was driven by an amplified 285MHz RF sinusoidal wave, which is the second harmonic pulse repetition frequency of the external cavity, as well as a ~220mA DC current. The amplified RF signal and DC current were combined with a bias-tee. There is an adjustable slit inside the cavity to control the spatial mode profile into the MQW SA and IBTSOA.

Multiple Quantum Well Saturable Absorber: As shown in Table 3, the **MQW SA** consists of 75 repetitive layers of 8.5nm $In_{0.18}Ga_{0.82}As$ quantum well and a 10nm $Al_{0.35}Ga_{0.65}As$ barrier on a GaAs substrate and both surfaces are anti-reflection coated with silicon nitride [39]. The unsaturated absorption with respect to wavelength is characterized with a spectrophotometer (Cary 500 Spectrophotometer) and an excitonic absorption peak at room temperature was observed near 970nm (Figure 19(b)). As shown in Figure 1 (a), the MQWSA with an electrical contact can be biased to shift the peak wavelength of excitonic absorption (Figure 19(c) and (d)). It could be used to adjust an absorption recovery time as well as to tune the center wavelength of a mode-locked oscillator.
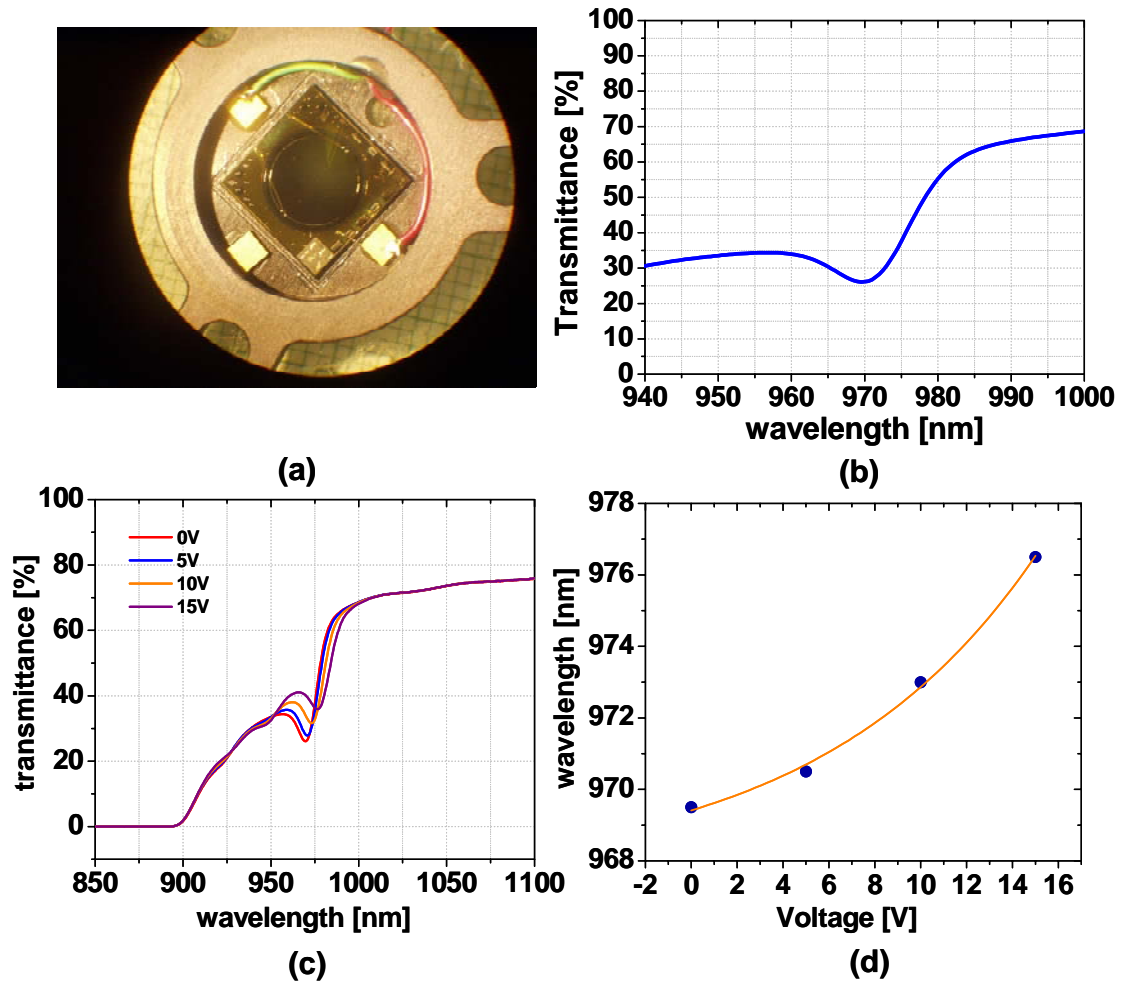
Figure 19 (a) Photograph of MQW SA, (b) transmittance of MQW SA at unsaturated regime, (c) transmittance of MQW SA with difference reverse biased condition, (d) plot of excitonic peak shift with respect to reserve biased voltage

Table 3. MQW SA epi-wafer structure

Material	purpose	thickness	doping	concentration
SiN	AR	125nm		
GaAs	p-contact	1um	p-doped	3x10^18
GaAs	buffer	0.25um	undoped	
$Al_{0.35}Ga_{0.65}As$	barrier	10nm x 75 layers		
$In_{0.18}Ga_{0.82}As$	QW	8.5nm x 75 layers		
GaAs	buffer	50nm	undoped	
GaAs	n-contact	1um	n-doped	3x10^18
SiN	AR	125nm		

The **IBTSOA** used as a gain medium inside the CPMLL cavity has the design of a 1mm-long InGaAs inverse bowtie shaped stripe at an angle of ~6 degrees with respect to the facets, linearly tapered from a 10um width at the facet to about 20um width at the center (addressed in chapter 3-3-1). The 10um aperture on both facets makes the output beam closer to diffraction limited and a wide tapered center region is incorporated for generating high power [11, 40].

By optimizing the location of IBTSOA and MQWSA and the output coupler, >20pJ output pulse energy can be generated directly by the oscillator. The prominent feature of the CPMLL is that 40~50ps compressible up-chirped pulses are generated directly from the oscillator (Figure 20). This feature of generating a pre-chirped pulse is helpful for minimizing nonlinearities inside the CFBG when used as a compression stage. In Figure 21, the output optical spectrum from the CPMLL has a typical spectral shape from passively mode-locked semiconductor lasers using MQWSAs [7] and its bandwidth is from 971nm to 977nm.
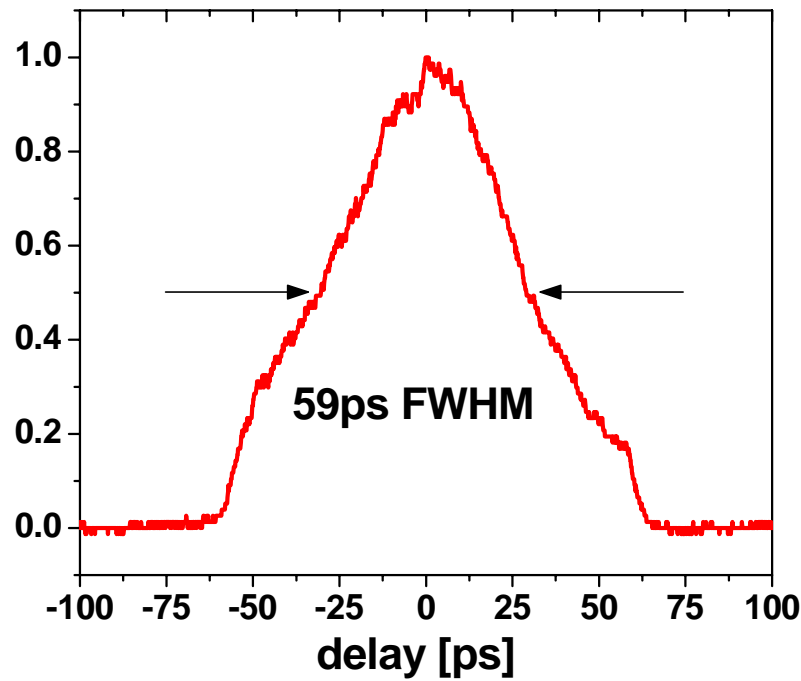
Figure 20. Autocorrelation trace of a compressible pre-chirped pulse directly from CPMLL

Compensating the impressed chirp by an external dual bulk grating compressor (addressed in chapter 3-7), the ~45ps pulse from the oscillator was compressed down to 0.92ps (FWHM at autocorrelation trace, Figure 21). With the assumption of a hyperbolic secant pulse, the deconvolved pulse width becomes 0.52ps, which is ~3.5times the transform-limited pulse duration.
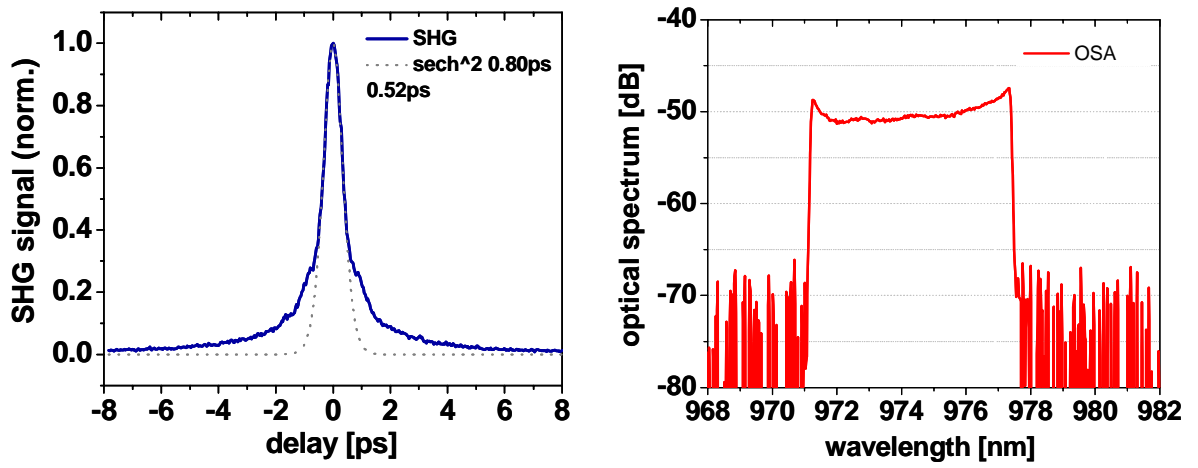
Figure 21. Autocorrelation trace of a compressed pulse from CPMLL after the bulk grating compressor (left) and optical spectrum of the amplified CPMLL (right)

3-2. Optical Pulse Pre-stretcher: Single Mode Fiber Spool

Even if a 40~50ps pre-stretched pulse was directly generated from the CPMLL to reduce the detrimental nonlinearity that causes optical pulse distortion, as the output power from the X-CPA system is increased to a certain power level, the amount of pre-stretching generated from the CPMLL is not enough to prevent optical pulse distortion. At the moment, in order to reduce the detrimental nonlinearity, more stretching of the optical pulse from the CPMLL will be necessary. As an optical pulse pre-stretcher, simply a spool of 980nm single mode fiber can be used in the X-CPA system. Fortunately, the sign of pre-chirping of the optical pulse from the CPMLL is matched with the dispersion sign of the commercially available 980nm single mode fiber (HI1060). The accumulated pre-chirping from the CPMLL and single mode fiber (SMF) spool is compensated by a bulk grating pulse compressor (Chapter 3-7). Current bulk grating pulse compressors limit the length of a single mode fiber to ~300m.

3-3. eXtreme Pulse Stretcher and Compressor: Chirped Fiber Bragg Grating

A highly dispersive chirped fiber Bragg grating (Figure 22, manufactured by 3M) used as an extreme pulse stretcher and compressor plays an important role in realizing the X-CPA concept [41]. As shown in Figure 23, the group delay of the CFBG is linear and ~ 1600 ps/nm with 6nm bandwidth at a 974nm center wavelength. The physical length of the CFBG ($t_{stretch} = \dfrac{c}{2nL}$) is about 0.96m considering the refractive index of the fiber core. The grating is written in a photosensitive PS1060 fiber that supports a single spatial mode (MFD~5.9um^2) within the reflectance wavelength band. Due to cladding modes [42, 43] of the CFBG, the reflected blue shifted wavelengths from the red port of the CFBG experiences more loss than the
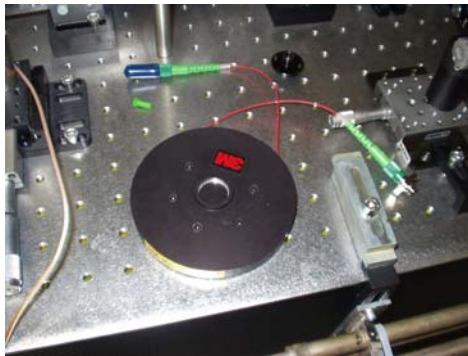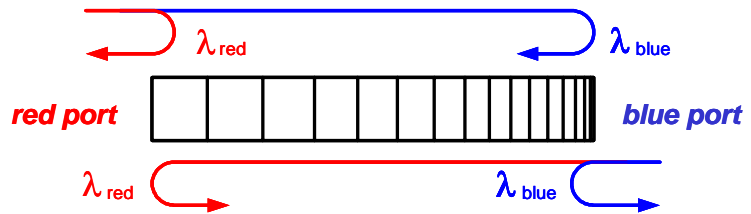
(a)   (b)

Figure 22. (a) photograph of packaged CFBG and (b) CFBG as a extreme chirped pulse stretcher and compressor

red shifted wavelengths. This is clearly seen from the reflectance spectrum measured from the red port (Figure 23). However, the reflectance band of the blue port is flat (Figure 23). The maximum stretched pulse will be ~ 9.6ns which realizes at least ten times larger energy extraction from the SOA considering <1ns energy storage lifetime of the SOA.
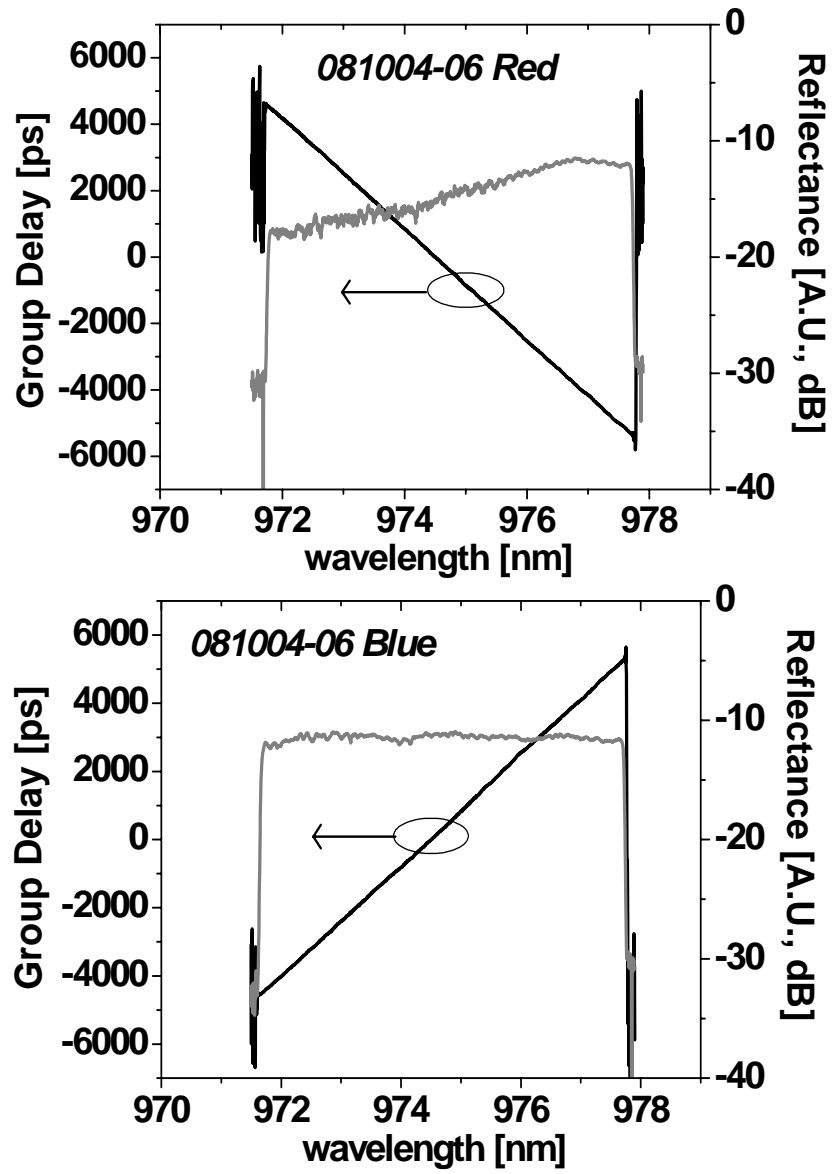
Figure 23. Group delay and reflectance of red port (top) and blue port (bottom) of the CFBG
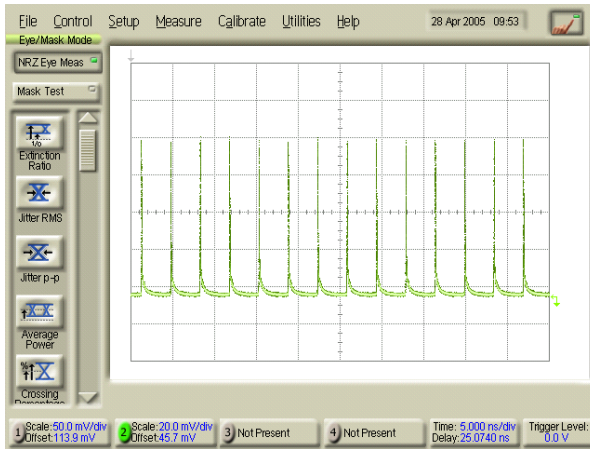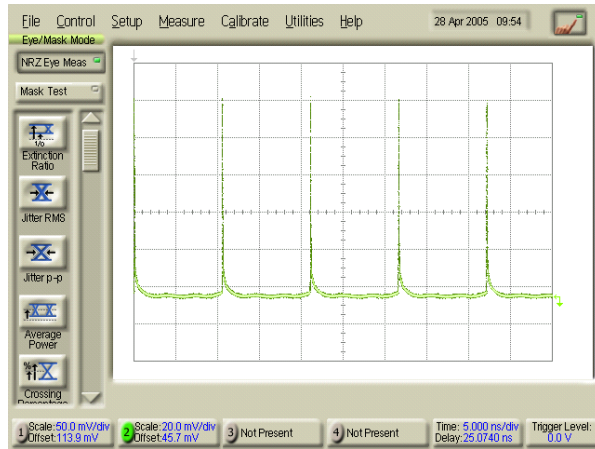
(a)   (b)

Figure 24. Sampling scope trace of (a) 285MHz CPMLL and (b) 95MHz pulse train after the
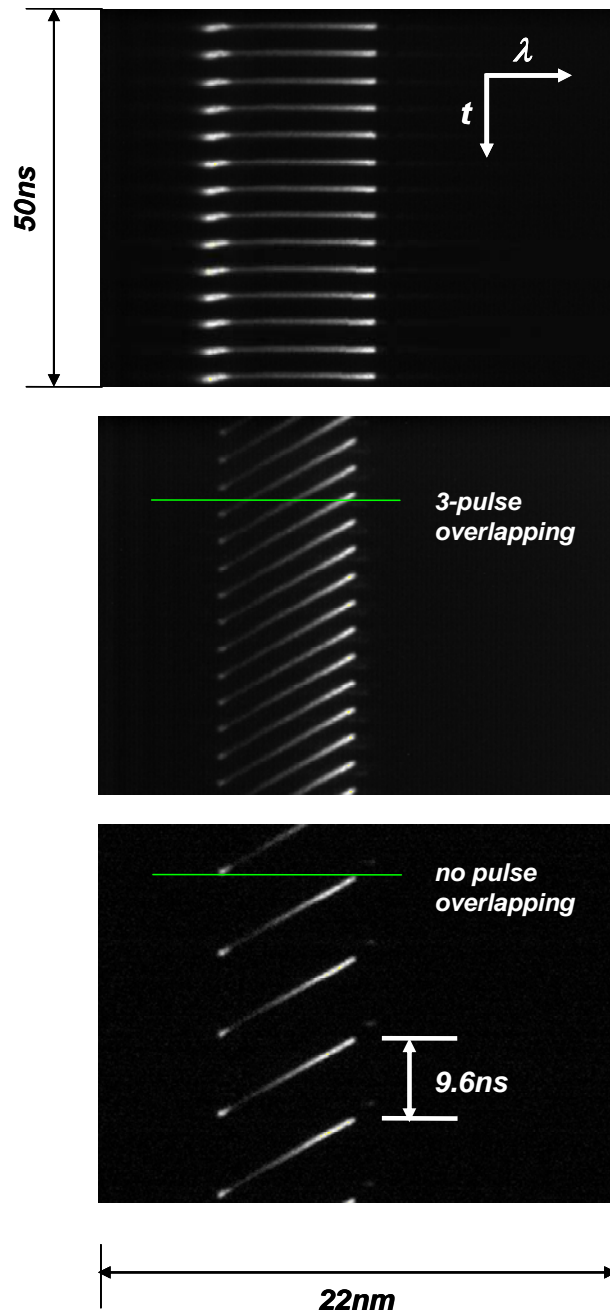
SOA pulse picker

Figure 25. Streak camera images, vertical axis – time window, horizontal axis – spectral window, (a) 285MHz CPMLL, (b) 285MHz extremely stretched pulse, and (c) 95MHz extremely stretched pulse

45

3-4. SOA Pulse Picker: Intensity Modulator with Optical Gain

If a 285MHz pulse train from the CPMLL (Figure 24(a) and Figure 25(a)) is stretched directly using a CFBG that possesses a 1600ps/nm with 6nm bandwidth, then three pulses will temporally overlap, leading to gain competition and a reduction of the efficiency of the energy extraction from the cascaded semiconductor optical amplifier chain (Figure 25(b)). In order to prevent temporal pulse overlapping, an SOA pulse picker was inserted between the CPMLL and the extreme pulse stretcher. A 1mm long IBTSOA, identical to the SOA inside the oscillator, was used as the pulse picker and was pulse biased to reduce the repetition rate from 285MHz (Figure 24(a) and Figure 25(a)) down to 95MHz (Figure 24(b) and Figure 25(c)). The pulse picker was driven by a ~3ns electrical pulse at 95MHz amplified through a high power RF amplifier and the pulse picker setup is illustrated in Figure 26 and Figure 27. The salient feature of the SOA pulse picker is that we are able to amplify the optical pulse to compensate for the loss arising from single mode fiber coupling and the insertion loss inside the CFBG as an extreme pulse stretcher, as well as reduce the pulse repetition rate. Also, by applying a reverse bias between forward biased 95MHz electrical pulses, the transmitted pulses under an unbiased condition can be suppressed by absorption which improves the signal to noise ratio of the 95MHz pulse train. The 95MHz pulse train after the pulse picker is extremely stretched to 9.6ns after reflecting from the red port of the CFBG (Figure 25(c)).
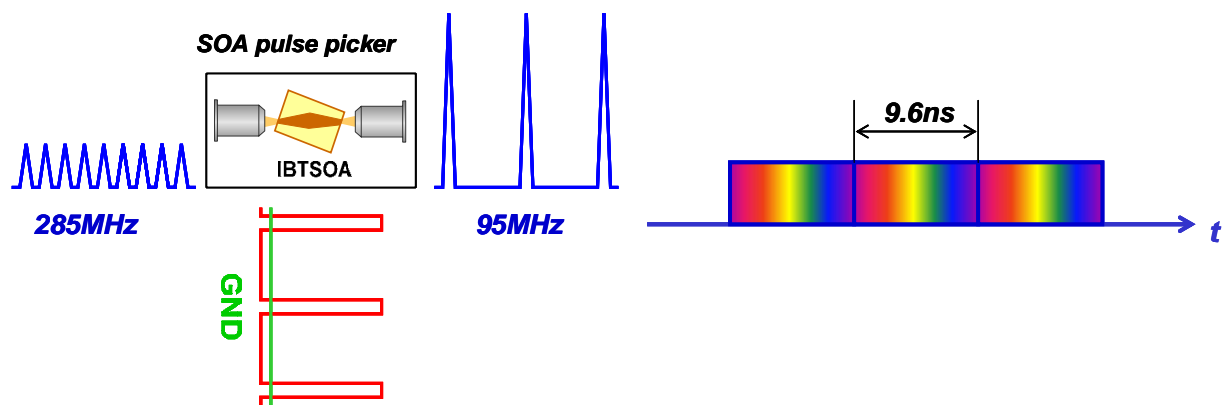
Figure 26. Operating concept of the SOA pulse picker
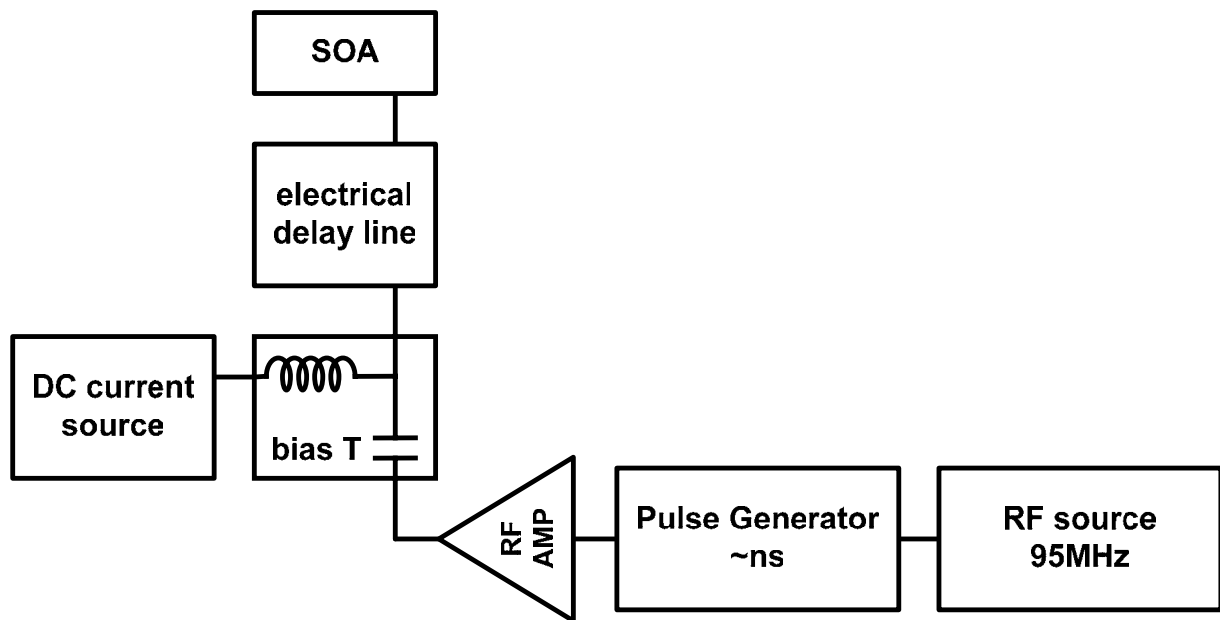
Figure 27. Electronics diagram of the SOA pulse picker driver

3-5. Free Space Optical Circulator

In this experiment, an optical circulator consisting of a quarter wave plate (QWP) and a polarizing beam splitter (PBS) (Figure 28) produces a spectral modulation of the reflectance band of the CFBG which is difficult to minimize (Figure 29). The spectral modulation makes energy extraction less efficient and causes distortion of the recompressed optical pulse. Therefore an optical circulator consisting of a polarizing beam splitter (PBS), Faraday rotator (FR), and a polarization controller (PC) was implemented in this experiment (Figure 30). As shown in Figure 25(c) and Figure 31, the spectral modulation occurring in the previous setup was
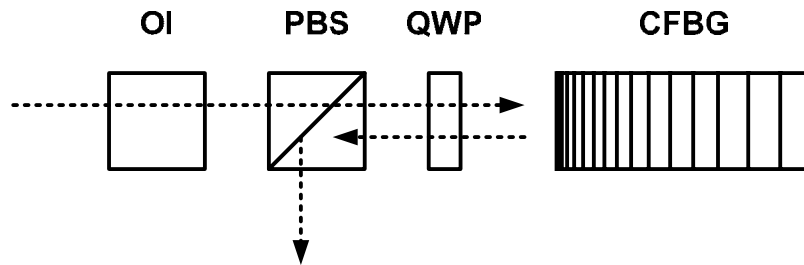
Figure 28. Optical circulator using PBS and QWP

nearly minimized by optimizing the polarization controller. Another advantage of the optical circulator is that it is a polarization sensitive component. When a single CFBG is used as both an extreme pulse stretcher and a compressor, it is possible to make the polarization state of the transmitted light from the red port orthogonal to the polarization state of the reflected light from the blue port and vice versa. It helps to minimize detrimental closed loop lasing from cascaded amplifiers.

(a)   (b)
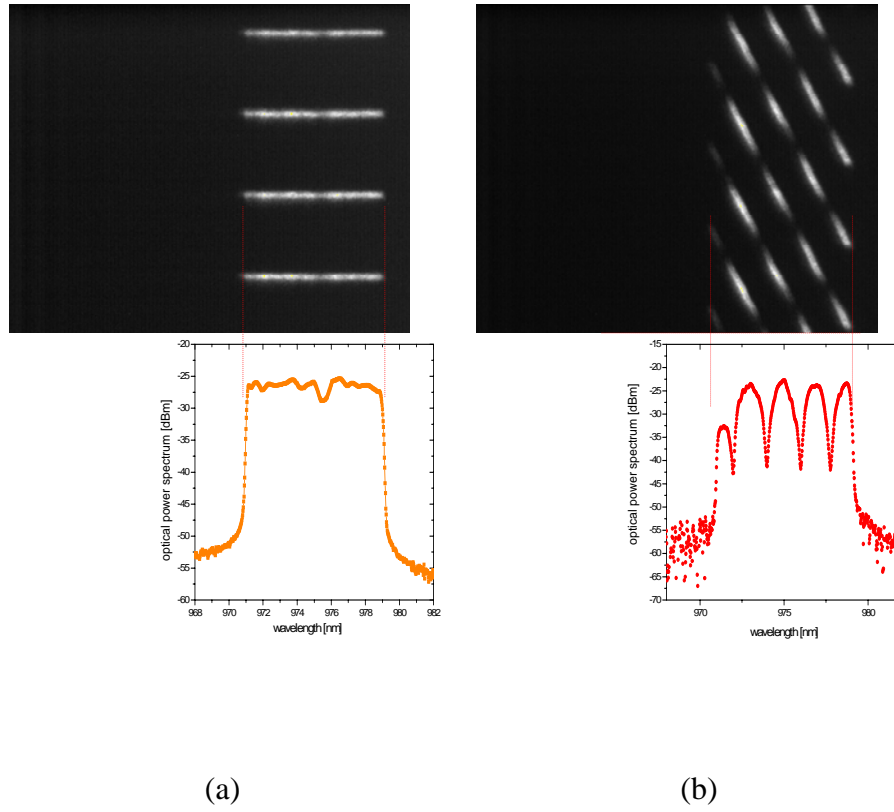
Figure 29. (a) streak camera image and optical spectrum of optical pulses directly from the gain flattened actively mode-locked semiconductor laser (GFMLL, Appendix B-1) and (b) streak camera image and optical spectrum of extremely stretched pulses after CFBG by using the optical circulator consisting of QWP and PBS, streak camera image: vertical axis-time, horizontal axis-wavelength

49
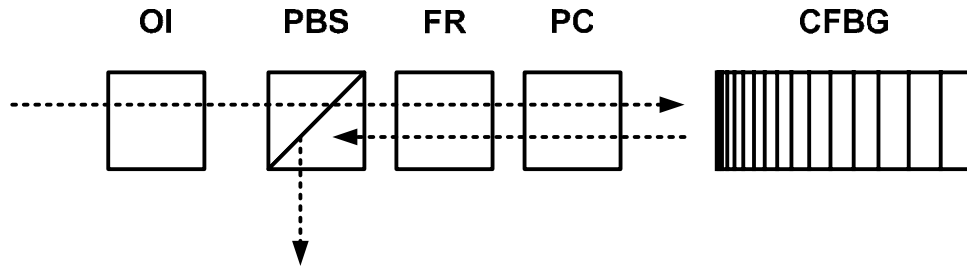
Figure 31. Optical circulator consisting of PBS, FR and PC

(a)   (b)
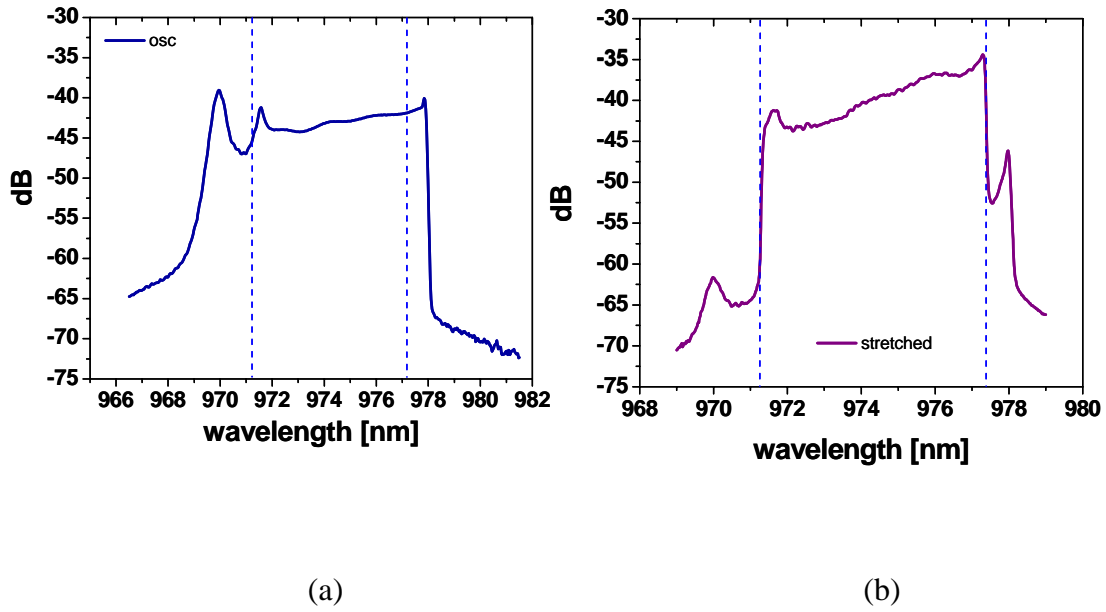
Figure 30. (a) optical spectrum of optical pulses directly from the CPMLL and (b) optical

spectrum of extremely stretched pulses after CFBG by using optical circulator consisting of

PBS, FR and PC

3-6. Semiconductor Optical Amplifiers

3-6-1. Inverse Bow-tie Semiconductor Optical Amplifier (IBTSOA)

Identical IBTSOAs (Sarnoff Corporation) are used as the gain medium inside the CPMLL cavity and pulse picker. The design of IBTSOA is a 1mm-long inverse bowtie shaped stripe at an angle of 6 degrees with respect to the facets to reduce the effective reflectivity and is linearly tapered from a 10um width at the facet to near 20um width at the center (Figure 32). The 10um aperture on both facets makes the output beam closer to diffraction limited and a wide tapered center region is incorporated for generating high power [11, 40]. The composition is based on a InGaAs quantum well on a GaAs substrate and an inverse bowtie shaped active region has a gain guided structure. The optical power and optical spectrum of the amplified spontaneous emission with respect to injected current are shown in Figure 33. In order to reduce
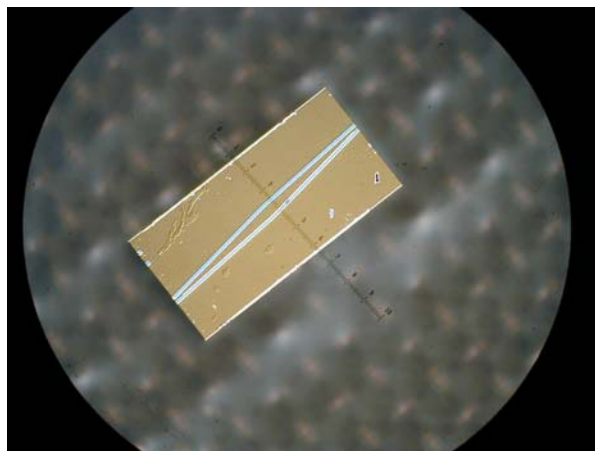
Figure 32. Photograph of the inverse bowtie semiconductor optical amplifier, Length: 1mm

Fresnel loss (~30%), both facets are anti-reflection coated.
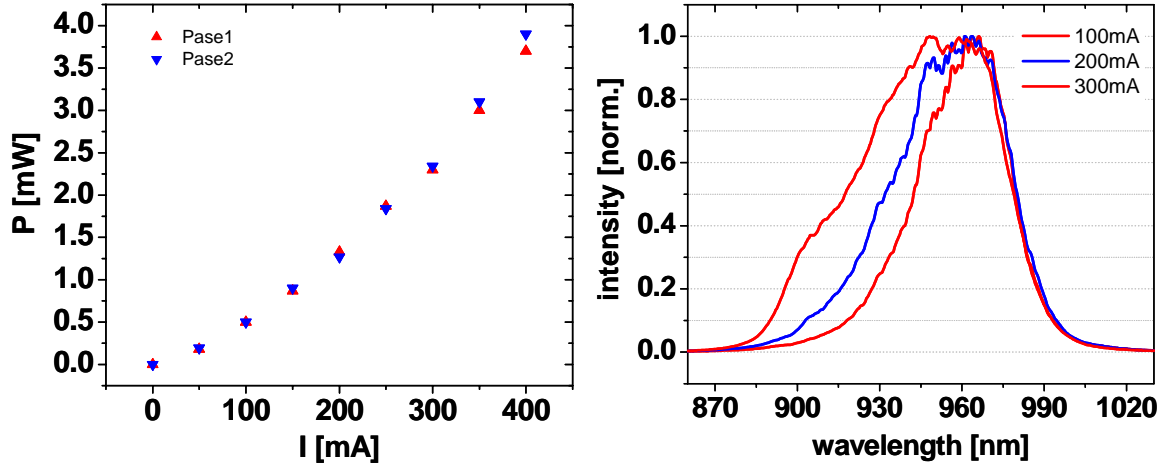
Figure 33. Spontaneous emission characteristics of IBTSOA, (a) L-I curve from both facets and (b) optical spectrum

3-6-2. Ridge Waveguide Semiconductor Optical Amplifier (RWGSOA)

In an X-CPA system, even though the SOA pulse picker is inserted, the average optical power after the extreme pulse stretcher is not enough to saturate a power amplifier, because of the coupling loss into the single mode fiber and insertion loss of the extreme pulse compressor. A customized 1.5mm long RWGSOA was inserted as a pre-amplifier between the extreme pulse stretcher and the power amplifier; this provided enough optical power after the pre-amplifier to saturate the power amplifier.

The RWGSOA (a custom device manufactured by Axcel Photonics) is a ridge waveguide based SOA which can support a single spatial mode. Based on basic parameters of the epi-wafer

structure and the ridge waveguide structure (mode field diameter 4.8um, refractive index difference between core and cladding ~0.004) provided by Axcel Photonics, the effective reflectivity versus tilting angle was calculated based on reference 44 and the tilting angle was chosen to be ~5.8 degree given 10^{-5} of effective reflectivity (Figure 34). Both facets are passivated for high power operation and are anti-reflection coated to reduce Fresnel reflection loss. The device length of the RWGSOA used as a preamplifier is 1.5mm long. The optical power and optical spectrum of the ASE versus the injected current are characterized (Figure 35). At a 500mA injection current, the optical power from both facets was >80mW and shows a symmetric behavior. At a low current peak wavelength the ASE is located near 950nm and as the injection current is increased, the n=2 state excitation of quantum well was observed in the optical spectrum. In Figure 36, catastrophic optical mirror damage (COMD) of the 1.5mm long RWGSOA is investigated. This particular device shows COMD at a 230mW output power.
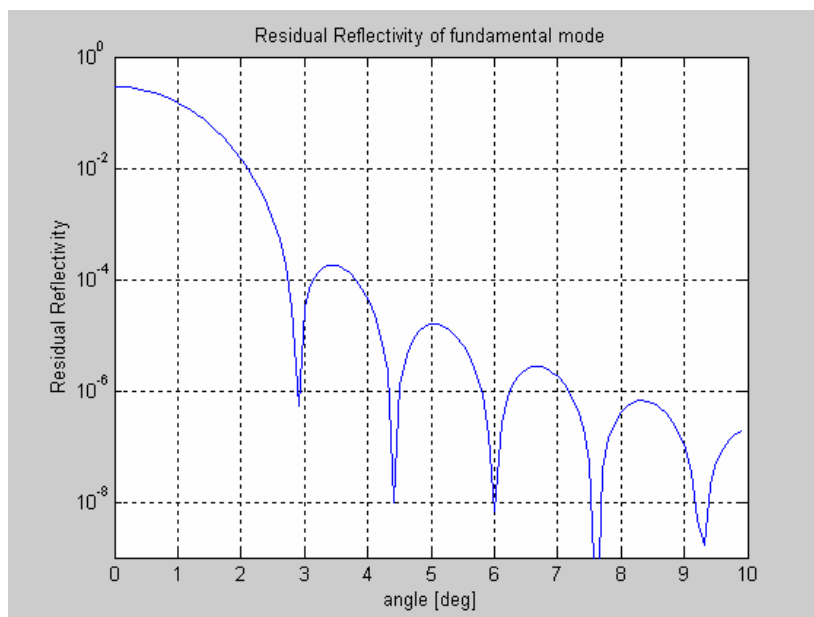
Figure 34. Calculated effective reflectivity vs. tilted angle of the ridge waveguide of the

RWGSOA based on parameters provided by Axcel Photonics
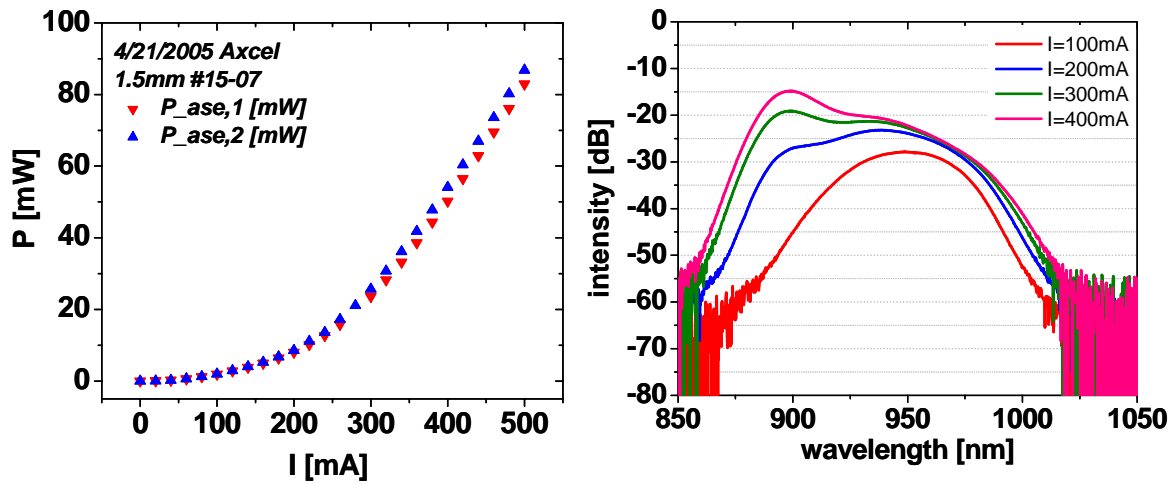
Figure 35. Spontaneous emission characteristics of the 1.5mm long RWGSOA. (a) L-I curve and (b) optical spectrum
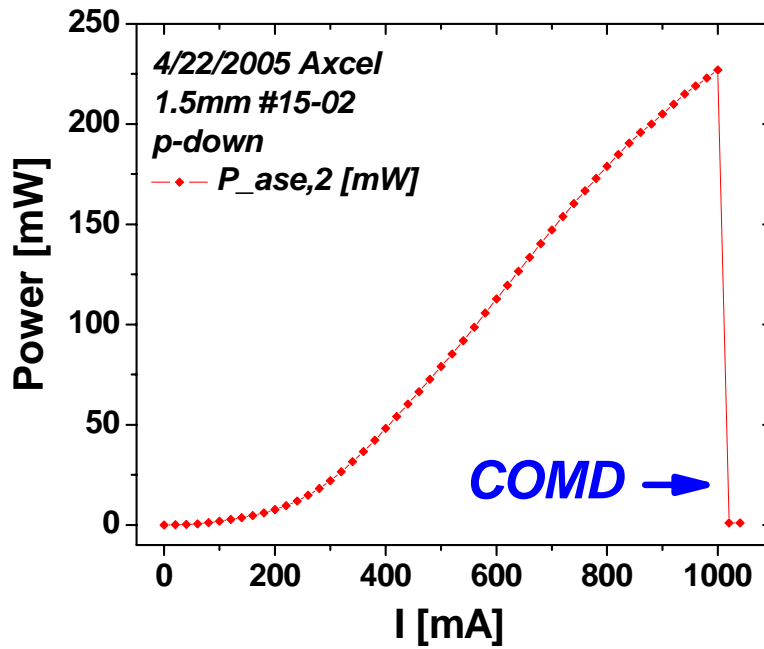
Figure 36. Catastrophic optical mirror damage of the 1.5mm long RWGSOA. L-I curve

3-6-3. Tapered Semiconductor Optical Amplifier (TA)

As a power amplifier in an X-CPA system, a tapered amplifier (Eagleyard Photonics, GmbH) was implemented between the preamplifier and the extreme pulse compressor. There are two noticeable characteristics of the tapered amplifier (TA) which are very useful in the X-CPA system; one is that the TA is an optical amplifier with a high optical saturation power and the other is the output beam profile is close to the diffraction limit. Because the output from the TA

should be coupled into a single mode fiber, a good quality beam profile is needed to get more output power from the X-CPA system.

The TA is a ~3mm long two section device with a ~3um input aperture and a ~200um output aperture. After a straight 3um ridge waveguide used as a spatial filter and a preamplifier, the beam from the 3um ridge waveguide is diffracted through a tapered region and therefore a single spatial mode is kept inside the tapered amplifier. At the same time, due to a 200um large output aperture that can support high power operation, the output power is increased through the tapered region. Both facets are anti-reflection coated to prevent chip lasing and the TA is mounted on a c-mount with p-down. The optical power and optical spectrum of the spontaneous emission from the TA versus the injected current were measured (Figure 37).
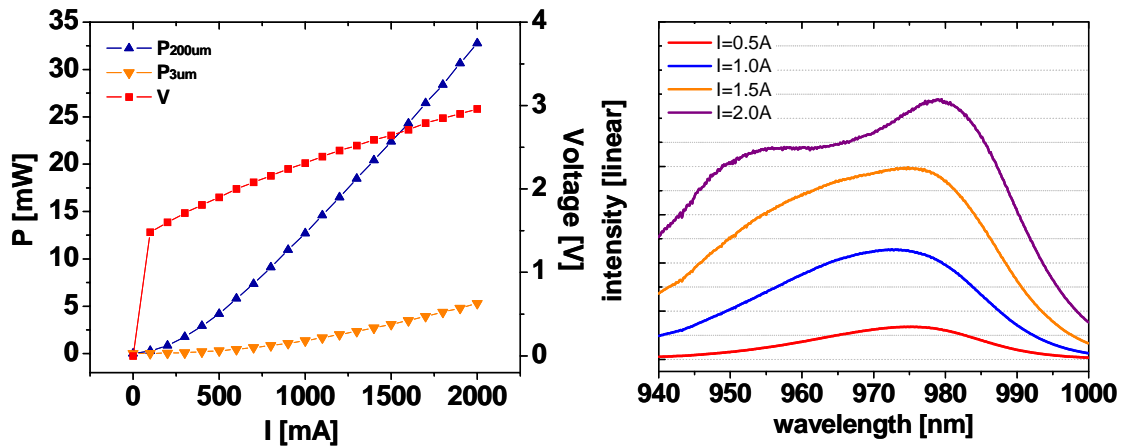
Figure 37. Spontaneous emission characteristics of a 3mm long TA. (a) L-I-V curve and (b) optical spectrum

3-6-4. Flared Semiconductor Optical Amplifier (FA)

The flared amplifier (customized device, Coherent, Inc.) is a high power, gain guided multi-spatial mode device and the input and output apertures typically support multi spatial modes. In this experiment, the FA was implemented to study the limitation of energy extraction of the semiconductor optical amplifier developed with current technology. The epi-structure of the FA consists of a large optical cavity (LOC) and a separate confinement hetero-structure with an InGaAs quantum well (QW) active region (Table 4). The length of the FA is 6 mm. The emitting output aperture is 700um wide to the increase output saturation power and the input coupling aperture is 200um wide. Both facets of the amplifier are anti-reflection coated (by K-Lab & Covega). The amplifier was mounted p-side down on a heatsink. Spontaneous characteristics of the FA using a customized 2kA pulsed current source were measured (Figure

Table 4. Epi-structure of the flared amplifier

Layer #	Material	Layer Description
0	n-GaAs Substrate	
1	GaAs:Si	buffer layer
2	$Al_yGa_{1-y}As$:Si	n-cladding
3	$Al_xGa_{1-x}As$	waveguide
4	**$In_{1-x}Ga_xAs$**	**QW**
5	$Al_xGa_{1-x}As$	waveguide
6	$Al_yGa_{1-y}As$:C	p-cladding
7	GaAs:C	p-contact

38 and 39).
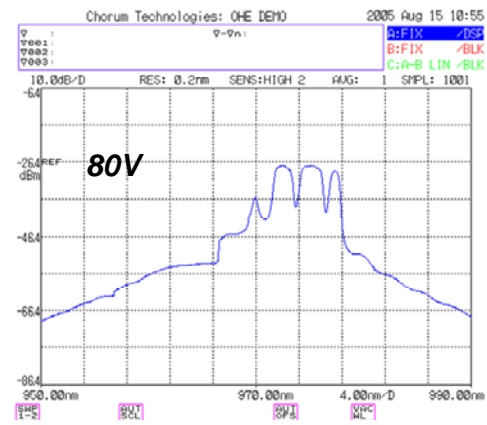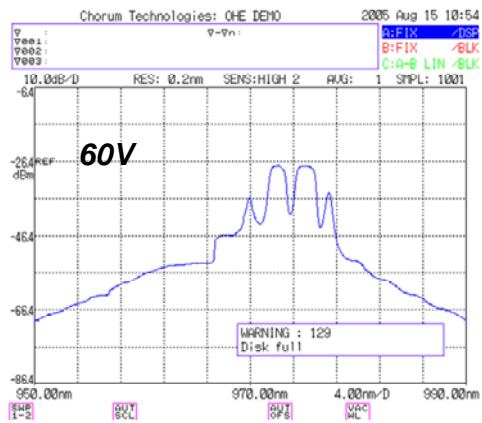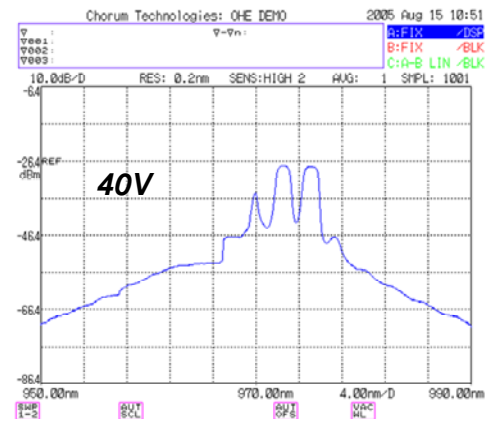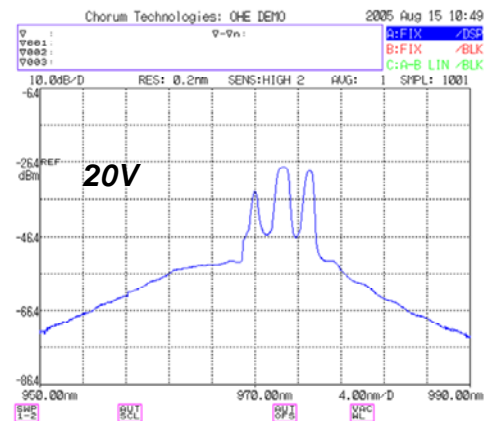
Figure 38. Optical spectrum of the spontaneous emission from the flared amplifier at different

bias
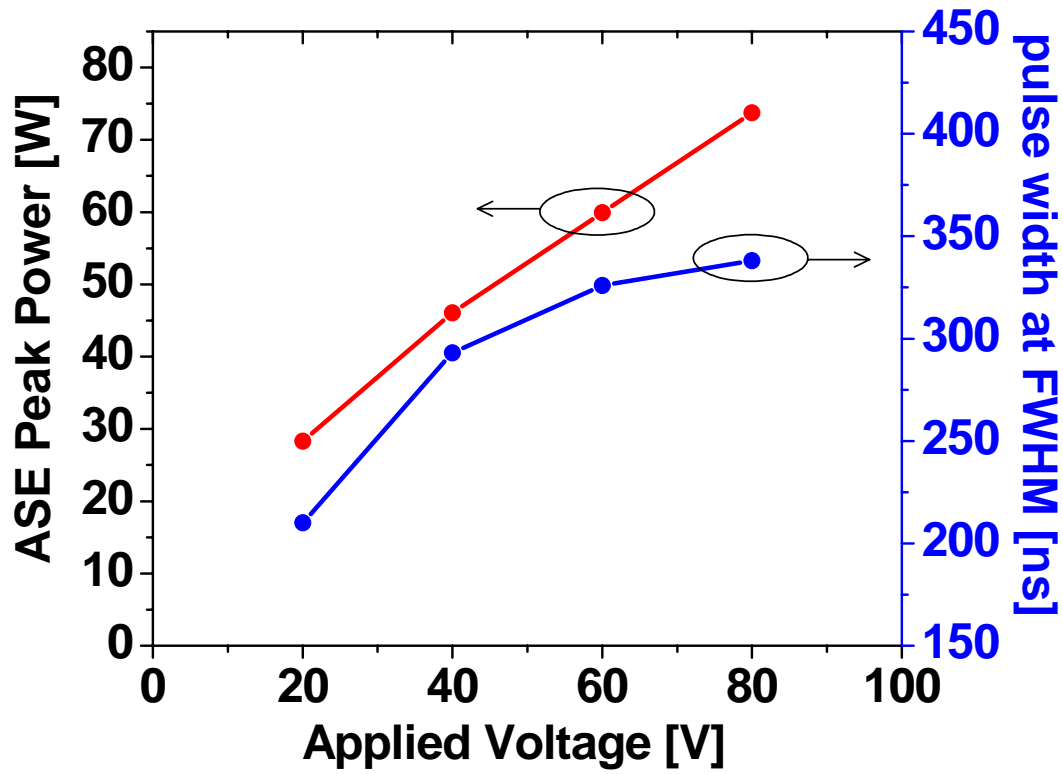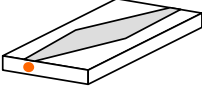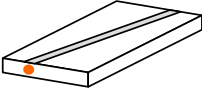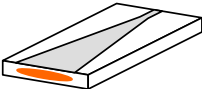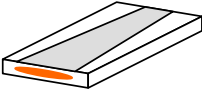
Figure 39. Spontaneous emission power and optical pulse width of the flared amplifier driven by a customized 2kA pulsed current source

In the X-CPA experiment, the FA was used to investigate the maximum extractable energy from the SOA developed using current technology.

Table 5. SOAs used in the X-CPA experiment and their basic characteristics

	type	dimension	description
oscillator & pulse picker	inverse bowtie SOA (IBTSOA)	1mm long 10um input & output	gain-guided close to diffraction limit medium power Sarnoff Corp.
pre-amplifier	ridge waveguide SOA (RWGSOA)	1.5mm long	ridge waveguide single spatial mode low power with high gain Axcel Photonics
power amplifier	tapered amplifier (TA)	3mm long 3um input 200um output	ridge waveguide + gain guided close to diffraction limit, M2~1.06 high power Eagleyard Photonics
power amplifier	flared amplifier (FA)	6mm long 200um input 700um output	gain-guided multi-spatial mode high power Coherent, Inc.

3-7. Bulk Grating Pulse Compressor and Stretcher

The bulk grating compressor plays two roles in an X-CPA system. One is to compensate the pre-chirping of an optical pulse that was directly generated by an oscillator and/or imposed from a single mode fiber pre-stretcher. The other is to access the Fourier plane to manipulate unwanted optical spectrum and to investigate the phase relation of the optical spectrum.
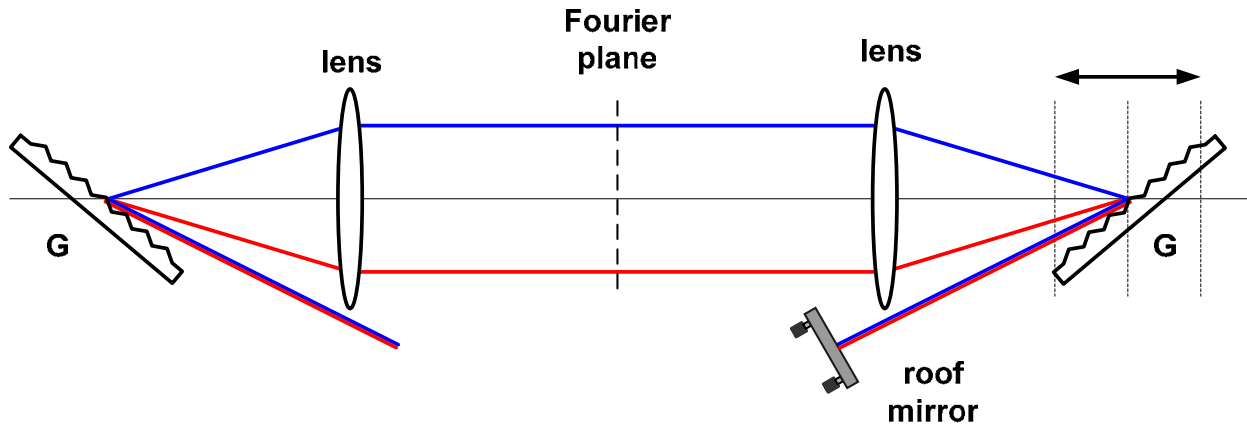
Figure 40. Bulk grating pulse compressor and stretcher, G: grating

A typical dual grating compressor with two lenses (achromat, f=20cm), which allows access to both negative and positive group delay dispersions (GDD) [45], consists of two holographic gratings, two AR coated achromat lenses (f=20cm) and one roof mirror. The grating has 1800 lines/mm of groove density and its size is 2 inch x 2 inch. To maximize the angular dispersion and for alignment purposes on the optical table, an incident angle into the grating compressor is set to be ~55 degree. Given the input angle and the groove density, the calculated

dispersion parameter (D) [46] is ~1.66ps/nm/cm. Considering losses from the grating, lenses, and roof mirror, the total throughput of the bulk grating compressor was ~57%.

3-8. All-Semiconductor Mode-Locked X-CPA System: >kW High Peak Power Generation

Combining i) master oscillator, ii) pre-stretcher + pre-amplifier, iii) SOA pulse picker, iv) optical circulator, v) extreme pulse stretcher and compressor (CFBG), vi) cascaded amplifiers, and vii) bulk grating pulse compressor, an all-semiconductor mode-locked X-CPA system has been demonstrated.

In this experiment, the CPMLL (Chapter 3-1) generates 39pJ per pulse with compressible
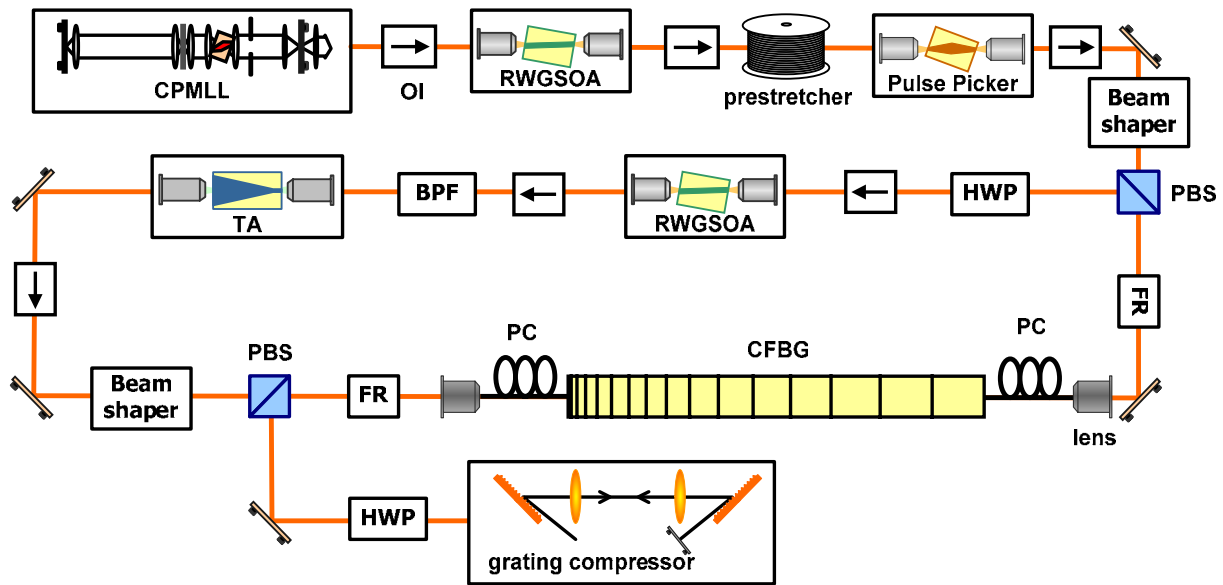
Figure 41. Schematic diagram of the all-semiconductor mode-locked X-CPA system, CPMLL: colliding pulse mode-locked semiconductor laser, OI: optical isolator, RWGSOA: ridge waveguide SOA, PBS: polarizing beam splitter, FR: Faraday rotator, PC: polarization controller, CFBG: chirped fiber Bragg grating, HWP: half wave plate, BPF: band pass filter, TA: tapered amplifier

up-chirped ~38ps pulses at 285MHz and 6.5nm bandwidth at the center wavelength of 974nm which matches the center wavelength of the CFBG. As mentioned previously, the ~38ps pre-chirped pulse width was expected to reduce the peak power at the end of the extreme pulse compression stage. Therefore, detrimental nonlinearities such as instantaneous self phase modulation and Raman scattering, which cause pulse distortion at high peak power, is expected to be reduced. But as the output energy was increased in the X-CPA system, the amount of pre-chirping was not sufficient to suppress the nonlinearities, causing side band generation and spectral modulation in the optical spectrum as well as temporal wings in the autocorrelation trace. To further to reduce the nonlinearities in the system, 300m of single mode fiber (SMF) was added to the X-CPA system. The type of SMF used as an optical pulse pre-stretcher was Corning HI1060 and its mode field diameter is ~5.9um^2 at the operating wavelength (Chapter 3-2). In order to compensate SMF coupling loss, a RWGSOA (Chapter 3-6-2) identical to the pre-amplifier in cascaded amplifiers was implemented between the CPMLL and the optical pulse pre-stretcher. The injection DC current into the pre-amplifier was set to 150mA. The optical pulse after the pre-amplifier and the optical pulse pre-stretcher became an up-chirped pulse of ~150ps which is within the range to be compensated by the dual bulk grating compressor. It provides an additional 4 times the pulse stretching factor, considering the ~39ps pulse from the CPMLL. The 150ps pre-stretched optical pulse train at 285MHz was injected into the SOA pulse picker to reduce the repetition rate down to 95MHz. As addressed in Chapter 3-4, the purpose of the reduction of the repetition rate is to avoid temporal pulse overlapping, which would lead to a reduction of the energy extraction efficiency in extreme chirped pulse amplification. The ~150ps optical pulse train at 95MHz was injected into the CFBG, used as the extreme pulse stretcher (Chapter 3-3), through a free space polarization dependent optical circulator consisting of a
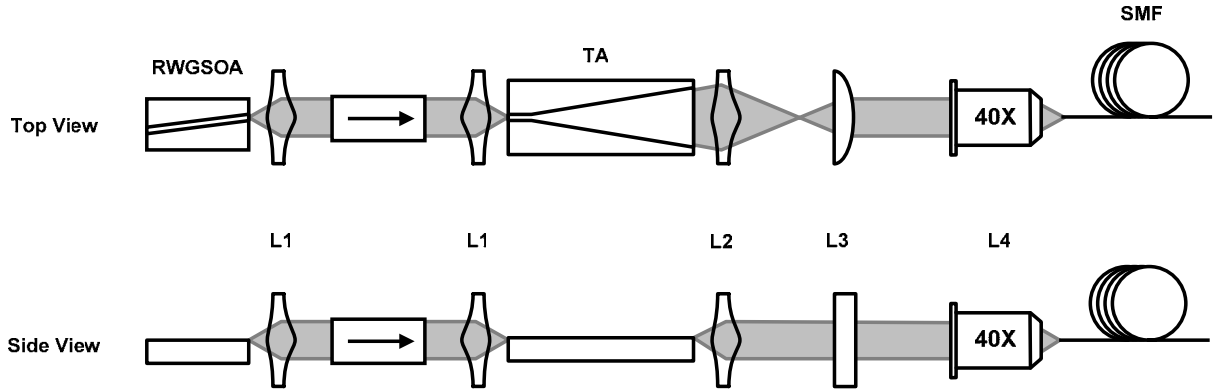
Figure 42. Experimental setup for SMF coupling with amplified signal from cascaded amplifiers, L1: aspheric lens (Thorlab, C240), L2: aspheric lens (CVI, FCA-0.67NA-2.84mm-970), L3: plano-convex cylindrical lens (Thorlab, f=40mm), L4: microscope objective lens (Newport, M-40X)

polarizing beam splitter, a Faraday rotator, and a three ring polarization controller (Chapter 3-5). The CFBG used in this experiment possess a finite transmission which is sufficient to allow for closed-loop lasing by the high gain, cascaded semiconductor optical amplifiers. By implementing the free space polarization dependant optical circulator, the polarization state of the reflected light from the red port of the CFBG becomes nearly orthogonal to that of transmitted light injected into the blue port of the CFBG and vice versa. In this way, the detrimental closed loop lasing is prevented.

In this experiment, the red port of the CFBG was used as the extreme pulse stretcher and the blue port of the CFBG was used as the extreme pulse compressor in order to best exploit the pre-up chirped pulses generated from the CPMLL. The reason is that if the red port of the CFBG was used as the extreme pulse compressor, then detrimental nonlinearities will be increased significantly. The ~150ps pre-stretched pulse train at 95MHz is extremely stretched to ~9.6ns after reflecting from the CFBG. Experiencing a SMF coupling loss, the insertion loss of CFBG and the free space optical circulator, the average power of the stretched pulse was ~1mW which
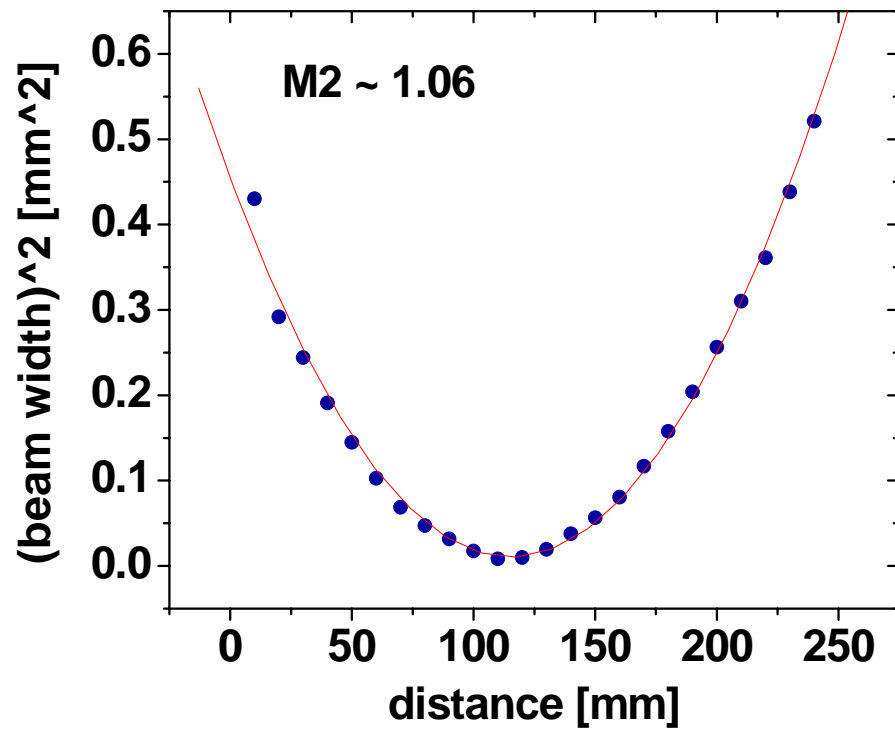
Figure 43. M2 measurement of the beam profile from the tapered amplifier, normal to the p-n junction

is sufficient to saturate the 1.5mm long RWGSOA used as the pre-amplifier biased at 150mA. Even though the free space polarization dependant optical isolator was implemented to prevent closed-loop lasing at low current operation, at high current operation a wavelength out-of-band of the CFBG starts to exhibit closed loop lasing. Therefore, a band pass filter was inserted between the preamplifier and the tapered amplifier to further prevent closed loop lasing. After boosting the optical power after the pulse stretcher through the pre-amplifier, the optical power, after the preamplifier, passes through an optical isolator and a band pass filter, yielding ~20mW of average power. The 20mW average power at this stage is also sufficient to saturate the tapered amplifier, which is biased at 2.5ADC, and maximized through the tapered amplifier. After the tapered amplifier, a maximum average optical power of 1.4W was obtained with ~20mW input power from the preamplifier. The significant feature of extreme chirped pulse amplification is that the 9.6ns extremely stretched pulses at 95MHz nearly fill the time window between pulses and thus simulates c.w. optical injection into the cascaded amplifiers. This allows us to have an extremely good optical signal to noise ratio (Chapter 2-3-2) and results in most of the 1.4W output power from the tapered amplifier being contained within amplified signal (Figure 44). It should be noted that this corresponds to a 14nJ per 9.6ns extremely stretched pulse and clearly demonstrates the advantage of energy extraction using the X-CPA concept. Given 39pJ input energy directly from the CPMLL and 14nJ output energy after the tapered amplifier, the X-CPA power gain is 26dB. The measured M2 of spatial beam profile normal to p-n junction was 1.06, which means the beam profile is close to the diffraction limit (Figure 43). Incorporating beam shaping optics which consists of an aspheric lens (f=2.84mm, 0.67NA) as a collimator, a cylindrical lens (f=40mm) as an astigmatism compensator and a microscope objective lens (40X) as a single mode fiber coupler (Figure 42), the SMF coupling efficiency was maximized

(maximum coupling efficiency achieved from this configuration was ~60%), and given the insertion loss of the CFBG as an extreme pulse compressor and the external dual grating compressor as a final pulse compressor, an average output power of 228mW was measured after compressing the optical pulse. The optical spectrum of the recompressed pulse was measured to possess a 6nm bandwidth which matches the bandwidth of the CFBG (Figure 45). The energy per pulse was 2.4nJ and the autocorrelation trace of the recompressed pulse was 1.06ps at FWHM (Figure 46). With the assumption of a hyperbolic secant pulse shape, a deconvolved pulse width becomes 0.69ps, which is ~4.1times of the transform-limited pulse duration. Considering the energy in the center lobe of the autocorrelation trace, a peak power of 1.4kW was generated from the all-semiconductor X-CPA system. This peak power is the highest peak power and first >kW demonstration generated from an all-semiconductor mode-locked laser system. As compared with the result without the optical pulse pre-stretcher, by inserting the optical pulse pre-stretcher, detrimental nonlinearities are reduced and therefore side band generation in optical spectrum and temporal wings in autocorrelation are reduced (Figure 48). However, the FWHM in autocorrelation of the compressed pulse was increased by 17% as compared to results without the optical pulse pre-stretcher and I believe that this is caused by an accumulated third order of dispersion due to the 300m SMF pulse pre-stretcher and different operating conditions of the master oscillator which can be investigated by carefully analyzing the optical phase of the recompressed pulse with and without the 300m SMF pulse pre-stretcher.
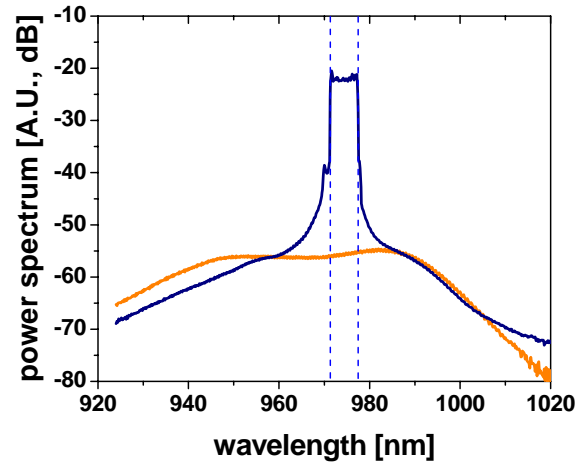
Figure 44. Optical spectrum from the tapered amplifier with (blue) and without (orange) injection
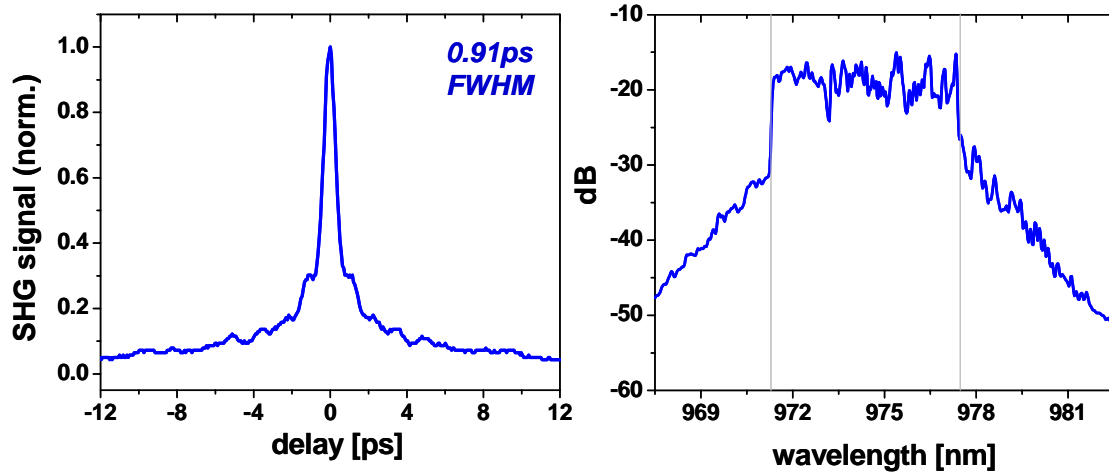
(a)

(b)

Figure 45. (a) autocorrelation and (b) optical spectrum of recompressed pulse from the all-semiconductor X-CPA system with an optical pulse pre-stretcher

It should be noted that through the extreme pulse compressor, the 9.6ns extremely stretched pulses were recompressed down to 0.69ps (Figure 25 (c) → Figure 45(a)), as demonstrated, which represents near 14,000 times the extreme pulse recompression. Without utilizing the optical pulse pre-stretcher, near 16,000 times the extreme pulse compression was also demonstrated (Figure 25(c) → Figure 48(a), 9.6ns → 0.59ps). It should be noted that since the output beam is obtained directly from a single mode fiber, the spatial beam quality from the X-CPA system is purely diffraction limited. By replacing the PS1060 CFBG with a large mode area CFBG or/and by replacing the tapered/flared amplifier with a higher saturation power and diffraction limited beam, the X-CPA system performance in terms of output energy will be increased.

These results imply that it is a significant step toward a high energy, compact all-semiconductor mode-locked laser system using the X-CPA concept.

3-9. Nonlinearity from CFBG in an X-CPA system

In this section, experimental data regarding nonlinearities due to high peak power inside a CFBG will be shown. Figure 46 shows the optical spectrum of a recompressed pulse from the X-CPA system at low power and at high power. Owing to increased peak power inside the CFBG, enhanced spectral sideband generation as well as enhanced spectral modulation was observed at high power operation. In Figure 47, temporal side wing of the recompressed pulse at high power operation was increased as compared to low power operation; this was due to the enhanced nonlinearities at the extreme chirped pulse compression stage.

(a)   (b)
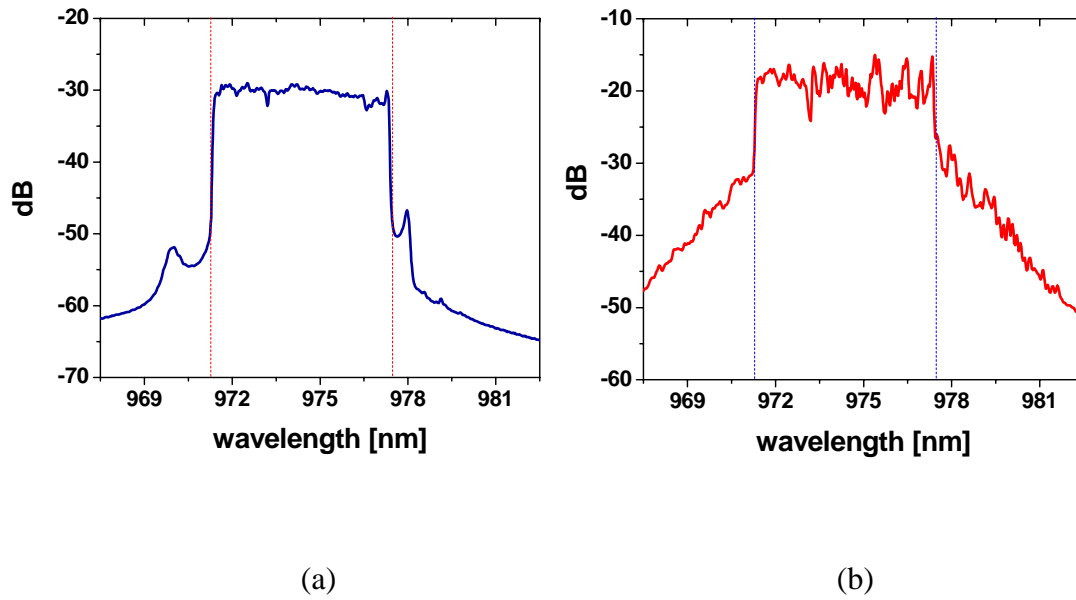
Figure 46. Optical spectrum of a recompressed pulse from the X-CPA system at (a) low and (b) high power

(a)   (b)
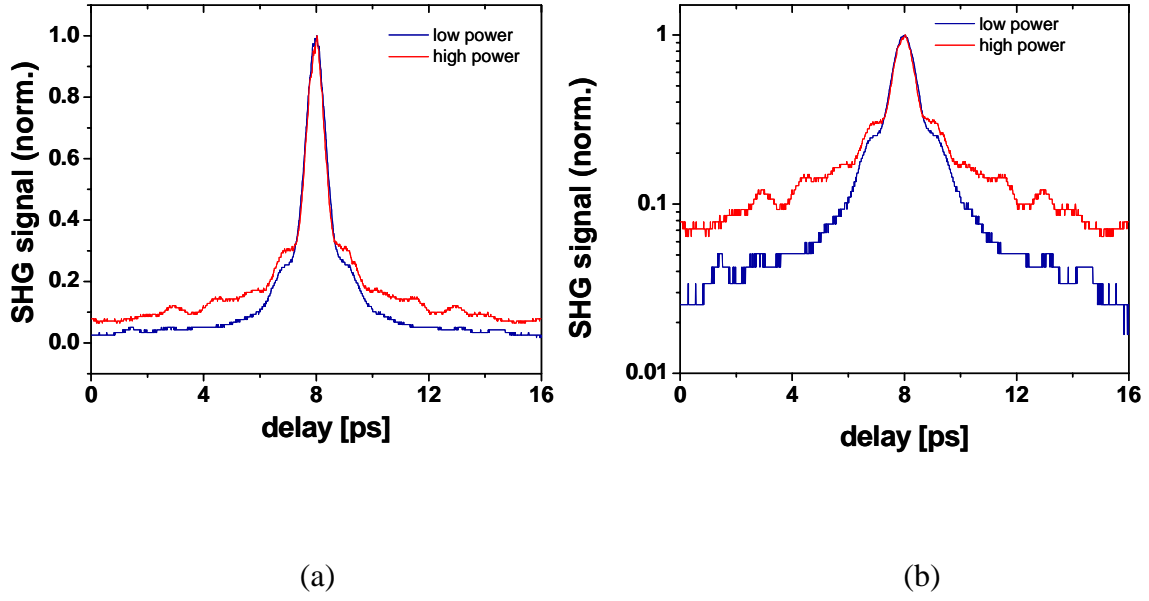
Figure 47. Autocorrelation trace of a recompressed pulse from the X-CPA at low power (blue)

and high power (red), (a) linear scale and (b) log scale
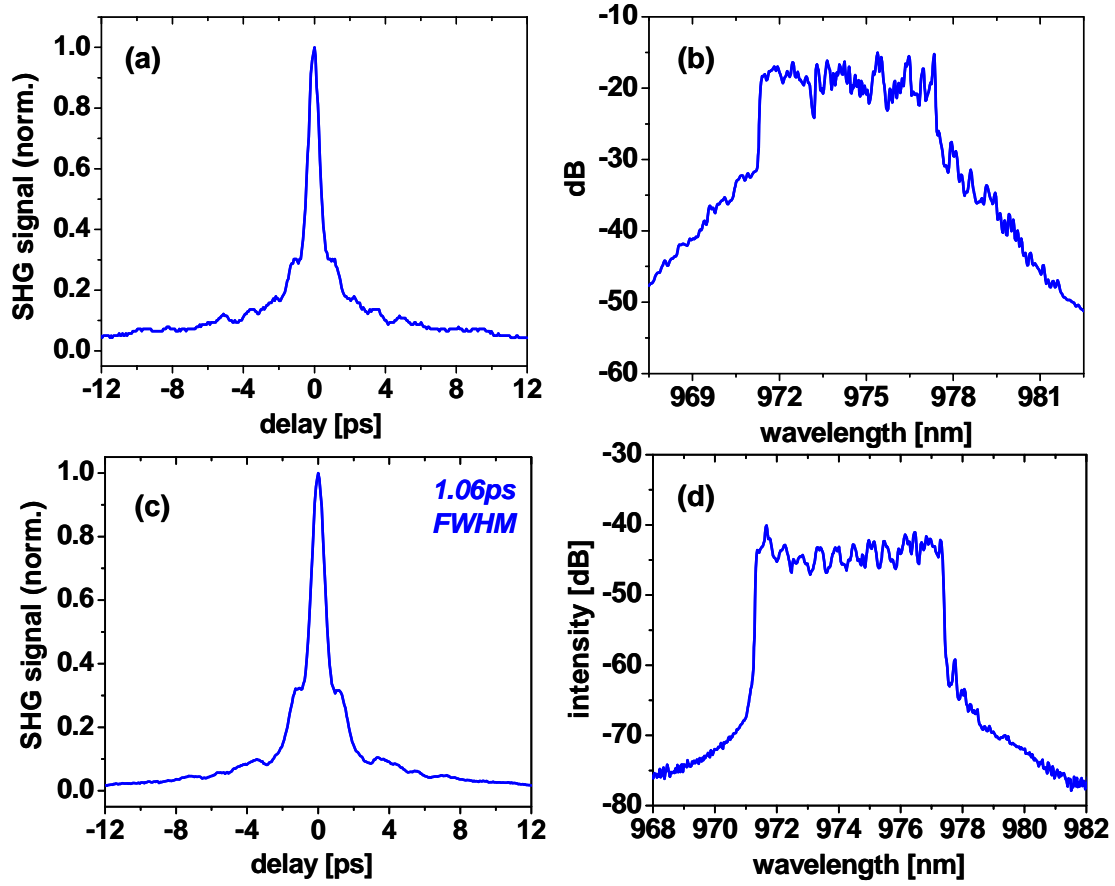
Figure 48. Comparison of the experimental data with and without the optical pulse pre-stretcher, (a) autocorrelation trace and (b) optical spectrum without the optical pulse pre-stretcher, (c) autocorrelation trace and (d) optical spectrum with the optical pulse pre-stretcher

3-10. Optical Spectrum from an X-CPA system

Figure 49(a) shows the optical spectrum from the CPMLL and the spectral bandwidth of the optical spectrum which is broader than bandwidth of the CFBG. The shape of the optical spectrum from the CPMLL has sharp edges on both the red and blue sides; this is the typical shape of a passively mode-locked semiconductor laser incorporating a multiple quantum well saturable absorber [7]. After passing through an SOA pulse picker, combined effects of the integrated self phase modulation as well as the gain saturation of an up-chirped pulse directly generated from the CPMLL cause a red peak in the optical spectrum and was enhanced more than 10dB (Figure 49(b)) [7]. Because the bandwidth of a CFBG is narrower than that of the optical spectrum from a CPMLL, as shown in Figure 49(c), the enhanced red peak was cut. A ~9.6ns extremely stretched pulse at 95MHz, which simulates c.w. injection was amplified through a cascade amplifier consisting of a RWGSOA and a TA. The shape of the optical spectrum after the cascade amplifier was flattened (Figure 49(d)) and I believe that it was because of the spectral shape of the gain bandwidth of the cascade amplifier. Finally the optical spectrum of a recompressed pulse from the X-CPA system (without the optical pulse pre-stretcher, Figure 49(d)) is similar to that of a pulse after the cascade amplifier owing to the spectral shape of the reflectance bandwidth of the blue port of the CFBG (Figure 23, bottom graph). In addition, due to detrimental nonlinearities caused by high peak power at the extreme chirped compression stage, generation of a sideband as well as a spectral modulation in the optical spectrum can be seen in Figure 49(e). As mentioned in Chapter 3-8 and 3-9, By

incorporating an optical pulse pre-stretcher, the detrimental nonlinearities at the extreme chirped compression stage was reduced significantly.
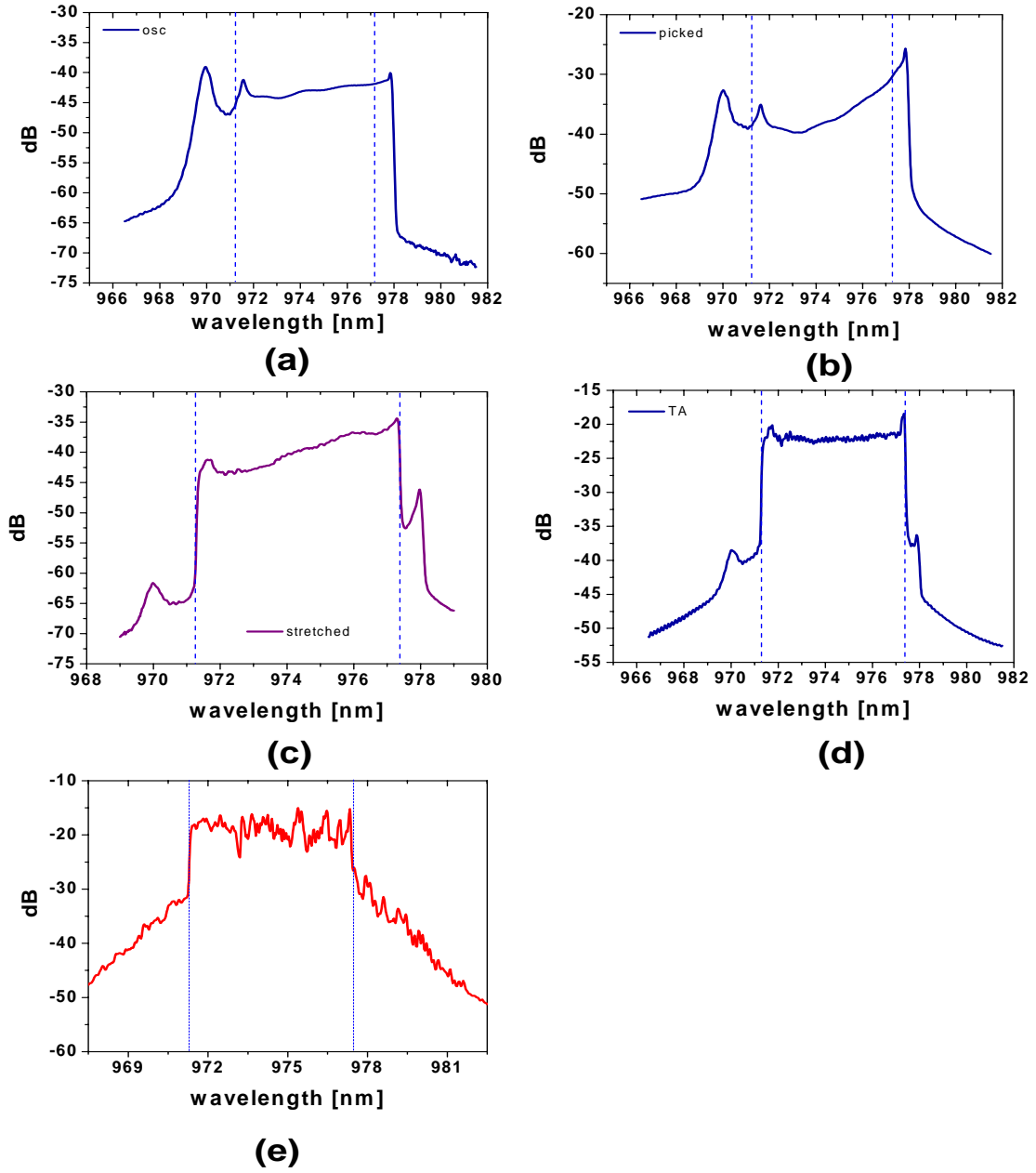
Figure 49. Optical spectra from the X-CPA system (a) from the CPMLL, (b) after the SOA pulse picker, (c) extremely stretched pulse after the CFBG, (d) after the TA, (e) recompressed pulse after the bulk grating compressor

3-11. Micro-joule Energy Extraction

Apart from the limitation of detrimental nonlinearities at the extreme pulse compression stage, a question arises regarding the limitation of energy extraction from a semiconductor optical amplifier. In order to answer this question, an energy extraction experiment was performed by adding a high power flared amplifier after the tapered amplifier.
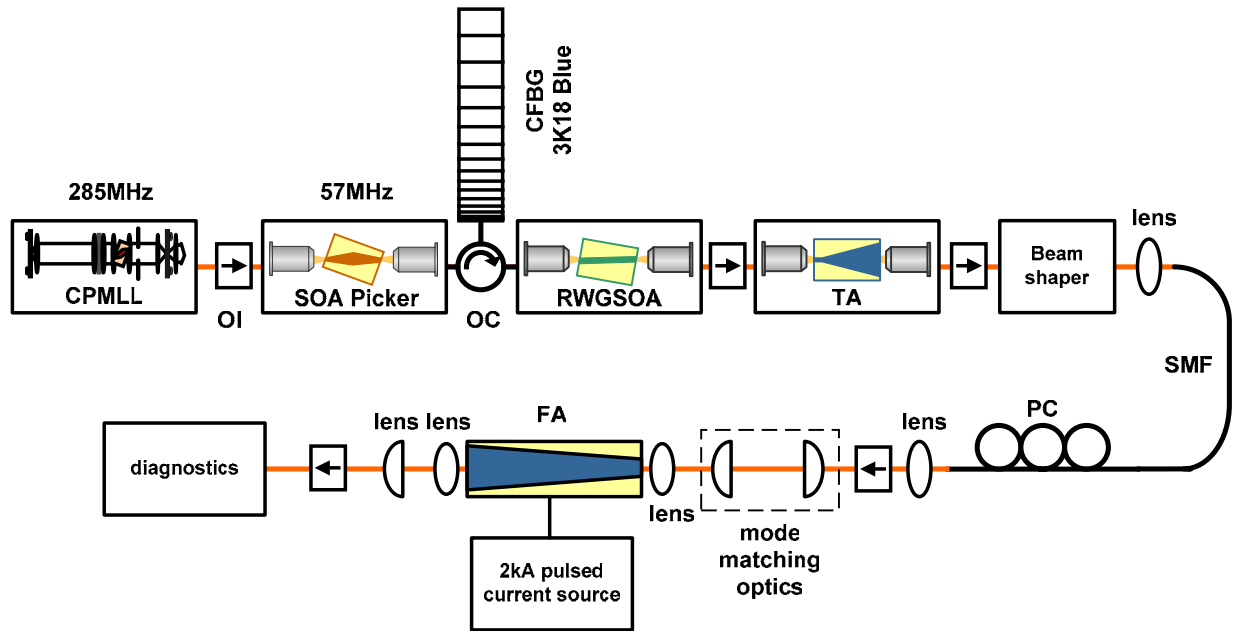
Figure 50. High energy extraction experiment setup with a flared amplifier and a 2kA high peak current source, SMF: single mode fiber, PC: polarization controller, FA: flared amplifier

Experimental setup

Figure 50 illustrates a schematic diagram of the energy extraction experimental setup. The 285MHz optical pulse train from the CPMLL was reduced to 57MHz after the SOA pulse picker to prevent temporal pulse overlapping and the 57MHz optical pulse train was extremely stretched to 20ns after a CFBG which possess a dispersion of ~4000ps/nm with a 5nm bandwidth centered at 974nm. The 20ns extremely stretched pulses were injected into cascaded amplifiers consisting of a RWGSOA as a preamplifier and a tapered amplifier as a medium power amplifier. The amplified signal after the tapered amplifier was coupled into a SMF and its output polarization was controlled by a three ring polarization controller attached to the SMF. The coupled amplified signal was collimated and injected into mode-matching optics consisting of two cylindrical lenses. The flared amplifier (Chapter 3-6-4) implemented for the high energy extraction experiment is a 6mm long InGaAs single quantum well amplifier (Coherent Inc.) with a 200um input aperture and 700um output aperture. Specifications show a highly astigmatic beam profile between the normal and parallel directions to the p-n junction. By adjusting the position of the mode-matching optics and one coupling lens in front of the 200um input aperture of the flared amplifier, a position where all the gain volume is filled by the injected input beam can be found by monitoring the beam profile from the 700um output aperture using a CCD camera. In order to increase the catastrophic optical mirror damage threshold and to avoid the thermal management burden at high current injection, the flared amplifier was pulse biased with a specially designed high peak current source which can generate a >200ns electrical pulse at a repetition rate of 1kHz (Novatron, customized high current pulse source). The high peak current source was designed to generate a peak current up to 2kA. Because the electrical pulse width was increased as the injected current was increased (Figure 51(a)), the optical pulse width was

monitored at each injected current with a 1GHz photodiode (Thorlabs, DET210) (Figure 51(b)).

Owing to the long electrical pulse from the high peak current source, 10 to 20 optical pulses in aggregate were amplified inside one electrical pulse at 1kHz. After amplification, the optical pulse, optical spectrum and average optical power were measured to calculate the amplified optical energy based on a 20ns extremely stretched optical pulse and its OSNR.
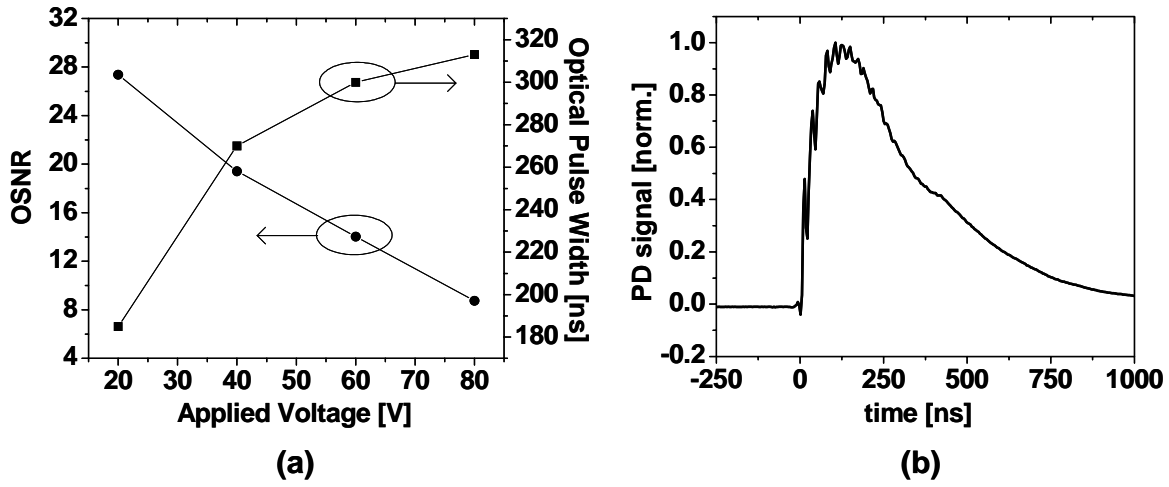
Figure 51. High energy extraction experimental results (a) optical signal to noise ratio and optical pulse width vs. applied voltage, (b) oscilloscope trace of the amplified stretched pulse

Experimental results

Approximately 400mW of average optical power was injected into the flared amplifier with the mode-matching optics and the coupling lens being adjusted to give the maximum output power from the flared amplifier. Figure 51 shows the optical signal to noise ratio and the optical pulse width with respect to the applied voltage. Due to the lack of a peak current probe, applied

voltage was chosen instead of the injected peak current to plot experimental results such as the peak power, energy per pulse and OSNR. The peak current corresponding to an applied voltage of 80V was estimated to be ~150A based on measurements without a load. As mentioned previously, when the injected current was increased, the optical pulse width was increased and for a fixed input power the OSNR was decreased. The optical pulse shape of the amplified pulse at the applied voltage of 80V was measured using a 1GHz photodiode (Figure 51(b)). Considering the OSNR, the average power and FWHM of the optical pulse width, a ~1.6uJ amplified output energy per 20ns extremely stretched pulse was obtained (Figure 52) and given 39pJ input energy from the CPMLL, it represents the energy gain of 46dB from the extreme chirped pulse amplification. The results imply that based on the concept of extreme chirped pulse amplification, micro-joule output energy can be obtained from semiconductor optical amplifiers based on current technology. As a future prospective for demonstrating a micro-joule, femtosecond source with a semiconductor gain medium, an air-guiding photonic crystal fiber [35] that possesses low loss, low nonlinearity, and a high dispersion might be a future candidate as an extreme pulse compressor.
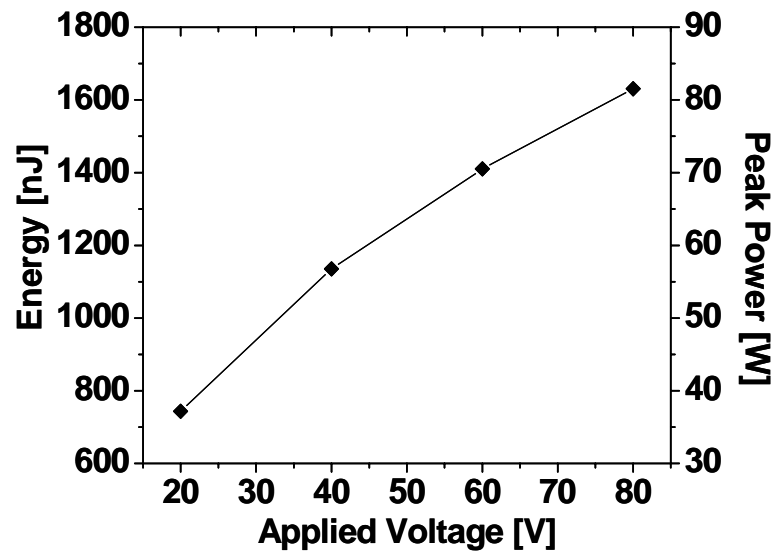
Figure 52. Extracted output energy and peak power of amplified stretched pulse through FA vs.

applied voltage

CHAPTER 4: APPLICATION OF THE X-CPA SYSTEM

As one of the applications utilizing the X-CPA system, second harmonic generation (SHG) is demonstrated (Figure 53).

Nonlinear crystals used in this experiment are 2mm x 2mm x 5mm $KNbO_3$. The $KNbO_3$ crystal is cut to be 13 degrees from b-axis to a-axis, which provides a critical phase matching condition at room temperature with small spatial walk-off. Both facets are AR coated for 976nm and 488nm. Owing to a high peak power from the mode-locked X-CPA system, a simple single pass SHG setup was chosen (Figure 53). Figure 55 shows the optical spectra of the fundamental and the second harmonic. Because of a long nonlinear crystal, the spectral bandwidth of the second harmonic becomes narrow. Figure 54 shows the second harmonic power and conversion efficiency with respect to the fundamental power. With 100mW of fundamental power, nearly 10% second harmonic conversion efficiency was achieved.
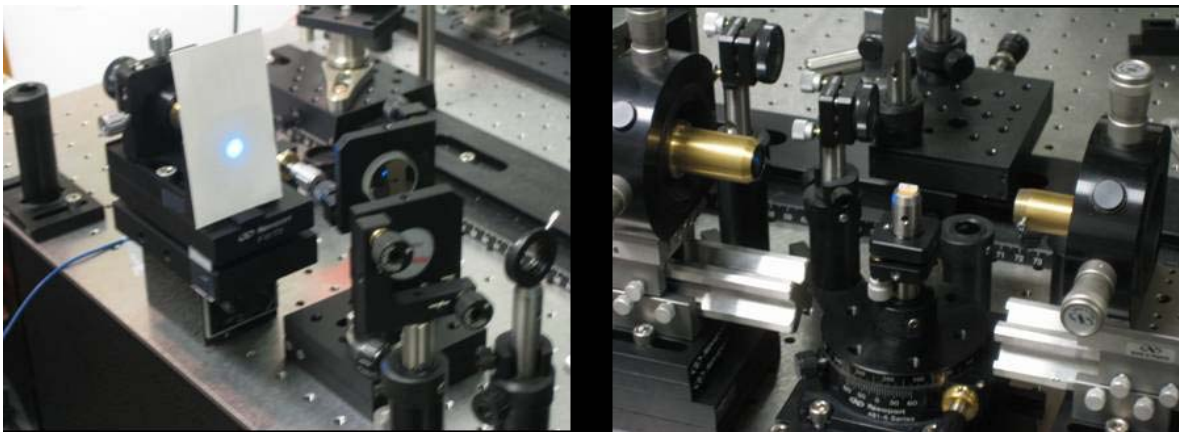
Figure 53. Photographs of the experimental setup of SHG (right) and the generated blue light on screen (left)
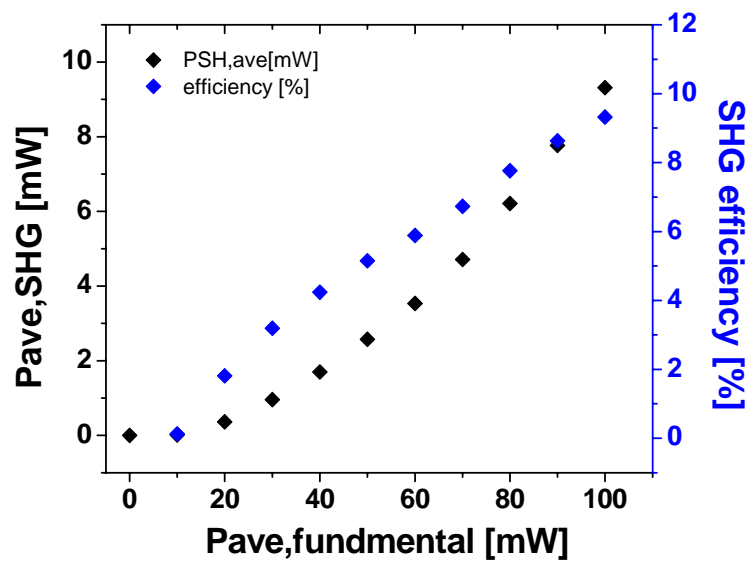
Figure 54. Second harmonic power and conversion efficiency vs. fundamental power
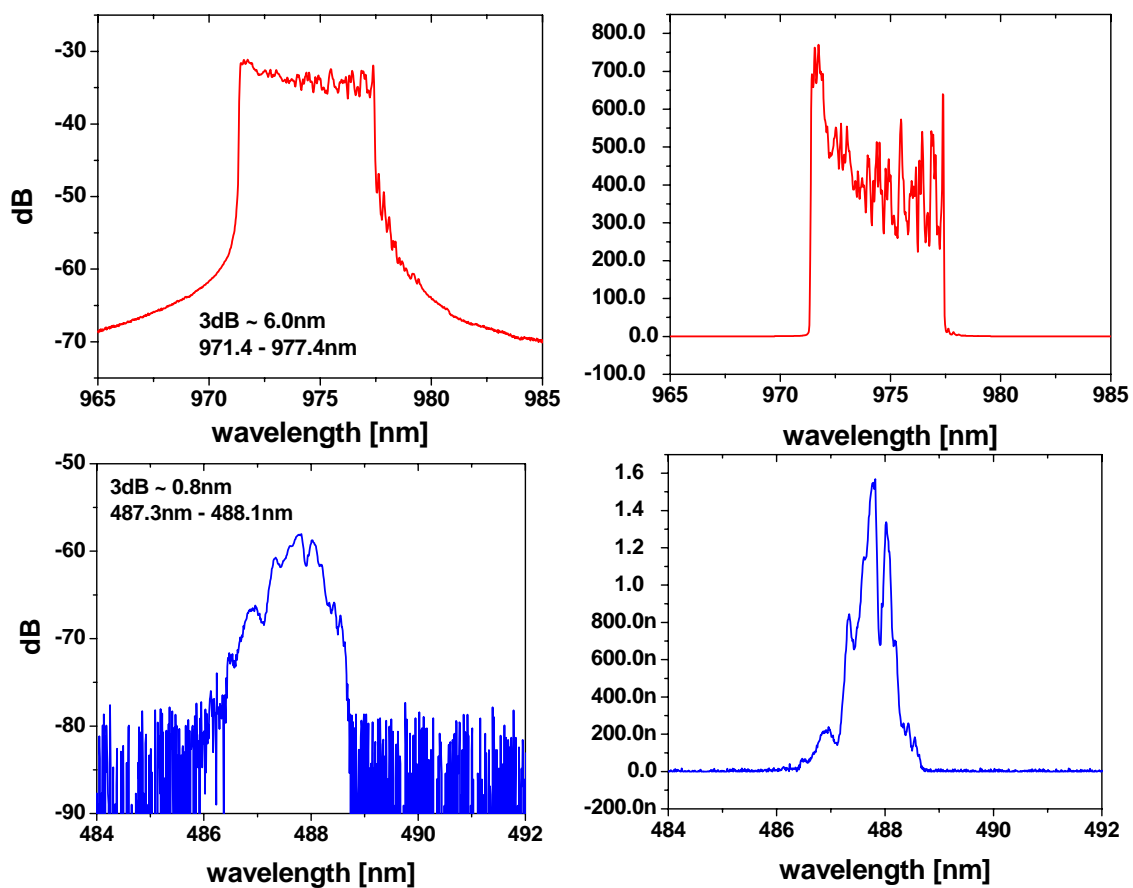
Figure 55. Optical spectrum of the fundamental (top) and the second harmonic (bottom)

CHAPTER 5: EXTERNAL CAVITY, ACTIVELY MODE-LOCKED GRATING COUPLED SURFACE EMITTING LASER AND AMPLIFICATION CHARACTERISTICS OF GRATING COUPLED SURFACE EMITTING SEMICONDUCTOR OPTICAL AMPLIFIER

An external cavity, active mode-locked grating coupled surface emitting laser (GCSEL) is demonstrated. The optical pulse duration from the actively mode-locked oscillator is 22.6ps and a 3dB optical spectrum bandwidth is 0.07nm at 976nm. The average power from the oscillator is 0.72mW and its peak power is 108mW. The amplification characteristics of a grating coupled surface emitting semiconductor optical amplifier (GCSOA), optically injected with a continuously operated external cavity GCSEL are also demonstrated. Despite the observation of lasing from the device, injection locking can be performed using an external source. At 4A peak current injection, 375mW output was achieved with 12mW injection.

5-1. Introduction

Angled stripe semiconductor optical amplifiers (SOA) have been used widely in mode-locked semiconductor lasers owing to their very low facet reflectivity ($<10^{-4}$). Facet reflectivity is an important parameter for successful mode locking of external-cavity lasers because facet reflections, and consequent etalon filtering, impose bandwidth limitations on the optical spectrum [7]. Grating-coupled surface-emitting semiconductor lasers (GCSELs) [47-50] and grating-coupled semiconductor optical amplifiers (GCSOAs) are attractive alternatives to angled stripe SOAs because these devices possess an output-coupled grating that is detuned from the second-order Bragg condition and provide potentially low effective reflectivity [51].

In addition, their large emission area allows a higher surface damage threshold as compared to conventional edge emitting SOAs at high power operation. The GCSEL/GCSOA can directly generate optical beams with low divergence, thus reducing the need of high numerical aperture optics and simplified coupling into optical fibers. These features of high power and low beam divergence due to the large emission area make these devices excellent candidates as gain and amplifier elements for short pulse, high power generation using the master oscillator power amplifier (MOPA) scheme.

In this Chapter, I report the first experimental demonstration of an actively mode-locked GCSEL master oscillator, and demonstrate the potential for high power amplification using GCSOAs that incorporate two identical detuned gratings applied as in- and out-couplers accordingly. These GCSOA devices can be used as a single pass amplifier in the MOPA configuration allowing mode-locked operation and is qualitatively different to previously developed integrated GCSEL- MOPA [52, 53].
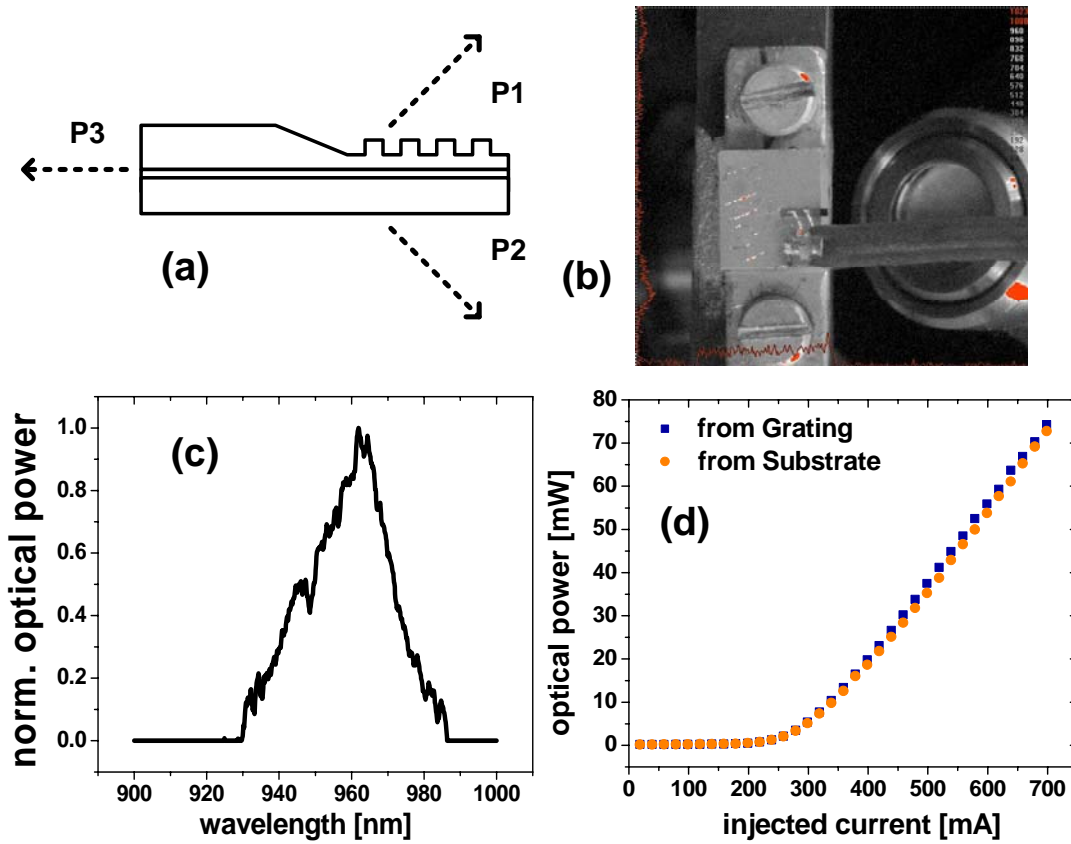
Figure 56. GCSEL spontaneous emission characteristics, (a) three output ports (grating port -P1, substrate port – P2 and cleaved facet port – P3), (b) photograph of mounted GCSEL device, (c) optical spectrum from cleaved facet (P3) at I=100mA, (d) L-I curve (from grating port (P1) and substrate port (P2))

5-2. Device Characteristics

The GCSEL device used in the experiment is shown schematically in Figure 56(a) and is fabricated from an InGaAs/AlGaAs GRINSCH-SQW wafer grown by IQE (Cardiff, UK). The GCSEL was realized by fabricating a grating structure that evanescently couples out light from the gain layer of a conventional Fabry-Perot semiconductor laser structure. The fabricated gain

stripe width was chosen to be 0.1mm, and the length of gain section is 1.95mm long. The wide gain stripe inherently enables the oscillation of multiple transverse modes. The length of the grating section is 0.33mm with a grating period of 325nm. The grating was fabricated using a holographic technique with the grating period chosen to enable off resonant operation near the gain peak of the InGaAs quantum well, ~ 970nm. The salient feature of an off-resonance grating is that output coupled light is not normal to the surface, and light reflected from the grating structure is not coupled back into the gain region, thus reducing the internal effective reflectivity [51]. The device can therefore be used as an SOA without the need of AR coatings. The grating was also designed to provide the maximum output in the 1st diffracted order and its output angle at 970nm is approximately 18 degrees normal to surface. As shown in Figure 56(a), there are three main outputs from the GCSEL; one is from the cleaved facet (P3; R~30%) and the other two outputs by diffraction are from the grating (P1) and the substrate (P2). The diffraction efficiency from the two outputs P1&P2 was estimated to be in the range of 50~60% and is similar to that reported in reference 54.

The optical spectrum was measured using light from the cleaved facet. The measurement shows a peak in the spontaneous emission at 960nm, with a 3dB spectral width of 22nm (Figure 56(c)). The L-I characteristic was measured from both the grating and substrate ports, and displays the typical super-luminescence behavior seen from conventional angle-striped SOAs. The L-I curve appears kink-free for bias currents up to 700mA (Figure 56(d)).
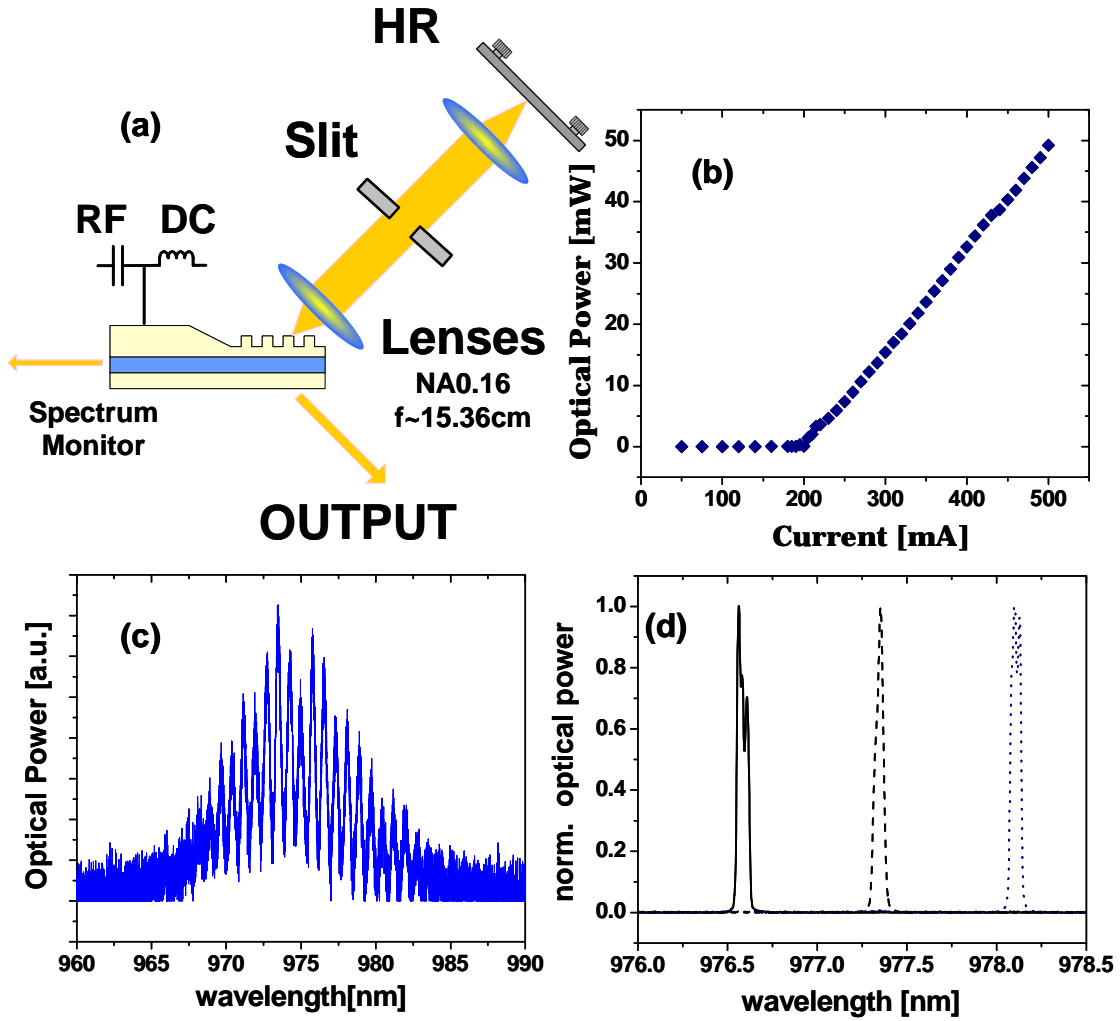
Figure 57. (a) external cavity setup with GCSEL (b) L-I curve from the output port (c) spectrum modulation due to a residual reflection from the substrate. Spontaneous emission spectrum from grating port (P1) at 200mA using a ball-lensed multimode fiber (core diameter: 100um) (d) discrete wavelength tuning characteristics of a continuously-operated external cavity with a GCSEL

5-3. C.W. Operation of the External Cavity Laser with a GCSEL

The external cavity with a GCSEL was realized by using two low N.A. aspheric lenses (0.16 N.A., f~15cm), one HR mirror and an adjustable slit, (Figure 57(a)). The grating port was used to provide optical feedback that defines the external cavity, whereas the substrate port was used as an output port. From the output port, the optical power and spatial beam profile were measured; while the optical spectrum was monitored using light collected from the cleaved facet that was used as one of the external cavity mirrors. The wavelength can be coarsely-tuned by rotating the GCSEL or the HR mirror and fine tuning can be achieved by adjusting a slit inside the cavity or translating the HR mirror. This type of device has previously demonstrated greater than 100nm of wavelength tuning [48]. The threshold injection current of the external cavity GCSEL was 193 mA, and produced a cw lasing peak at 977nm (Figure 57(b)). It should be noted that there was a residual reflection from the substrate which creates an internal etalon within the GCSEL. This is caused by the interference between the upward diffracted light and the downward diffracted light which is subsequently reflected from the substrate (R~30%). This effect gives a high contrast spectral modulation which is easily observed on a spontaneous emission spectrum from the grating port or substrate port, and also manifests itself from the tuning characteristics of the c.w. operation of the external cavity GCSEL (Figure 57(c) and (d)). The average spacing of the modulated optical spectrum was 0.77nm and corresponds to ~0.147mm substrate thickness of the GCSEL device. The slope efficiency of the c.w. external cavity GCSEL is 0.16W/A (Figure 56(b)).

Far-field beam profiles of the continuously-operated external cavity with the GCSE at three different distances from substrate output port (P2) shows that the vertical and horizontal beam divergences are near 14mrad and 3mrad with 25.5cm data without collimating optics (Figure 58) which are originated from a large emission area of the grating port.
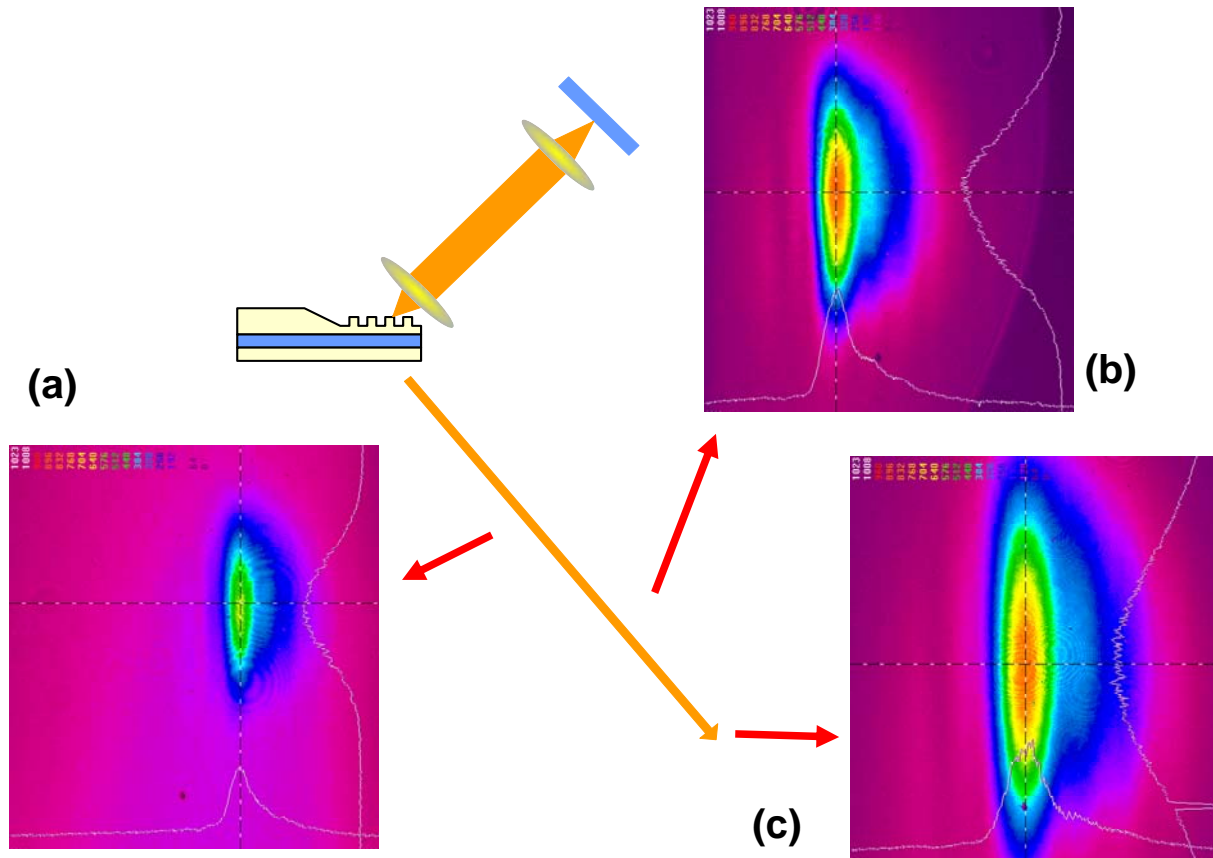
Figure 58. Far field beam profiles of the c.w. operated GCSEL with an external cavity at a distance of (a) 12cm, (b) 17cm and (c) 26cm

5-4. Mode-Locked Operation of an External Cavity Laser with a GCSEL

After obtaining c.w. operation of the external cavity GCSEL, mode-locking of the external cavity GCSEL was achieved by modulating the injection current of the gain section. The fundamental pulse-repetition frequency of the external cavity is near 297MHz. A 297MHz sinusoidal wave from an RF synthesizer was amplified through a 1W RF amplifier and was applied through a bias-tee in order to combine with a DC current. The temporal pulse profile as well as the spatial beam profile and optical power were measured from the substrate output port. The 3dB spectral bandwidth was 0.07nm at 965nm and the spectral broadening by mode-locking was limited by two factors. One is due to the residual reflection from the substrate and the other is due to the cavity design combined with the spectral dispersion of the grating (Figure 59(b)). The temporal pulse profile was characterized using a 50GHz digital sampling scope and a 25GHz InGaAs fast photodiode. A 27.1ps pulse width was measured directly from the sampling oscilloscope and detection system, and deconvolving the system response of the system suggests an optical pulse duration of 22.6ps (Figure 59(a)). The pulse duration and intensity spectral width implies a time bandwidth product of 0.50. The measured average optical power from the substrate output port was 0.72mW and implies a peak power of a 108mW. Without any collimating optics a low divergence beam was generated from the output port. The full divergence angles at half maximum were 0.76^o parallel to the p-n junction and 0.20^o normal to the p-n junction (Figure 59(c) and (d)). The latter corresponds to the fast axis divergence of a conventional edge-emitting diode and this illustrates one of the key advantages associated with the large emission area of the GCSEL. The asymmetric beam shape normal to the p-n junction in

the far field pattern is due to wavelength dispersion from the grating output coupler. In comparison with the c.w. beam width, the beam width normal to the p-n junction from the mode-locked oscillator is increased owing to the spectral broadening due to mode-locking.
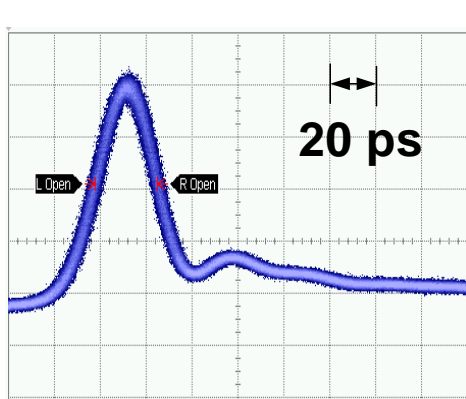
(a)
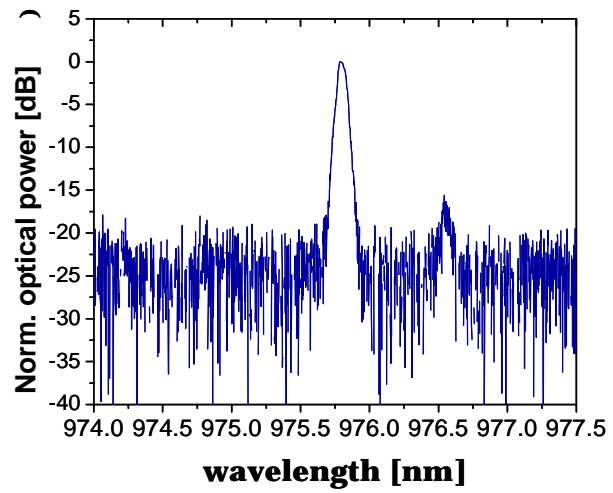
(b)
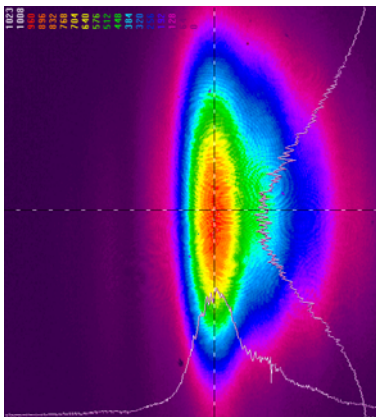
(c)
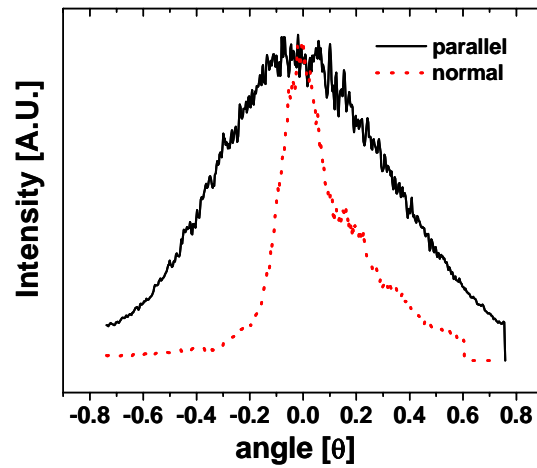
(d)

Figure 59. (a) optical pulse from the actively mode-locked GCSEL with an external cavity in a digital sampling oscilloscope and (b) the optical spectrum of the mode-locked GCSEL with an external cavity. (c) And (d) far field beam pattern from the substrate output port of the actively mode-locked GCSEL with an external cavity (parallel and normal to the device p-n junction)

5-5. Amplification Characteristics of GCSOA

In order to test the feasibility of high power amplification a GCSOA was fabricated. The GCSOA device was simply realized by cleaving the device such that two grating structures are on either end of the gain section. In this configuration, the GCSEL is transformed into a GCSOA and can operate as a semiconductor optical amplifier (SOA). The GCSOA in this experiment has the same grating periods. The length of the grating section is 330um and the length of gain section is 4mm. The device exhibits classic super-luminescence behavior up to bias currents of 2A. Beyond this pumping level, evidence of spectral narrowing was observed, suggesting the tendency towards lasing operation. A c.w. external cavity GCSEL was used as the master oscillator. It should be noted that the internally generated background spontaneous emission of the 4mm gain section length is large compared to the average output power of the external cavity modelocked GCSEL laser, making the injection locking process difficult owing to gain competition. Nonetheless, the amplification characteristics of a GCSOA device under c.w. optical injection locking conditions can provide critical information that can predict the amplification performance with the injection of a c.w. modelocked pulse train. The average input power from the c.w. external cavity GCSEL can easily be controlled and increased by increasing the d.c. bias current. In order to optimize coupling, a 4f imaging system was employed between the GCSOA and the GCSEL master oscillator (Figure 60(a)). A low duty cycle electrical pulse (500ns duration at 1kHz repetition rate) was injected into the GCSOA to avoid thermal loading of the device. Figure 60(c) and 60(d) show the injection locking characteristics of the experimental setup. The signal from the oscillator, which has three main longitudinal mode clusters, was injected into the GCSOA and the optical spectra from GCSOA

were compared with and without injection. It is easily seen that the output spectrum from the GCSOA is dominated by the optical spectrum from the oscillator. At a 4A current injection level into the GCSOA, a 325mW peak output power of the amplified signal from the substrate port was obtained with 12mW of input average power injected from the master oscillator and the output power reported represents the amplified power without background amplified spontaneous emission. The signal-to-noise of the amplified output power was obtained from the spectral measurement of Figure 60(b).
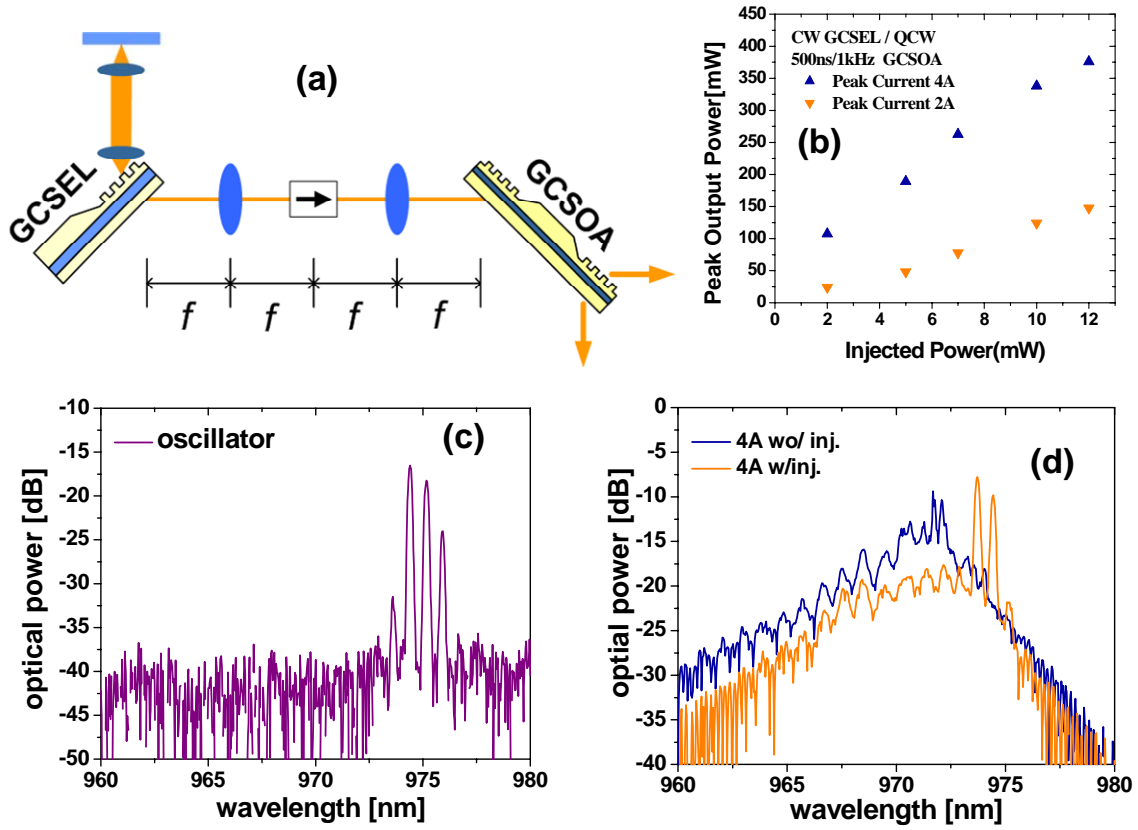
Figure 60. (a) Experimental setup of amplification with a GCSOA, (b) output signal power vs. input power at two QCW current injection (2A:triangle-down and 4A:triangle-up), optical spectra from (c) the oscillator and (d) amplifier without (dark line) and with (light line) injection.

CHAPTER 6: PASSIVE OPTICAL CAVITY AMPLIFICATION - FUTURE PERSPECTIVE

6-1. Fundamentals and Review

In principle, a passive optical cavity with a high quality factor (or high finesse) works as an energy storage reservoir. This characteristic is why passive optical cavity is implemented in various applications.

Applications utilizing a high finesse passive optical cavity include:

- efficient second harmonic generation and an optical parametric oscillator, [55]
- cavity dumped Ti:sapphire mode-locked laser, [56]
- cavity ring down spectroscopy, [57]
- high resolution optical spectrometer
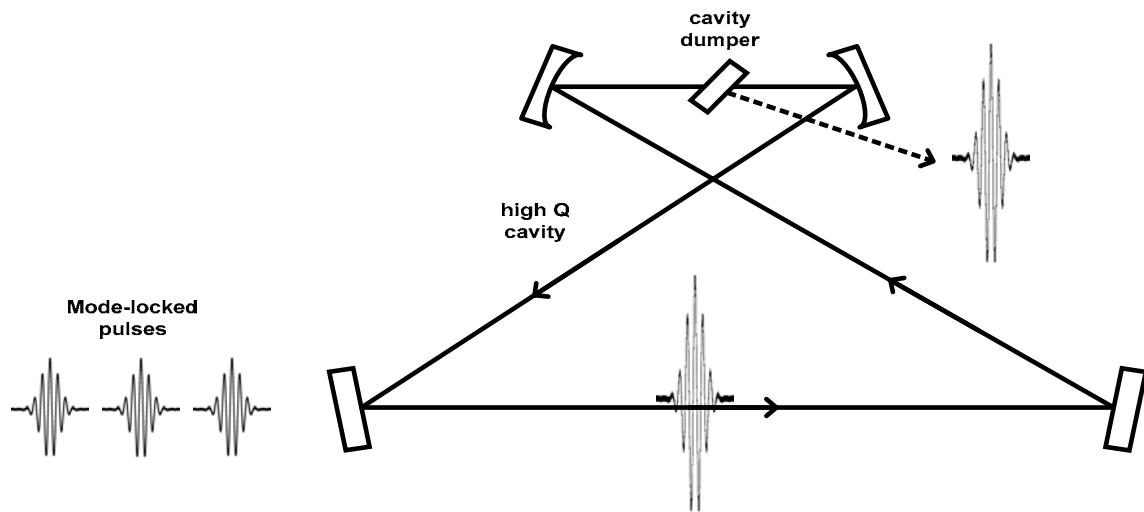
Figure 61. Concept of passive optical cavity amplification

The characteristic of the passive optical cavity (POC) as an energy storage reservoir can apply to the pulse amplification of a mode-locked laser as illustrated in Figure 61. Optical pulses from a mode-locked laser are injected into a high finesse POC with a length that is matched with the repetition rate of the mode-locked laser and combined coherently inside the POC. Peak power inside the POC is increased until reaching the cavity build-up time. After the cavity build-up time, a cavity dumper such as an acousto-optic modulator, electro-optic modulator, etc. is switched on to extract a coherently added optical pulse inside the POC. Then output energy from the POC is larger than the input energy from a mode-locked oscillator. However the conservation law of energy should be satisfied. Therefore, as output energy is increased, the repetition rate of mode-locked laser from POC is decreased. The technique of pulse amplification using the POC is called "passive optical cavity amplification" and has been demonstrated. Potma *et al.* demonstrated 30 times amplification with a picosecond Ti:sapphire mode-locked laser and an

output energy of 150nJ with a pulse width of 3.5ps [58]. In the experiment, a 76MHz pulse repetition rate was reduced to 0.253MHz. Also Jones *et al.* demonstrated the same concept with a femtosecond Ti:sapphire laser. Thirty times amplification with a 38fs optical pulse and 70 times amplification with a 58fs optical pulse were demonstrated [59].

Future perspective of the X-CPA system combined with a passive optical cavity amplification technique: As a future work to increase the output energy from the X-CPA system, the X-CPA system can be incorporated with a passive optical cavity amplification technique. Here, primary results of a POCA, which was combined with a mode-locked semiconductor laser, are presented.

Figure 62. Experimental setup of passive optical cavity amplification with a mode-locked laser, AOM: acousto-optic modulator, HR: high reflector, IC: input coupler, PZT: piezo-electric transducer, PD: photodiode, QWP: quarter wave plate, PBS: polarizing beam splitter, PID: PID controller, HV amp.: high voltage amplifier, rep rate: repetition rate

6-2. Passive Optical Cavity Amplification Setup and the Calculation of the Amplification Factor

Figure 62 illustrates the passive optical cavity amplification setup incorporated with the mode-locked semiconductor laser. The POC consists of one input coupler (IC), one cavity dumper (AOM), two concave high reflectors (HR), and three flat high reflectors (HR). Once optical loss of the components of the POC, except the input coupler, is measured or calculated,

the transcittance of the input coupler, which gives the highest amplification, can be easily calculated and is called "impedance matching" (Figure 63) [60, 61]
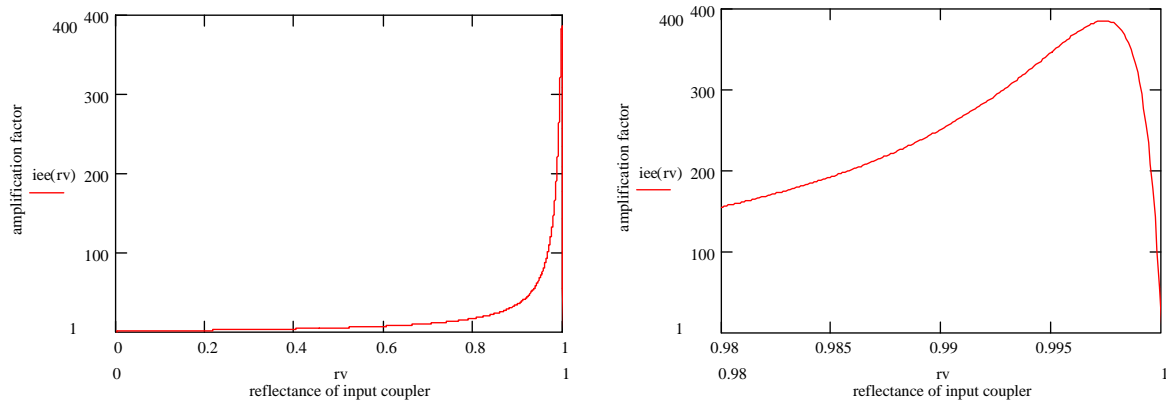
Figure 63. Calculated amplification factor with respect to the reflectance of the input coupler

Table 6 Optical components inside the passive optical cavity

POC component	reflectance / transmittance	company
Flat high reflector	99.998%R	RMI
Concave high reflector ROC ~ 10cm	99.998%R	RMI
Cavity dumper	99.75%R	Harris

6-3. Passive Optical Cavity Design

In order to design the POC, three constraints should be satisfied. First is the spot size inside the cavity dumper. In the specifications, to achieve 8~10ns rise time, the focused spot size inside the cavity dumper should be smaller than 100um. Second is the astigmatism caused by the cavity dumper at Brewster's angle should be compensated by finding the radius of curvature of the concave mirror and the proper incident angle into the mirror [62]. Third is the length of the POC should be matched to the repetition rate of the mode-locked laser. Based on these three constraints, the POC was designed using ABCD-matrix software. After finishing the design of the POC, mode-matching optics were properly chosen to achieve maximum coupling from a single mode fiber into the POC. In this configuration, two plano-convex lenses were used as mode-matching optical components.

6-4. Linewidth of the Mode-locked Laser

In order to get an efficient amplification from the POC, the linewidth of an optical comb from the mode-locked laser system should not be more than the linewidth of a passive optical cavity. In a current configuration, the linewidth of the POC was estimated to be ~190kHz. Using a "delayed self homodyne" method (Figure 64) [63], the linewidth of the CPMLL was measured [64]. In the delayed self-homodyne measurement setup, a 6.5km long single mode fiber which is able to measure the linewidth of 32kHz without a coherent ring was inserted into one arm of the interferometer to make two split beams incoherent. The measured 3dB linewidth was ~270kHz (Figure 65(a)) with the optical spectrum from the CPMLL in Figure 65(b). In this configuration,

the reflectance of the output coupler of the CPMLL was ~30%. One way to make the linewidth narrower is to increase the cavity finesse by using an output coupler which possesses a higher reflectance.

Later the output coupler was changed to one with 70% reflectance which is expected to narrow the linewidth of the optical comb from the CPMLL. The error signal from the POC with the mode-locked laser depends on the operating condition of the CPMLL and as a result the optical spectrum, with a sharp edge on both sides, shows a stable and clean error signal from the POC (Figure 66).
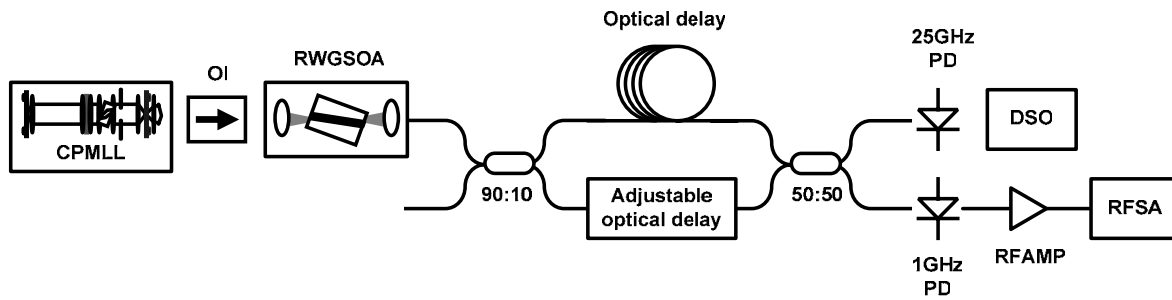
Figure 64. Schematic of the delayed self-homodyne method, CPMLL: Colliding pulse mode-locked semiconductor laser, OI: optical isolator, RWGSOA: ridge waveguide semiconductor optical amplifier, 90:10: 2x2 fiber coupler with 90/10 split ratio, 50:50: 2x2 fiber coupler with 50/50 split ratio, PD: photodiode, DSO: digital sampling oscilloscope, RFAMP: RF amplifier, RFSA: RF spectrum analyzer
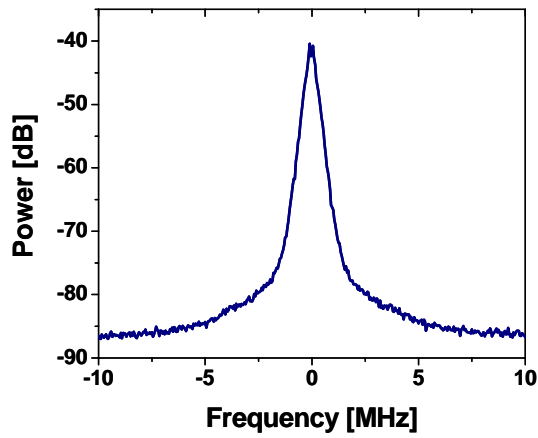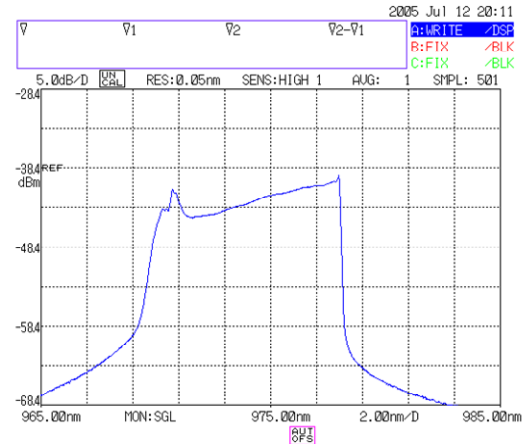
(a)   (b)

Figure 65. (a) Measured linewidth and (b) the optical spectrum of the CPMLL with an output coupler with reflectance of 30%
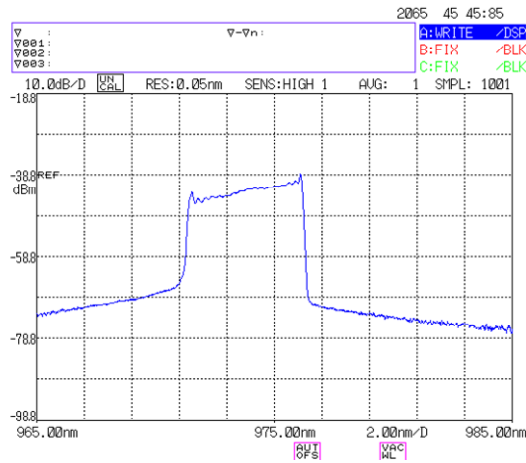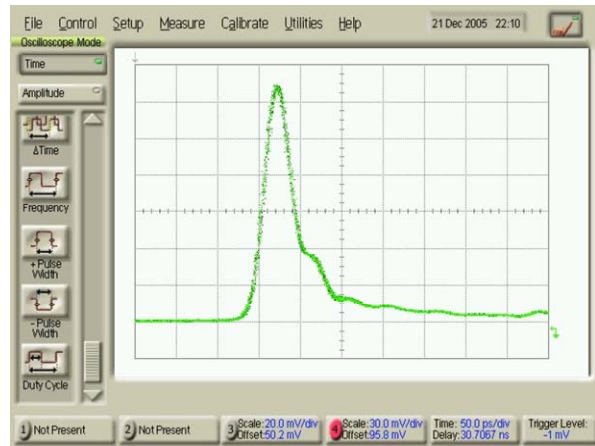
(a)   (b)

Figure 66. (a) Optical spectrum [h-axis: 2nm/div, v-axis: 5dB/div] and (b) digital sampling scope trace [h-axis: linear, v-axis: 50ps/div] of CPMLL with output coupler which possesses the reflectance of 70%

6-5. Cavity Stabilization

In order to perform the passive optical cavity amplification experiment, it is necessary to stabilize the POC with respect to the mode-locked laser system. There are several methods to stabilize an optical cavity. One of the methods is called the "Hanch-Couillaud" method and it was applied to this experiment [65]. Two orthogonal states of polarization experience a different phase shift from the POC. Light reflected from the input coupler was injected into a balanced receiver after a quarter wave plate and a polarizing beam splitter. The generated electrical error signal from the balanced detector was used for cavity stabilization. The error signal was sent to the PID controller and the output of the PID controller was amplified through an analog high voltage amplifier to drive a piezo-electric transducer (PZT) attached to one of the flat high reflectors of the POC.

(a)   (b)
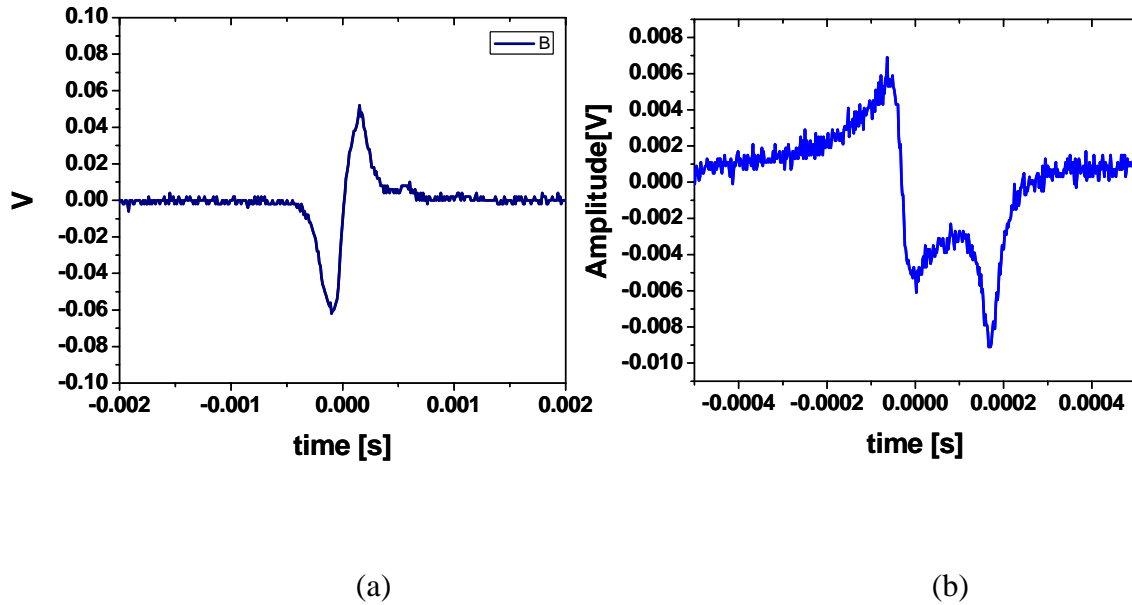
Figure 67. Measured error signals in the case of (a) 90%R and (b) 99%R input couplers

With an input coupler with reflectance of 90%, an error signal is monitored by scanning the PZT (Figure 67(a)). Using the error signal, the POC is stabilized successfully. But with an input coupler with reflectance of ~99%, two overlapped error signals which are very close to each other were observed (Figure 67(b)). This behavior makes cavity stabilization difficult. More studies will be needed to understand this behavior to perform the passive optical cavity amplification experimemt.

6-6. Cavity Dumper and Its Driver

As a cavity dumper, an acousto-optic modulator (Harris, H-101) made of SiO_2 was used. Even if it was optimized for a visible wavelength, it can still be used for near infrared wavelength. However the diffraction efficiency will be less than that of the designed wavelength. The AOM was mounted on a rotation stage, a XYZ stage and a tilting stage to find the optimal location of the acoustic wave inside the AOM. Figure 68 illustrates the schematic diagram of the electronics to generate an AOM driving signal. The carrier frequency for the AOM is near 400MHz and the maximum input power into AOM is 1W at c.w. operation and 10W at pulsed operation with <10% duty cycle. A 400MHz carrier frequency was combined with the ~10ns electrical pulse through a frequency mixer. A mixed signal was amplified through a broadband RF amplifier (Figure 69(a)).
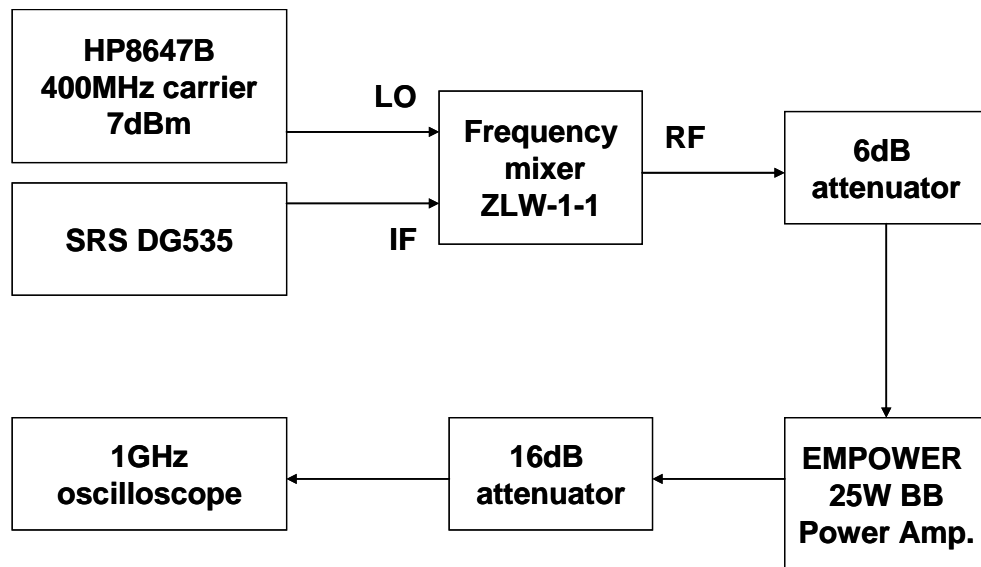
Figure 68. Schematic diagram of electronics to generate an AOM driving electrical signal

(a)

(b)
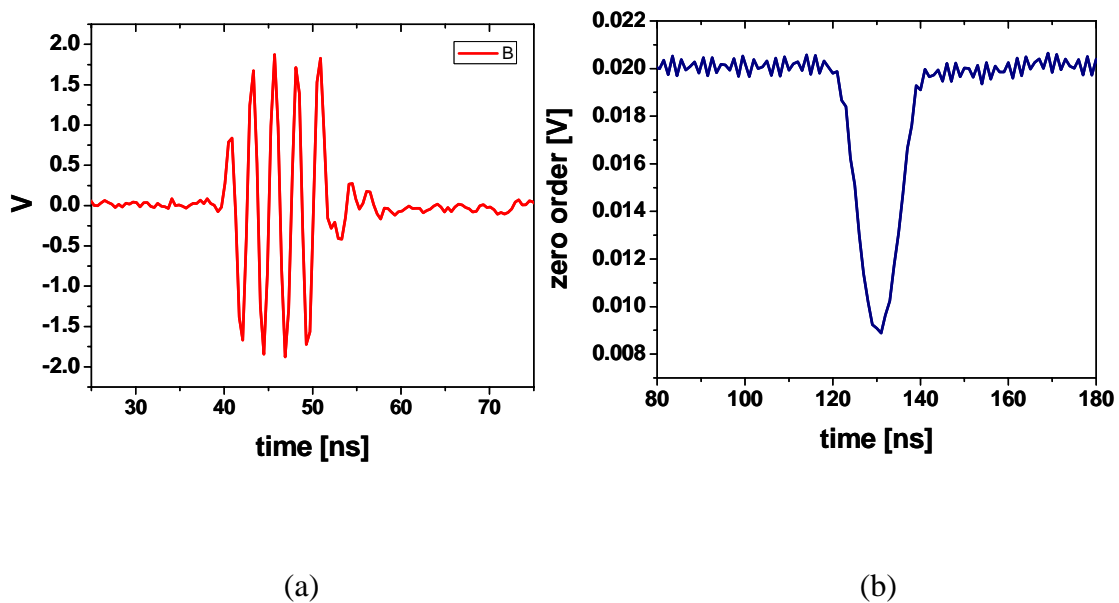
Figure 69. (a) AOM driving signal, 10W peak power after 16dB attenuator (b) time response of AOM with HeNe laser

With the generated AOM driving signal and HeNe laser, the time response of the AOM was measured (Figure 69(b)) and is ~10ns at FWHM. It shows the entire bandwidth of the AOM driving signal was coupled into the AOM driver.
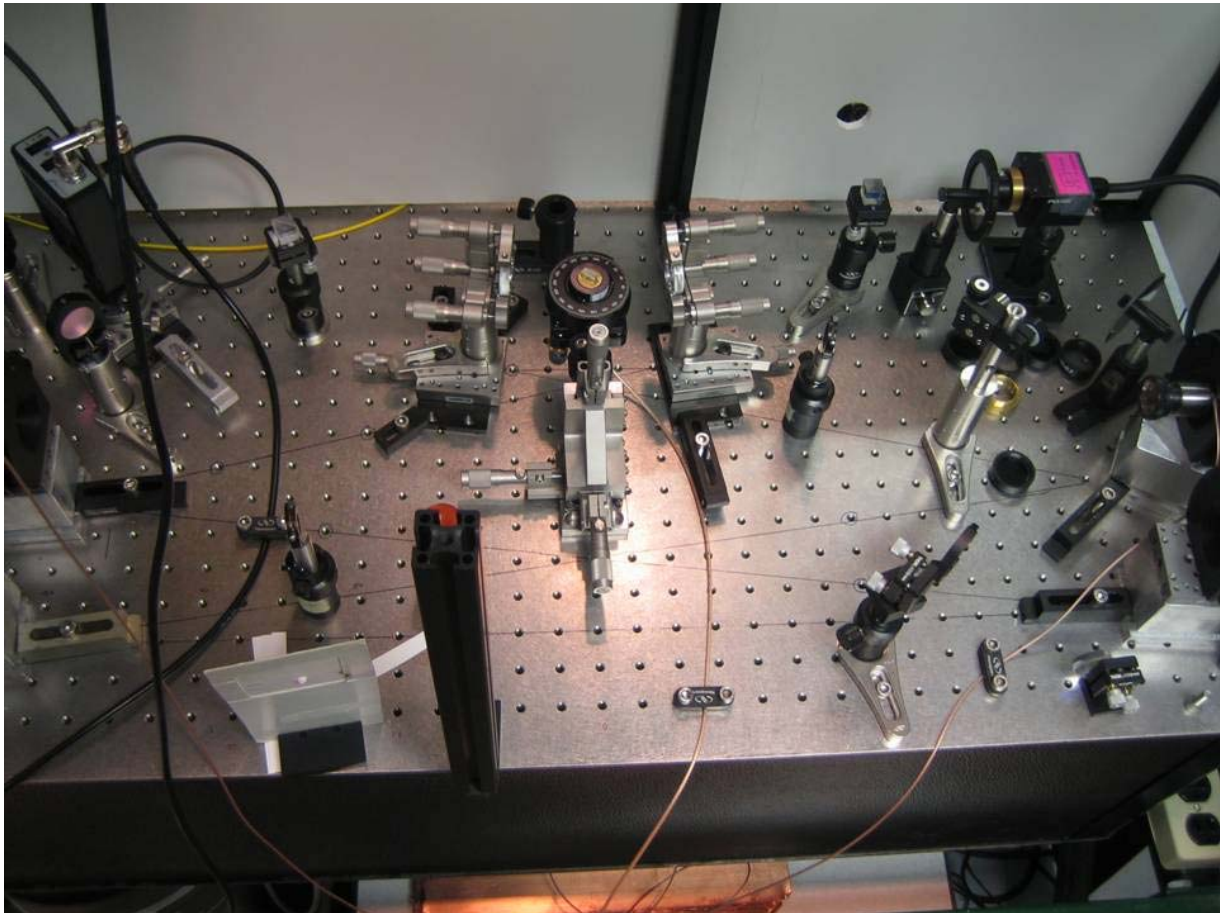
Figure 70. Photograph of the current POC setup

CHAPTER 7: CONCLUSION

In ultrashort pulse amplification, a semiconductor optical amplifier is considered as an inappropriate amplifier because of its fundamental characteristics of small storage energy. A novel method to overcome the fundamental limit of the small storage energy inside a semiconductor gain medium is proposed and called "**eXtreme Chirped Pulse Amplification (X-CPA)**". The concept of X-CPA is proved theoretically and experimentally.

Based on the concept of X-CPA, an all-semiconductor X-CPA system is developed and demonstrated successfully. The X-CPA system consists of

i)   a master oscillator: colliding pulse, hybrid mode-locked semiconductor laser,

ii)   an optical pulse pre-stretcher: single mode fiber spool,

iii)   an SOA pulse picker,

iv)   free space polarization-dependent optical circulator,

v)   an extreme pulse stretcher/compressor: a chirped fiber Bragg grating,

vi)   cascaded amplifiers: a ridge waveguide SOA and a tapered amplifier, and

vii)   a bulk grating pulse compressor

The X-CPA system generates **>kW record peak power** from an all-semiconductor mode-locked laser system and the key benefits of the X-CPA system addressed in this dissertation are **1) the fundamental energy storage limit of an SOA is overcome, 2) detrimental nonlinearities during pulse amplification are reduced, 3) optical signal to noise ratio in pulse amplification is significantly improved, and 4) the beam profile is diffraction limited due to output from a single mode fiber**. In addition, 1.6uJ energy with a 20ns

extremely stretched pulses is obtained and represents an energy gain of 46dB. These results represent a significant step toward realizing a high energy, compact mode-locked semiconductor laser system (Figure 71).
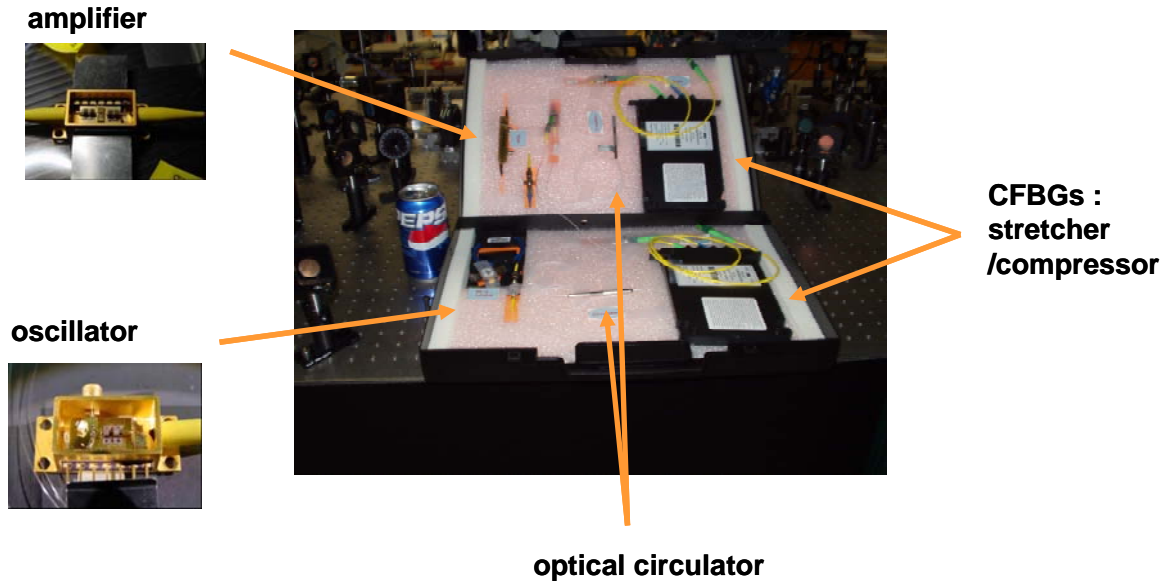
Figure 71. Toward a high energy, compact mode-locked semiconductor laser system

As an application of the X-CPA system, a single pass second harmonic generation experiment was performed using a long nonlinear crystal.

As a candidate device for high power generation, grating coupled surface emitting semiconductor devices were studied experimentally. Active mode-locking of GCSEL with an external cavity was demonstrated for the first time. In addition, a single pass amplification experiment using a GCSOA was also performed. The experiments generate optical pulse trains of 22psec at a 297 MHZ pulse repetition frequency, centered at 965nm, while the c.w. injection

locked amplification experiments have generated ~ 0.3 watts of peak intensity. Also these results are a first step toward high power optical pulse generation novel grating coupled and semiconductor optical amplifiers.

As a future perspective to increase the energy per optical pulse, a technique called "passive optical cavity amplification" was studied theoretically and experimentally. Primary study of passive optical cavity amplification indicates a strong possibility to increase the energy with more than a hundred times the amplification factor.

Appendix A: MATLAB CODE FOR SIMULATION OF X-CPA

A-1. CASE I: PULSE WIDTH << CARRIER LIFETIME

```
% case I ) tp << tc
% pulse width of stretched pulse after CFBG is much shorter than carrier lifetime of amplifier

%%%%%%%%%%%%%%%%%%%%%%%%%%%%%%%%%%%%%%%%%%%%%%%%%%%%%%%%%%%%%%%%%%%%
%%%   BEAM PROPAGATION THROUGH CPA SYSTEM WHICH CONSISTS OF      %%%
%%%   TWO CHIRPED FIBER BRAGG GRATINGS AND ONE SOA              %%%
%%%                                                              %%%
%%%                                      06/2005 Kyungbum Kim    %%%
%%%%%%%%%%%%%%%%%%%%%%%%%%%%%%%%%%%%%%%%%%%%%%%%%%%%%%%%%%%%%%%%%%%%

%%% initial values are
%%%  - input energy(Ein),
%%%  - input pulse width(tp),
%%%  - GVD(d),
%%%  - saturation energy(Esat),
%%%  - CFBG length(x)
%%%  - linewidth enhancement factor(alpha)
%%%  - and small signal gain(gol)

%%% input optical pulse
%%% et_in : temporal electric field
%%% et_in_amp : temporal amplitude of electric field
%%% et_in_arg : temporal phase (argument) of electric field
%%% pt_in : temporal intensity
%%% ew_in : spectral electric field
%%% pw_in : spectral intensity

%%% stretched pulse after CFBG
%%% et_CFBG1 : temporal electric field
%%% et_CFBG1_amp : temporal amplitude of electric field
%%% et_CFBG1_arg : temporal phase (argument) of electric field
%%% pt_CFBG1 : temporal intensity
%%% ew_CFBG1 : spectral electric field
%%% pw_CFBG1 : spectral intensity

%%% amplified stretched pulse after amplifier
%%% et_SOA : temporal electric field
%%% et_SOA_amp : temporal amplitude of electric field
%%% et_SOA_arg : temporal phase (argument) of electric field
%%% pt_SOA : temporal intensity
%%% ew_SOA : spectral electric field
%%% pw_SOA : spectral intensity

%%% recompressed pulse after CFBG
%%% et_CFBG2 : temporal electric field
%%% et_CFBG2_amp : temporal amplitude of electric field
%%% et_CFBG2_arg : temporal phase (argument) of electric field
%%% pt_CFBG2 : temporal intensity
%%% ew_CFBG2 : spectral electric field
%%% pw_CFBG2 : spectral intensity


%%%%%%%%%%%%%%%%%%%%%%%%%%%%%%%%%%%%%%%%%%%%%%%%%%%%%%%
%%%%%%%%%%%%%%%%%%%%%%%%%%%%%%%%%%%%%%%%%%%%%%%%%%%%%%%
%%%%%%   ONE. PULSE STRETCHING USING A CFBG    %%%%%%%
%%%%%%%%%%%%%%%%%%%%%%%%%%%%%%%%%%%%%%%%%%%%%%%%%%%%%%%
%%%%%%%%%%%%%%%%%%%%%%%%%%%%%%%%%%%%%%%%%%%%%%%%%%%%%%%
```

```matlab
disp('start ...');

%%%%%%%%%%%%%%%%%%%%%%%%%%%%%%%%%%%%%%%%%%%%%%%%%%%
%%% 1. generate a gaussain pulse & initial values %%%
%%%%%%%%%%%%%%%%%%%%%%%%%%%%%%%%%%%%%%%%%%%%%%%%%%%

% time domain 1 point = 0.01 ps

% check the input pulse and the stretched pulse and then find a proper N
% the number of point for FFT "N" should be governed by those two pulses


clear all;
tic;
utime=10^(-14);       % unit time = 0.01 ps
c=3*10^8*utime;       % speed of light [m/0.01ps]
l=975*10^(-9);        % center wavelength [m]
d=-8750/10^(-9)/0.15; % GVD [ps/nm/1.6m]                    %%%%%%%%%%%%%%%%%  initial value
%%%%%%%%%%%%%%%%
N=2^16;               % number of points for FFT           %%%%%%%%%%%%%%%%%  initial value
%%%%%%%%%%%%%%%%
save n N;
t=1:N;                % define a temporal unit step, unit of time [0.1ps]
tp=100;               % pulse duration [0.01ps]            %%%%%%%%%%%%%%%%%  initial value
%%%%%%%%%%%%%%%%
to=tp/sqrt(4*log(2));
Ein=5*10^(-12);       % input energy [Joule]               %%%%%%%%%%%%%%%%%  initial value
%%%%%%%%%%%%%%%%
a=Ein/to/sqrt(pi);    % field constant [J/0.1ps=power]
x=0; %0.15;           % beam propagation length [m]        %%%%%%%%%%%%%%%%%  initial value
%%%%%%%%%%%%%%%%
disp('total temporal window[ps]='); disp(N*utime*1e12);
% FYI : time-bandwidth product of transform-limited Gaussian pulse
% tp*dv = 0.441 and tp*dw = 2*pi*0.441

et_in=sqrt(a)*exp(-(t-N/2).^2/(sqrt(2)*to)^2); %-i*wc.*(t-N/2));   % input gaussian field
pt_in=(abs(et_in)).^2;

%pt_in_sum=sum(pt_in)  % total energy of input pulse in time domain
save pt_in pt_in; clear pt_in;

bw=1/utime;           % total bandwidth according to sampling
tbw=bw*2*pi*1e-12;save tbw tbw;     % total bandwidth according to sampling
disp('total spectral window[rad THz]='); disp(tbw);
w=2*pi*t./N;          % [rad Hz]
sf=(w(2)-w(1))/2/pi;  % scaling factor
w2=tbw/N*t; save w2 w2; clear w2;
save t t; clear t;
save w w; clear w;
%%% Nyquist theory  sampling dt (= "1") < 1/(dw)( = dt = "30")


%%%%%%%%%%%%%%%%%%%%%%%%%%%%%%%%%%%%%%%%%%%%%%%%%%%%
%%% Plot the temporal phase before the transmission %%%
%%%%%%%%%%%%%%%%%%%%%%%%%%%%%%%%%%%%%%%%%%%%%%%%%%%%
et_in_arg=angle(et_in); %atan(imag(et_in)./real(et_in));
save et_in_arg et_in_arg; clear et_in_arg;

disp('CFBG1 FFT ... running ...');


%%%%%%%%%%%%%%%%%%%%%%%%%%
%%% FFT of input pulse %%%
%%%%%%%%%%%%%%%%%%%%%%%%%%
ew_in=sqrt(sf)*fftshift(fft(et_in));
save et_in et_in; clear et_in;
pw_in=(abs(ew_in)).^2;
```

```
%pw_in_sum=sum(pw_in)  % total energy of input pulse in frequency domain
save pw_in pw_in; clear pw_in;

%%%%%%%%%%%%%%%%%%%%%%%%%%%%%%%%%%%%
%%% spectral phase of input pulse  %%%
%%%%%%%%%%%%%%%%%%%%%%%%%%%%%%%%%%%%
ew_in_arg=atan(imag(ew_in)./real(ew_in)); %angle(ew_in);

save ew_in_arg ew_in_arg; clear ew_in_arg;


disp('CFBG1 BPM ... running ...');

%%%%%%%%%%%%%%%%%%%%%%%%%%%%%%%%%%%%%%%%%
%%% beam propagation in frequency domain %%%
%%%%%%%%%%%%%%%%%%%%%%%%%%%%%%%%%%%%%%%%%%
beta=-l^2/(2*pi*c)*(d);  % dispersion parameter beta2
a=i/2*beta;
load w;
ew_CFBG1=ew_in.*exp(-a*(w).^2*x);   %sqrt(0.9)
clear w;
save ew_in ew_in; clear ew_in;


pw_CFBG1=(abs(ew_CFBG1)).^2;
%pw_CFBG1_sum=sum(pw_CFBG1)   %total enegy in frequency domain after CFBG1
save pw_CFBG1 pw_CFBG1; clear pw_CFBG1;


%%%%%%%%%%%%%%%%%%%%%%%%%%%%%%%%%%%%%%%%
%%% see a spectral phase after CFBG 01 %%%
%%%%%%%%%%%%%%%%%%%%%%%%%%%%%%%%%%%%%%%%
ew_CFBG1_arg=angle(ew_CFBG1);
save ew_CFBG1_arg ew_CFBG1_arg; clear ew_CFBG1_arg;

disp('CFBG1 IFFT ... running ...');


%%%%%%%%%%%%%%%%%%%
%%% inverse FFT %%%
%%%%%%%%%%%%%%%%%%%
et_CFBG1=1/sqrt(sf)*(ifft(ew_CFBG1));
save ew_CFBG1 ew_CFBG1; clear ew_CFBG1;

pt_CFBG1=(abs(et_CFBG1)).^2;

%pt_CFBG1_sum=sum(pt_CFBG1) %total energy in time domain after CFBG1
save pt_CFBG1 pt_CFBG1; clear pt_CFBG1;


%%%%%%%%%%%%%%%%%%%%%%%%%%%%%%%%%%%%%%%%%%%%%%%
%%% plot the temporal phase after transmission %%%
%%%%%%%%%%%%%%%%%%%%%%%%%%%%%%%%%%%%%%%%%%%%%%%%%
et_CFBG1_arg=angle(et_CFBG1);  %atan(imag(et_CFBG1)./(real(et_CFBG1+10^(-100)))));
save et_CFBG1 et_CFBG1; clear et_CFBG1;

%disp('FWHM of pt_CFBG1 = ');fwhm(pt_CFBG1,N,t)

save et_CFBG1_arg et_CFBG1_arg; clear et_CFBG1_arg;




%%%%%%%%%%%%%%%%%%%%%%%%%%%%%%%%%%%%%%%%%%%%%%%%%%%%%%%%%%%%%%
%%%%%%%%%%%%%%%%%%%%%%%%%%%%%%%%%%%%%%%%%%%%%%%%%%%%%%%%%%%%%%%
%%%%%%    TWO. PULSE AMPLIFICATION THROUGH THE SOA        %%%%%
%%%%%%%%%%%%%%%%%%%%%%%%%%%%%%%%%%%%%%%%%%%%%%%%%%%%%%%%%%%%%%%
%%%%%%%%%%%%%%%%%%%%%%%%%%%%%%%%%%%%%%%%%%%%%%%%%%%%%%%%%%%%%%%
```

116

```
disp('SOA gain ... running ...');

%%%%%%%%%%%%%%%%%%%%%%%%%%%%%%%%%%%%%%%%%%%%%%
%%% 2. initial values for SOA gain dynamics %%%
%%%%%%%%%%%%%%%%%%%%%%%%%%%%%%%%%%%%%%%%%%%%%%
load t;
ssg = 20;             % small signal gain [dB]               %%%%%%%%%%%%%%%%  initial value
%%%%%%%%%%%%%%%
gol = log(10^(ssg/10));
h(1)=gol;             % gain at t=0
dt=t(3)-t(1);         % unit time step [0.1 ps]
tc=20000;             % carrier lifetime                     %%%%%%%%%%%%%%%%  initial value
%%%%%%%%%%%%%%%
Esat=30*10^(-12);     % saturation energy [Joule]            %%%%%%%%%%%%%%%%  initial value
%%%%%%%%%%%%%%%
alpha = 10;            % line enhancement factor              %%%%%%%%%%%%%%%%  initial value
%%%%%%%%%%%%%%%
Psat=Esat/tc;         % saturation power


load pt_CFBG1;

%%%%%%%%%%%%%%%%%%%%
%%% gain of SOA %%%
%%%%%%%%%%%%%%%%%%%%

h=-log(1-(1-1/exp(gol))*exp(-cumsum(pt_CFBG1)/Esat));
% plot(t,cumsum(pt_CFBG1));

% %%% Fourth Order Runge-Kutta Algorithm %%%
% for m = 2:N-1
%     k0=dt*((gol-h(m-1))/tc-pt_CFBG1(t(m-1))/Esat*(exp(h(m-1))-1));
%     k1=dt*((gol-(h(m-1)+k0/2))/tc-pt_CFBG1(t(m-1)+dt/2)/Esat*(exp(h(m-1)+k0/2)-1));
%     k2=dt*((gol-(h(m-1)+k1/2))/tc-pt_CFBG1(t(m-1)+dt/2)/Esat*(exp(h(m-1)+k1/2)-1));
%     k3=dt*((gol-(h(m-1)+k2))/tc-pt_CFBG1(t(m-1)+dt)/Esat*(exp(h(m-1)+k2)-1));
%     h(m)=h(m-1)+1/6*(k0+2*k1+2*k2+k3);
% end
% h(N)=h(N-1);  % because of the step d=2, it is difficult to calculate h(N)
%
%%%%%%%%%%%%%%%%%%%%%%%%%%%%%%%%%%%%%%%%%%%%
%%% output intensity profile after SOA %%%
%%%%%%%%%%%%%%%%%%%%%%%%%%%%%%%%%%%%%%%%%%%%
pt_SOA=pt_CFBG1.*exp(h);                       % output intensity profile after SOA
clear pt_CFBG1;

%pt_SOA_sum=sum(pt_SOA)  %total energy in time domain after SOA

%%%%%%%%%%%%%%%%%%%%%%%%%%%%%%%
%%% output phase after SOA %%%
%%%%%%%%%%%%%%%%%%%%%%%%%%%%%%%
et_SOA_amp = sqrt(pt_SOA);                 % amplitude after SOA
save pt_SOA pt_SOA; clear pt_SOA;
load et_CFBG1_arg;
et_SOA_arg = et_CFBG1_arg-1/2*alpha*h;        % phase after SOA
save h h ; clear h;
clear et_CFBG1_arg;

et_SOA = et_SOA_amp.*exp(i*et_SOA_arg);  %(cos(et_SOA_arg)+i*sin(et_SOA_arg));  % electric field
after SOA
save et_SOA_amp et_SOA_amp; clear et_SOA_amp;
save et_SOA_arg et_SOA_arg; clear et_SOA_arg;

clear pt_SOA;



%%%%%%%%%%%%%%%%%%%%%%%%%%%%%%%%%%%%%%%%%%%%%%%%%%%%%%%%%%%%%%%%%%
%%%%%%%%%%%%%%%%%%%%%%%%%%%%%%%%%%%%%%%%%%%%%%%%%%%%%%%%%%%%%%%%%%
%%%%%     THREE. PULSE COMPRESSION USING CFBG     %%%%%%%%%%%%%%%
%%%%%%%%%%%%%%%%%%%%%%%%%%%%%%%%%%%%%%%%%%%%%%%%%%%%%%%%%%%%%%%%%%
```

117

```
%%%%%%%%%%%%%%%%%%%%%%%%%%%%%%%%%%%%%%%%%%%%%%%%%%%%%%%%%%%%%%
disp('CFGBG2 FFT ... running ...');

%%%%%%%%%%%%%%%%%%%%%%%%%%%%%%%%%%
%%% 3.1 FFT of pulse after SOA %%%
%%%%%%%%%%%%%%%%%%%%%%%%%%%%%%%%%%%%
ew_SOA=sqrt(sf)*(fft(et_SOA));
save et_SOA et_SOA; clear et_SOA;

pw_SOA=(abs(ew_SOA)).^2;

%pw_SOA_sum=sum(pw_SOA)   %total enegy in frequency domain after SOA
save pw_SOA pw_SOA; clear pw_SOA;


%%%%%%%%%%%%%%%%%%%%%%%%%%%%%%%%%%%%%%
%%%   Spectral phase after SOA    %%%
%%%%%%%%%%%%%%%%%%%%%%%%%%%%%%%%%%%%%%
ew_SOA_arg=angle(ew_SOA);

save ew_SOA_arg ew_SOA_arg; clear ew_SOA_arg;

disp('CFBG2 BPM ... running ...');

%%%%%%%%%%%%%%%%%%%%%%%%%%%%%%%%%%%%%%%%%%%%%
%%% beam propagation in frequency domain %%%
%%%%%%%%%%%%%%%%%%%%%%%%%%%%%%%%%%%%%%%%%%%%%%%
beta2=-l^2/(2*pi*c)*(-d);  % dispersion parameter beta2
a2=i/2*beta2;
load w;
ew_CFBG2=ew_SOA.*exp(-a2*(w).^2*x);   %sqrt(0.9)
clear w;
save ew_SOA ew_SOA; clear ew_SOA;

pw_CFBG2=(abs(ew_CFBG2)).^2;
save pw_CFBG2 pw_CFBG2; clear pw_CFBG2;


%%%%%%%%%%%%%%%%%%%%%%%%%%%%%%%%%%%%%%%
%%%    Spectral phase after CFBG2  %%%
%%%%%%%%%%%%%%%%%%%%%%%%%%%%%%%%%%%%%%%
ew_CFBG2_arg=angle(ew_CFBG2);

save ew_CFBG2_arg ew_CFBG2_arg; clear ew_CFBG2_arg;

%pw_CFBG2_sum=sum(pw_CFBG2);    %total enegy in frequency domain after CFBG2

disp('CFBG2 IFFT ... running ...');

%%%%%%%%%%%%%%%%%%%%
%%% inverse FFT %%%
%%%%%%%%%%%%%%%%%%%
et_CFBG2=1/sqrt(sf)*(ifft(ew_CFBG2));
save ew_CFBG2 ew_CFBG2; clear ew_CFBG2;

pt_CFBG2=(abs(et_CFBG2)).^2;
%fwhm(pt_CFBG2,N,t);

%pt_CFBG2_sum=sum(pt_CFBG2)    %total enegy in time domain after CFBG2
save pt_CFBG2 pt_CFBG2; clear pt_CFBG2;


%%%%%%%%%%%%%%%%%%%%%%%%%%%%%%%%%%%%%%%%%%%%%%%%%%%%%%%%%%%%%
%%% plotting the temporal phase after transmission %%%
%%%%%%%%%%%%%%%%%%%%%%%%%%%%%%%%%%%%%%%%%%%%%%%%%%%%%%%%%%%%
et_CFBG2_arg=angle(et_CFBG2);

save et_CFBG2_arg et_CFBG2_arg; clear et_CFBG2_arg;
save et_CFBG2 et_CFBG2; clear et_CFBG2;
```

```
disp('Done ...');
toc;
disp(toc);
```

A-2. CASE II: PULSE WIDTH ~ CARRIER LIFETIME

```
% case II ) tp ~ tc
% pulse width of stretched pulse after CFBG is comparable to carrier lifetime of amplifier

%%%%%%%%%%%%%%%%%%%%%%%%%%%%%%%%%%%%%%%%%%%%%%%%%%%%%%%%%%%%%%%%
%%%   BEAM PROPAGATION THROUGH CPA SYSTEM WHICH CONSISTS OF       %%%
%%%   TWO CHIRPED FIBER BRAGG GRATINGS AND ONE SOA               %%%
%%%                                                             %%%
%%%                                   06/2005 Kyungbum Kim      %%%
%%%%%%%%%%%%%%%%%%%%%%%%%%%%%%%%%%%%%%%%%%%%%%%%%%%%%%%%%%%%%%%%

%%% initial values are
%%%  - input energy(Ein),
%%%  - input pulse width(tp),
%%%  - GVD(d),
%%%  - saturation energy(Esat),
%%%  - CFBG length(x)
%%%  - linewidth enhancement factor(alpha)
%%%  - and small signal gain(gol)

%%% input optical pulse
%%% et_in : temporal electric field
%%% et_in_amp : temporal amplitude of electric field
%%% et_in_arg : temporal phase (argument) of electric field
%%% pt_in : temporal intensity
%%% ew_in : spectral electric field
%%% pw_in : spectral intensity

%%% stretched pulse after CFBG
%%% et_CFBG1 : temporal electric field
%%% et_CFBG1_amp : temporal amplitude of electric field
%%% et_CFBG1_arg : temporal phase (argument) of electric field
%%% pt_CFBG1 : temporal intensity
%%% ew_CFBG1 : spectral electric field
%%% pw_CFBG1 : spectral intensity

%%% amplified stretched pulse after amplifier
%%% et_SOA : temporal electric field
%%% et_SOA_amp : temporal amplitude of electric field
%%% et_SOA_arg : temporal phase (argument) of electric field
%%% pt_SOA : temporal intensity
%%% ew_SOA : spectral electric field
%%% pw_SOA : spectral intensity

%%% recompressed pulse after CFBG
%%% et_CFBG2 : temporal electric field
%%% et_CFBG2_amp : temporal amplitude of electric field
%%% et_CFBG2_arg : temporal phase (argument) of electric field
%%% pt_CFBG2 : temporal intensity
%%% ew_CFBG2 : spectral electric field
%%% pw_CFBG2 : spectral intensity


%%%%%%%%%%%%%%%%%%%%%%%%%%%%%%%%%%%%%%%%%%%%%%%%%%%%%
%%%%%%%%%%%%%%%%%%%%%%%%%%%%%%%%%%%%%%%%%%%%%%%%%%%%%
%%%%%%   ONE. PULSE STRETCHING USING A CFBG    %%%%%%%
%%%%%%%%%%%%%%%%%%%%%%%%%%%%%%%%%%%%%%%%%%%%%%%%%%%%%
%%%%%%%%%%%%%%%%%%%%%%%%%%%%%%%%%%%%%%%%%%%%%%%%%%%%%

disp('start ...');

%%%%%%%%%%%%%%%%%%%%%%%%%%%%%%%%%%%%%%%%%%%%%%%%%%%%%
%%% 1. generate a gaussain pulse & initial values %%%
%%%%%%%%%%%%%%%%%%%%%%%%%%%%%%%%%%%%%%%%%%%%%%%%%%%%%
```

```
% time domain 1 point = 0.01 ps

% check the input pulse and the stretched pulse and then find a proper N
% the number of point for FFT "N" should be governed by those two pulses


clear all;
tic;
utime=10^(-14);        % unit time = 0.01 ps
c=3*10^8*utime;      % speed of light [m/0.01ps]
l=975*10^(-9);           % center wavelength [m]
d=-1600/10^(-9)/1.6; % GVD [ps/nm/1.6m]                      %%%%%%%%%%%%%%%  initial value
%%%%%%%%%%%%%%%%
N=2^17;        % number of points for FFT                      %%%%%%%%%%%%%%%%  initial value
%%%%%%%%%%%%%%%
save n N;
t=1:N;      % unit of time [0.1ps]
tp=23.3;      % pulse duration [0.01ps]                        %%%%%%%%%%%%%%%%  initial value
%%%%%%%%%%%%%%%
to=tp/sqrt(4*log(2));
Ein=0.01*10^(-12);        % input energy [Joule]               %%%%%%%%%%%%%%%%  initial value
%%%%%%%%%%%%%%%%
a=Ein/to/sqrt(pi);    % field constant [J/0.1ps=power]
x=1.6; % beam propagation length [m]

% FYI : time-bandwidth product of transform-limited Gaussian pulse
% tp*dv = 0.441 and tp*dw = 2*pi*0.441

et_in=sqrt(a)*exp(-(t-N/2).^2/(sqrt(2)*to)^2); %-i*wc.*(t-N/2));    % input gaussian field
pt_in=(abs(et_in)).^2;

%pt_in_sum=sum(pt_in)  % total energy of input pulse in time domain
save pt_in pt_in; clear pt_in;

bw=1/utime;    % total bandwidth according to sampling
w=2*pi*t./N; % [rad Hz]
save t t; clear t;
sf=(w(2)-w(1))/2/pi; % scaling factor
save w w;clear w;
%%% Nyquist theory  sampling dt (= "1") < 1/(dw)( = dt = "30")


%%%%%%%%%%%%%%%%%%%%%%%%%%%%%%%%%%%%%%%%%%%%%%%%%%%%%%%
%%% Plot the temporal phase before the transmission %%%
%%%%%%%%%%%%%%%%%%%%%%%%%%%%%%%%%%%%%%%%%%%%%%%%%%%%%%%
et_in_arg=angle(et_in); %atan(imag(et_in)./real(et_in));
save et_in_arg et_in_arg; clear et_in_arg;

disp('CFBG1 FFT ... running ...');


%%%%%%%%%%%%%%%%%%%%%%%%%%
%%% FFT of input pulse %%%
%%%%%%%%%%%%%%%%%%%%%%%%%%
ew_in=sqrt(sf)*fftshift(fft(et_in));
save et_in et_in; clear et_in;
pw_in=(abs(ew_in)).^2;

%pw_in_sum=sum(pw_in)  % total energy of input pulse in frequency domain
save pw_in pw_in; clear pw_in;

%%%%%%%%%%%%%%%%%%%%%%%%%%%%%%%%%%%%%%%%%
%%% spectral phase of input pulse  %%%
%%%%%%%%%%%%%%%%%%%%%%%%%%%%%%%%%%%%%%%%%%
ew_in_arg=atan(imag(ew_in)./real(ew_in)); %angle(ew_in);

save ew_in_arg ew_in_arg; clear ew_in_arg;
```

121

```matlab
disp('CFBG1 BPM ... running ...');

%%%%%%%%%%%%%%%%%%%%%%%%%%%%%%%%%%%%%%%%%%
%%% beam propagation in frequency domain %%%
%%%%%%%%%%%%%%%%%%%%%%%%%%%%%%%%%%%%%%%%%%
beta=-l^2/(2*pi*c)*(d);   % dispersion parameter beta2
a=i/2*beta;
load w;
ew_CFBG1=ew_in.*exp(-a*(w).^2*x);    %sqrt(0.9)
clear w;
save ew_in ew_in; clear ew_in;


pw_CFBG1=(abs(ew_CFBG1)).^2;
%pw_CFBG1_sum=sum(pw_CFBG1)    %total enegy in frequency domain after CFBG1
save pw_CFBG1 pw_CFBG1; clear pw_CFBG1;


%%%%%%%%%%%%%%%%%%%%%%%%%%%%%%%%%%%%%%%%%%
%%% see a spectral phase after CFBG 01 %%%
%%%%%%%%%%%%%%%%%%%%%%%%%%%%%%%%%%%%%%%%%%
ew_CFBG1_arg=angle(ew_CFBG1);
save ew_CFBG1_arg ew_CFBG1_arg; clear ew_CFBG1_arg;

disp('CFBG1 IFFT ... running ...');


%%%%%%%%%%%%%%%%%%%%%
%%% inverse FFT %%%
%%%%%%%%%%%%%%%%%%%%%
et_CFBG1=1/sqrt(sf)*(ifft(ew_CFBG1));
save ew_CFBG1 ew_CFBG1; clear ew_CFBG1;

pt_CFBG1=(abs(et_CFBG1)).^2;

%pt_CFBG1_sum=sum(pt_CFBG1) %total energy in time domain after CFBG1
save pt_CFBG1 pt_CFBG1; clear pt_CFBG1;


%%%%%%%%%%%%%%%%%%%%%%%%%%%%%%%%%%%%%%%%%%%%%%%%%%
%%% plot the temporal phase after transmission %%%
%%%%%%%%%%%%%%%%%%%%%%%%%%%%%%%%%%%%%%%%%%%%%%%%%%
et_CFBG1_arg=angle(et_CFBG1);   %atan(imag(et_CFBG1)./(real(et_CFBG1+10^(-100))));
save et_CFBG1 et_CFBG1; clear et_CFBG1;

%disp('FWHM of pt_CFBG1 = ');fwhm(pt_CFBG1,N,t)

save et_CFBG1_arg et_CFBG1_arg; clear et_CFBG1_arg;




%%%%%%%%%%%%%%%%%%%%%%%%%%%%%%%%%%%%%%%%%%%%%%%%%%%%%%%%%%%%%%%
%%%%%%%%%%%%%%%%%%%%%%%%%%%%%%%%%%%%%%%%%%%%%%%%%%%%%%%%%%%%%%%
%%%%%     TWO. PULSE AMPLIFICATION THROUGH THE SOA       %%%%%
%%%%%%%%%%%%%%%%%%%%%%%%%%%%%%%%%%%%%%%%%%%%%%%%%%%%%%%%%%%%%%%
%%%%%%%%%%%%%%%%%%%%%%%%%%%%%%%%%%%%%%%%%%%%%%%%%%%%%%%%%%%%%%%
disp('SOA gain ... running ...');

%%%%%%%%%%%%%%%%%%%%%%%%%%%%%%%%%%%%%%%%%%%%%%%%%
%%% 2. initial values for SOA gain dynamics %%%
%%%%%%%%%%%%%%%%%%%%%%%%%%%%%%%%%%%%%%%%%%%%%%%%%
load t;
ssg = 20;  % small signal gain [dB]                        %%%%%%%%%%%%%%%%%%% initial value
%%%%%%%%%%%%%%%%%%%
gol = log(10^(ssg/10)); % small gain cofficient
h(1)= gol;         % gain at t=0
dt=t(3)-t(1);            % unit time step [0.02 ps]
```

```
tc=20000;                   % carrier lifetime [0.01ps]        %%%%%%%%%%%%%%%  initial value
%%%%%%%%%%%%%%%%
Esat=30*10^(-12);           % saturation energy [Joule]        %%%%%%%%%%%%%%%%  initial value
%%%%%%%%%%%%%%%%
alpha = 0;                  % line enhancement factor          %%%%%%%%%%%%%%%%  initial value
%%%%%%%%%%%%%%%%
Psat=Esat/tc;               % saturation power [J/0.01ps]

load pt_CFBG1;

%%%%%%%%%%%%%%%%%%%%
%%% gain of SOA %%%
%%%%%%%%%%%%%%%%%%%%
%%% Fourth Order Runge-Kutta Algorithm %%%
for m = 2:N-1
    k0=dt*((gol-h(m-1))/tc-pt_CFBG1(t(m-1))/Esat*(exp(h(m-1))-1));
    k1=dt*((gol-(h(m-1)+k0/2))/tc-pt_CFBG1(t(m-1)+dt/2)/Esat*(exp(h(m-1)+k0/2)-1));
    k2=dt*((gol-(h(m-1)+k1/2))/tc-pt_CFBG1(t(m-1)+dt/2)/Esat*(exp(h(m-1)+k1/2)-1));
    k3=dt*((gol-(h(m-1)+k2))/tc-pt_CFBG1(t(m-1)+dt)/Esat*(exp(h(m-1)+k2)-1));
    h(m)=h(m-1)+1/6*(k0+2*k1+2*k2+k3);
end
h(N)=h(N-1);  % because of the step d=2, it is difficult to calculate h(N)

%%%%%%%%%%%%%%%%%%%%%%%%%%%%%%%%%%%%%%%%%%%%
%%% output intensity profile after SOA %%%
%%%%%%%%%%%%%%%%%%%%%%%%%%%%%%%%%%%%%%%%%%%%
pt_SOA=pt_CFBG1.*exp(h);                     % output intensity profile after SOA
clear pt_CFBG1;

%pt_SOA_sum=sum(pt_SOA)  %total energy in time domain after SOA

%%%%%%%%%%%%%%%%%%%%%%%%%%%%%%%
%%% output phase after SOA %%%
%%%%%%%%%%%%%%%%%%%%%%%%%%%%%%%
et_SOA_amp = sqrt(pt_SOA);                   % amplitude after SOA
save pt_SOA pt_SOA; clear pt_SOA;
load et_CFBG1_arg;
et_SOA_arg = et_CFBG1_arg-1/2*alpha*h;       % phase after SOA
save h h ; clear h;
clear et_CFBG1_arg;

et_SOA = et_SOA_amp.*exp(i*et_SOA_arg);  %(cos(et_SOA_arg)+i*sin(et_SOA_arg));  % electric field
after SOA
save et_SOA_amp et_SOA_amp; clear et_SOA_amp;
save et_SOA_arg et_SOA_arg; clear et_SOA_arg;

clear pt_SOA;




%%%%%%%%%%%%%%%%%%%%%%%%%%%%%%%%%%%%%%%%%%%%%%%%%%%%%%%%%%%%%%%%%%%%%%%%%%
%%%%%%%%%%%%%%%%%%%%%%%%%%%%%%%%%%%%%%%%%%%%%%%%%%%%%%%%%%%%%%%%%%%%%%%%%%
%%%%%%     THREE. PULSE COMPRESSION USING CFBG     %%%%%%%%%%%%%%%%%%
%%%%%%%%%%%%%%%%%%%%%%%%%%%%%%%%%%%%%%%%%%%%%%%%%%%%%%%%%%%%%%%%%%%%%%%%%%
%%%%%%%%%%%%%%%%%%%%%%%%%%%%%%%%%%%%%%%%%%%%%%%%%%%%%%%%%%%%%%%%%%%%%%%%%%
disp('CFGBG2 FFT ... running ...');

%%%%%%%%%%%%%%%%%%%%%%%%%%%%%%%%%%%%%
%%% 3.1 FFT of pulse after SOA %%%
%%%%%%%%%%%%%%%%%%%%%%%%%%%%%%%%%%%%%
ew_SOA=sqrt(sf)*(fft(et_SOA));
save et_SOA et_SOA; clear et_SOA;

pw_SOA=(abs(ew_SOA)).^2;

%pw_SOA_sum=sum(pw_SOA)   %total enegy in frequency domain after SOA
save pw_SOA pw_SOA; clear pw_SOA;
```

123

```
%%%%%%%%%%%%%%%%%%%%%%%%%%%%%%%%%
%%%   Spectral phase after SOA    %%%
%%%%%%%%%%%%%%%%%%%%%%%%%%%%%%%%%%
ew_SOA_arg=angle(ew_SOA);

save ew_SOA_arg ew_SOA_arg; clear ew_SOA_arg;

disp('CFBG2 BPM ... running ...');

%%%%%%%%%%%%%%%%%%%%%%%%%%%%%%%%%%%%%%%%%
%%% beam propagation in frequency domain %%%
%%%%%%%%%%%%%%%%%%%%%%%%%%%%%%%%%%%%%%%%%%
beta2=-l^2/(2*pi*c)*(-d);  % dispersion parameter beta2
a2=i/2*beta2;
load w;
ew_CFBG2=ew_SOA.*exp(-a2*(w).^2*x);   %sqrt(0.9)
clear w;
save ew_SOA ew_SOA; clear ew_SOA;

pw_CFBG2=(abs(ew_CFBG2)).^2;
save pw_CFBG2 pw_CFBG2; clear pw_CFBG2;


%%%%%%%%%%%%%%%%%%%%%%%%%%%%%%%%%%%
%%%   Spectral phase after CFBG2   %%%
%%%%%%%%%%%%%%%%%%%%%%%%%%%%%%%%%%%%
ew_CFBG2_arg=angle(ew_CFBG2);

save ew_CFBG2_arg ew_CFBG2_arg; clear ew_CFBG2_arg;

%pw_CFBG2_sum=sum(pw_CFBG2);    %total enegy in frequency domain after CFBG2

disp('CFBG2 IFFT ... running ...');

%%%%%%%%%%%%%%%%%%%%%
%%% inverse FFT %%%
%%%%%%%%%%%%%%%%%%%%%
et_CFBG2=1/sqrt(sf)*(ifft(ew_CFBG2));
save ew_CFBG2 ew_CFBG2; clear ew_CFBG2;

pt_CFBG2=(abs(et_CFBG2)).^2;
%fwhm(pt_CFBG2,N,t);

%pt_CFBG2_sum=sum(pt_CFBG2)   %total enegy in time domain after CFBG2
save pt_CFBG2 pt_CFBG2; clear pt_CFBG2;


%%%%%%%%%%%%%%%%%%%%%%%%%%%%%%%%%%%%%%%%%%%%%%%%%%
%%% plotting the temporal phase after transmission %%%
%%%%%%%%%%%%%%%%%%%%%%%%%%%%%%%%%%%%%%%%%%%%%%%%%%%
et_CFBG2_arg=angle(et_CFBG2);

save et_CFBG2_arg et_CFBG2_arg; clear et_CFBG2_arg;
save et_CFBG2 et_CFBG2; clear et_CFBG2;

disp('Done ...');
```

A-3. CASE III: PULSE WIDTH >> CARRIER LIFETIME

```
% case III ) tp >> tc
% pulse width of stretched pulse after CFBG is much longer than carrier lifetime of amplifier

%%%%%%%%%%%%%%%%%%%%%%%%%%%%%%%%%%%%%%%%%%%%%%%%%%%%%%%%%%%%%%%%%
%%%   BEAM PROPAGATION THROUGH CPA SYSTEM WHICH CONSISTS OF     %%%
%%%   TWO CHIRPED FIBER BRAGG GRATINGS AND ONE SOA             %%%
%%%                                                            %%%
%%%                                     06/2005   Kyungbum Kim %%%
%%%%%%%%%%%%%%%%%%%%%%%%%%%%%%%%%%%%%%%%%%%%%%%%%%%%%%%%%%%%%%%%%

%%% initial values are
%%%  - input energy(Ein),
%%%  - input pulse width(tp),
%%%  - GVD(d),
%%%  - saturation energy(Esat),
%%%  - CFBG length(x)
%%%  - linewidth enhancement factor(alpha)
%%%  - and small signal gain(gol)

%%% input optical pulse
%%% et_in : temporal electric field
%%% et_in_amp : temporal amplitude of electric field
%%% et_in_arg : temporal phase (argument) of electric field
%%% pt_in : temporal intensity
%%% ew_in : spectral electric field
%%% pw_in : spectral intensity

%%% stretched pulse after CFBG
%%% et_CFBG1 : temporal electric field
%%% et_CFBG1_amp : temporal amplitude of electric field
%%% et_CFBG1_arg : temporal phase (argument) of electric field
%%% pt_CFBG1 : temporal intensity
%%% ew_CFBG1 : spectral electric field
%%% pw_CFBG1 : spectral intensity

%%% amplified stretched pulse after amplifier
%%% et_SOA : temporal electric field
%%% et_SOA_amp : temporal amplitude of electric field
%%% et_SOA_arg : temporal phase (argument) of electric field
%%% pt_SOA : temporal intensity
%%% ew_SOA : spectral electric field
%%% pw_SOA : spectral intensity

%%% recompressed pulse after CFBG
%%% et_CFBG2 : temporal electric field
%%% et_CFBG2_amp : temporal amplitude of electric field
%%% et_CFBG2_arg : temporal phase (argument) of electric field
%%% pt_CFBG2 : temporal intensity
%%% ew_CFBG2 : spectral electric field
%%% pw_CFBG2 : spectral intensity


%%%%%%%%%%%%%%%%%%%%%%%%%%%%%%%%%%%%%%%%%%%%%%%%%%%%%%
%%%%%%%%%%%%%%%%%%%%%%%%%%%%%%%%%%%%%%%%%%%%%%%%%%%%%%
%%%%%%   ONE. PULSE STRETCHING USING A CFBG    %%%%%%
%%%%%%%%%%%%%%%%%%%%%%%%%%%%%%%%%%%%%%%%%%%%%%%%%%%%%%
%%%%%%%%%%%%%%%%%%%%%%%%%%%%%%%%%%%%%%%%%%%%%%%%%%%%%%
disp('start ... running ...');
%%%%%%%%%%%%%%%%%%%%%%%%%%%%%%%%%%%%%%%%%%%%%%%%%%%%
%%% 1. generate a gaussain pulse & initial values %%%
%%%%%%%%%%%%%%%%%%%%%%%%%%%%%%%%%%%%%%%%%%%%%%%%%%%%
% time domain 1 point = 0.01 ps
```

```
% check the input pulse and the stretched pulse and then find a proper N
% the number of point for FFT "N" should be governed by those two pulses


clear all;
tic;
utime=10^(-14);        % unit time = 0.01 ps
c=3*10^8*utime;     % speed of light [m/0.01ps]
l=975*10^(-9);          % center wavelength [m]
d=-40000/10^(-9)/1.6; % GVD [ps/nm/1.6m]                     %%%%%%%%%%%%%%%%  initial value
%%%%%%%%%%%%%%%  16000 gives 9.6ns stretched pulse with 0.233ps pulse
N=2^21;        % number of points for FFT                    %%%%%%%%%%%%%%%%  initial value
%%%%%%%%%%%%%%%
t=1:N;        % unit of time [0.1ps]
save n N;
tp=23.3;          % pulse duration [0.01ps]                  %%%%%%%%%%%%%%%%  initial value
%%%%%%%%%%%%%%%
to=tp/sqrt(4*log(2));
Ein=500*10^(-12);              % input energy [Joule]              %%%%%%%%%%%%%%%%
initial value %%%%%%%%%%%%%%%%
a=Ein/to/sqrt(pi);    % field constant [J/0.1ps=power]
x=1.6; % beam propagation length [m]                         %%%%%%%%%%%%%%%%  initial value
%%%%%%%%%%%%%%%
disp('total temporal window[ps]=');disp(N*utime*1e12);

% FYI : time-bandwidth product of transform-limited Gaussian pulse
% tp*dv = 0.441 and tp*dw = 2*pi*0.441

et_in=sqrt(a)*exp(-(t-N/2).^2/(sqrt(2)*to)^2); %-i*wc.*(t-N/2));    % input gaussian field
pt_in=(abs(et_in)).^2;

%pt_in_sum=sum(pt_in)  % total energy of input pulse in time domain
save pt_in pt_in; clear pt_in;

bw=1/utime;            % total bandwidth according to sampling
tbw=bw*2*pi*1e-12;save tbw tbw;    % total bandwidth according to sampling      %
<<<<<<<<<<<<<<<<<<<<<<<<<<<<<<<<<<<<<<<<<<<<<<<<
disp('total spectral window[rad THz]=');disp(tbw);    %
<<<<<<<<<<<<<<<<<<<<<<<<<<<<<<<<<<<<<<<<<<<<<<<<
w=2*pi*t./N;          % [rad Hz]
sf=(w(2)-w(1))/2/pi;  % scaling factor
w2=tbw/N*t; save w2 w2; clear w2;
save t t; clear t;
save w w; clear w;


%%%%%%%%%%%%%%%%%%%%%%%%%%%%%%%%%%%%%%%%%%%%%%%%%%%%%%
%%% Plot the temporal phase before the transmission %%%
%%%%%%%%%%%%%%%%%%%%%%%%%%%%%%%%%%%%%%%%%%%%%%%%%%%%%%
et_in_arg=angle(et_in); %atan(imag(et_in)./real(et_in));
save et_in_arg et_in_arg; clear et_in_arg;

disp('CFBG1 fft start ... running ...');


%%%%%%%%%%%%%%%%%%%%%%%%%%
%%% FFT of input pulse %%%
%%%%%%%%%%%%%%%%%%%%%%%%%%
ew_in=sqrt(sf)*fftshift(fft(et_in));
save et_in et_in; clear et_in;
pw_in=(abs(ew_in)).^2;

%pw_in_sum=sum(pw_in)  % total energy of input pulse in frequency domain
save pw_in pw_in; clear pw_in;

%%%%%%%%%%%%%%%%%%%%%%%%%%%%%%%%%%%%%%%%%
%%% spectral phase of input pulse  %%%
%%%%%%%%%%%%%%%%%%%%%%%%%%%%%%%%%%%%%%%%%
ew_in_arg=atan(imag(ew_in)./real(ew_in)); %angle(ew_in);
```

126

```
save ew_in_arg ew_in_arg; clear ew_in_arg;


disp('CFBG1 BPM start ... running ...');

%%%%%%%%%%%%%%%%%%%%%%%%%%%%%%%%%%%%%%%
%%% beam propagation in frequency domain %%%
%%%%%%%%%%%%%%%%%%%%%%%%%%%%%%%%%%%%%%%
beta=-l^2/(2*pi*c)*(d);  % dispersion parameter beta2
a=i/2*beta;
load w;
ew_CFBG1=ew_in.*exp(-a*(w).^2*x);    %sqrt(0.9)
clear w;
save ew_in ew_in; clear ew_in;


pw_CFBG1=(abs(ew_CFBG1)).^2;
%pw_CFBG1_sum=sum(pw_CFBG1)   %total enegy in frequency domain after CFBG1
save pw_CFBG1 pw_CFBG1; clear pw_CFBG1;


%%%%%%%%%%%%%%%%%%%%%%%%%%%%%%%%%%%%%%
%%% see a spectral phase after CFBG 01 %%%
%%%%%%%%%%%%%%%%%%%%%%%%%%%%%%%%%%%%%%
ew_CFBG1_arg=angle(ew_CFBG1);
save ew_CFBG1_arg ew_CFBG1_arg; clear ew_CFBG1_arg;

disp('CFBG1 ifft start ... running ...');


%%%%%%%%%%%%%%%%%%
%%% inverse FFT %%%
%%%%%%%%%%%%%%%%%%
et_CFBG1=1/sqrt(sf)*ifft(ew_CFBG1);
save ew_CFBG1 ew_CFBG1; clear ew_CFBG1;

pt_CFBG1=(abs(et_CFBG1)).^2;

%pt_CFBG1_sum=sum(pt_CFBG1) %total energy in time domain after CFBG1
save pt_CFBG1 pt_CFBG1; clear pt_CFBG1;


%%%%%%%%%%%%%%%%%%%%%%%%%%%%%%%%%%%%%%%%%%%%%
%%% plot the temporal phase after transmission %%%
%%%%%%%%%%%%%%%%%%%%%%%%%%%%%%%%%%%%%%%%%%%%%
et_CFBG1_arg=angle(et_CFBG1);  %atan(imag(et_CFBG1)./(real(et_CFBG1+10^(-100))));
save et_CFBG1 et_CFBG1; clear et_CFBG1;

%disp('FWHM of pt_CFBG1 = ');fwhm(pt_CFBG1,N,t)

save et_CFBG1_arg et_CFBG1_arg; clear et_CFBG1_arg;


%%%%%%%%%%%%%%%%%%%%%%%%%%%%%%%%%%%%%%%%%%%%%%%%%%%%%%%%%%
%%%%%%%%%%%%%%%%%%%%%%%%%%%%%%%%%%%%%%%%%%%%%%%%%%%%%%%%%%
%%%%%%    TWO. PULSE AMPLIFICATION THROUGH THE SOA         %%%%%%
%%%%%%%%%%%%%%%%%%%%%%%%%%%%%%%%%%%%%%%%%%%%%%%%%%%%%%%%%%
%%%%%%%%%%%%%%%%%%%%%%%%%%%%%%%%%%%%%%%%%%%%%%%%%%%%%%%%%%

disp('SOA gain start ... running ...');


%%%%%%%%%%%%%%%%%%%%%%%%%%%%%%%%%%%%%%%%%%%%
%%% 2. initial values for SAO gain dynamics %%%
%%%%%%%%%%%%%%%%%%%%%%%%%%%%%%%%%%%%%%%%%%%%
ssg = 20; % small singal gain [dB]                      %%%%%%%%%%%%%%%%  initial value
%%%%%%%%%%%%%%%
gol = log(10^(ssg/10));
h(1)= gol;         % gain at t=0
```

```
tc=20000;                % carrier lifetime                        %%%%%%%%%%%%%%%%  initial value
%%%%%%%%%%%%%%%
Esat=30*10^(-12);        % saturation energy [Joule]               %%%%%%%%%%%%%%%%
initial value %%%%%%%%%%%%%%%
alpha=0;                 % line enhancement factor                 %%%%%%%%%%%%%%%%  initial
value %%%%%%%%%%%%%%%
Psat=Esat/tc;            % saturation power

%%%%%%%%%%%%%%%%%%%%%%%%%%%%%%%%%%%%%
%%% gain of SOA : Newton's Method  %%%
%%%%%%%%%%%%%%%%%%%%%%%%%%%%%%%%%%%%%

load pt_CFBG1;
x0=h(1)*ones(1,N);
x1=x0-(x0-gol+pt_CFBG1./Psat.*(exp(x0)-1))./(1+pt_CFBG1./Psat.*exp(x0));clear x0;
x2=x1-(x1-gol+pt_CFBG1./Psat.*(exp(x1)-1))./(1+pt_CFBG1./Psat.*exp(x1));clear x1;
x3=x2-(x2-gol+pt_CFBG1./Psat.*(exp(x2)-1))./(1+pt_CFBG1./Psat.*exp(x2));clear x2;
x4=x3-(x3-gol+pt_CFBG1./Psat.*(exp(x3)-1))./(1+pt_CFBG1./Psat.*exp(x3));clear x3;
x5=x4-(x4-gol+pt_CFBG1./Psat.*(exp(x4)-1))./(1+pt_CFBG1./Psat.*exp(x4));clear x4;
h=x5;clear x5;


%%%%%%%%%%%%%%%%%%%%%%%%%%%%%%%%%%%%%%%%%
%%% output intensity profile after SOA %%%
%%%%%%%%%%%%%%%%%%%%%%%%%%%%%%%%%%%%%%%%%%
pt_SOA=pt_CFBG1.*exp(h);                    % output intensity profile after SOA
clear pt_CFBG1;

pt_SOA_sum=sum(pt_SOA);  %total energy in time domain after SOA

%%%%%%%%%%%%%%%%%%%%%%%%%%%%%
%%% output phase after SOA %%%
%%%%%%%%%%%%%%%%%%%%%%%%%%%%%
et_SOA_amp = sqrt(pt_SOA);                  % amplitude after SOA
save pt_SOA pt_SOA; clear pt_SOA;
load et_CFBG1_arg;
et_SOA_arg = et_CFBG1_arg-1/2*alpha*h;      % phase after SOA
save h h ; clear h;
clear et_CFBG1_arg;

et_SOA = et_SOA_amp.*exp(i*et_SOA_arg);  %(cos(et_SOA_arg)+i*sin(et_SOA_arg));  % electric field
after SOA
save et_SOA_amp et_SOA_amp; clear et_SOA_amp;
save et_SOA_arg et_SOA_arg; clear et_SOA_arg;

clear pt_SOA;


%%%%%%%%%%%%%%%%%%%%%%%%%%%%%%%%%%%%%%%%%%%%%%%%%%%%%%%%%%%%%%%%%%
%%%%%%%%%%%%%%%%%%%%%%%%%%%%%%%%%%%%%%%%%%%%%%%%%%%%%%%%%%%%%%%%%%
%%%%%%    THREE. PULSE COMPRESSION USING CFBG    %%%%%%%%%%%%%%%%
%%%%%%%%%%%%%%%%%%%%%%%%%%%%%%%%%%%%%%%%%%%%%%%%%%%%%%%%%%%%%%%%%%
%%%%%%%%%%%%%%%%%%%%%%%%%%%%%%%%%%%%%%%%%%%%%%%%%%%%%%%%%%%%%%%%%%
disp('CFGBG2 fft start ... running ...');

%%%%%%%%%%%%%%%%%%%%%%%%%%%%%%%%%%
%%% 3.1 FFT of pulse after SOA %%%
%%%%%%%%%%%%%%%%%%%%%%%%%%%%%%%%%%
ew_SOA=sqrt(sf)*(fft(et_SOA));
save et_SOA et_SOA; clear et_SOA;

pw_SOA=(abs(ew_SOA)).^2;

%pw_SOA_sum=sum(pw_SOA)    %total enegy in frequency domain after SOA
save pw_SOA pw_SOA; clear pw_SOA;


%%%%%%%%%%%%%%%%%%%%%%%%%%%%%%%%%%%%%%%%%
%%%   Spectral phase after SOA    %%%
```

```
%%%%%%%%%%%%%%%%%%%%%%%%%%%%%%%%%%
ew_SOA_arg=angle(ew_SOA);

save ew_SOA_arg ew_SOA_arg; clear ew_SOA_arg;

disp('CFBG2 BPM start ... running ...');

%%%%%%%%%%%%%%%%%%%%%%%%%%%%%%%%%%%%%%%%%%%
%%% beam propagation in frequency domain %%%
%%%%%%%%%%%%%%%%%%%%%%%%%%%%%%%%%%%%%%%%%%%%
beta2=-l^2/(2*pi*c)*(-d);  % dispersion parameter beta2
a2=i/2*beta2;
load w;
ew_CFBG2=ew_SOA.*exp(-a2*(w).^2*x);   %sqrt(0.9)
clear w;
save ew_SOA ew_SOA; clear ew_SOA;

pw_CFBG2=(abs(ew_CFBG2)).^2;
save pw_CFBG2 pw_CFBG2; clear pw_CFBG2;


%%%%%%%%%%%%%%%%%%%%%%%%%%%%%%%%%%%%%
%%%    Spectral phase after CFBG2  %%%
%%%%%%%%%%%%%%%%%%%%%%%%%%%%%%%%%%%%%
ew_CFBG2_arg=angle(ew_CFBG2);

save ew_CFBG2_arg ew_CFBG2_arg; clear ew_CFBG2_arg;

%pw_CFBG2_sum=sum(pw_CFBG2);   %total enegy in frequency domain after CFBG2

disp('CFBG2 ifft start ... running ...');

%%%%%%%%%%%%%%%%%%%%
%%% inverse FFT %%%
%%%%%%%%%%%%%%%%%%%%
et_CFBG2=1/sqrt(sf)*ifft(ew_CFBG2);
save ew_CFBG2 ew_CFBG2; clear ew_CFBG2;

pt_CFBG2=(abs(et_CFBG2)).^2;
%fwhm(pt_CFBG2,N,t);

%pt_CFBG2_sum=sum(pt_CFBG2)   %total enegy in time domain after CFBG2
save pt_CFBG2 pt_CFBG2; clear pt_CFBG2;


%%%%%%%%%%%%%%%%%%%%%%%%%%%%%%%%%%%%%%%%%%%%%%%%%%%%%%%%%%%
%%% plotting the temporal phase after transmission %%%
%%%%%%%%%%%%%%%%%%%%%%%%%%%%%%%%%%%%%%%%%%%%%%%%%%%%%%%%%%%
et_CFBG2_arg=angle(et_CFBG2);

save et_CFBG2_arg et_CFBG2_arg; clear et_CFBG2_arg;
save et_CFBG2 et_CFBG2; clear et_CFBG2;

disp('done ...');
toc;
beep; beep; beep;
```

129

Appendix B: DEVELOPMENT OF MODE-LOCKED SEMICONDUCTOR LASER

B-1. Gain Flattened Actively Mode-locked Semiconductor Laser

Figure 72 shows the experimental setup of the gain flattened actively mode-locked semiconductor laser (GFMLL) and its temporal and spectral characteristics. The SOA used in the laser is identical to one used for a CPMLL in Chapter 3-1. A grating and a lens combination are employed as an intracavity spectrometer that has a Fourier filtering plane inside the cavity and provides the ability to independently control the optical spectrum. Employing a bandpass filter and a gain flattening filter in the intracavity spectrometer, the output optical spectral characteristics can be adjusted to match the optical reflection spectrum of the CFBG. The GFMLL is actively mode-locked by gain modulation and its temporal pulse duration and optical spectrum are ~190ps and ~8nm at 975nm (Figure 73 (a) and (b)). The pulse repetition rate of the GFMLL is 203MHz. The GFMLL was developed to get a broad band optical spectrum that is matched with early developed CFBG which has near 8nm spectral bandwidth. The gain flattened, actively mode-locked semiconductor laser was utilized to characterize the CFBG before the CPMLL was developed. The salient feature of the GFMLL is that incorporating with an MQW and SA a broader optical spectral bandwidth with better phase correlation could be achieved. With a broader optical spectral bandwidth, a shorter optical pulse can be generated from the oscillator. It means that a shorter optical pulse could be achieved from an X-CPA system. The peak power of the optical pulse from the X-CPA system increase as a result.

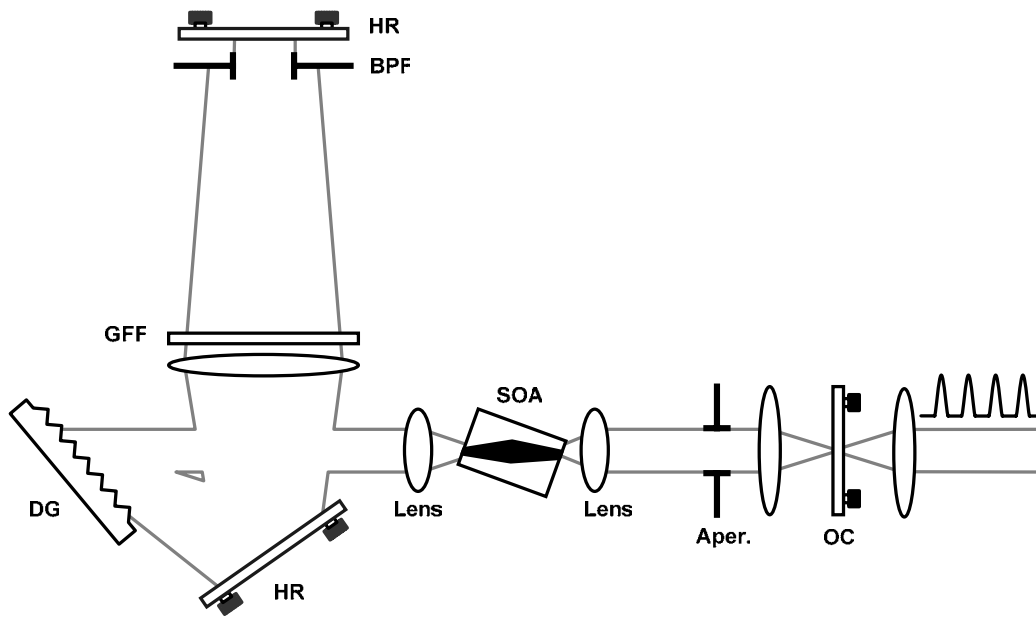Figure 72. Schematic diagram of the gain flattened actively mode-locked semiconductor laser.

HR: high reflector, BPF: band pass filter, GFF: gain flattening filter, DG: diffraction grating,

SOA: semiconductor optical amplifier, Aper.: aperture, OC: output coupler
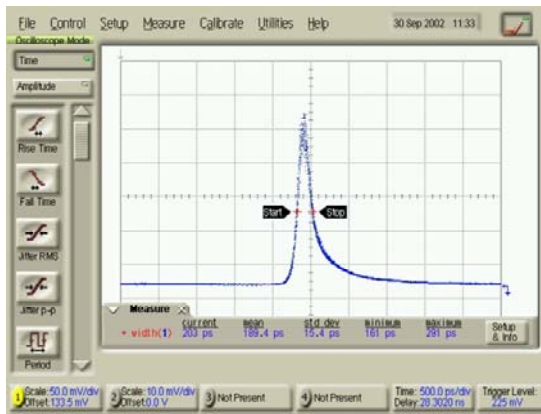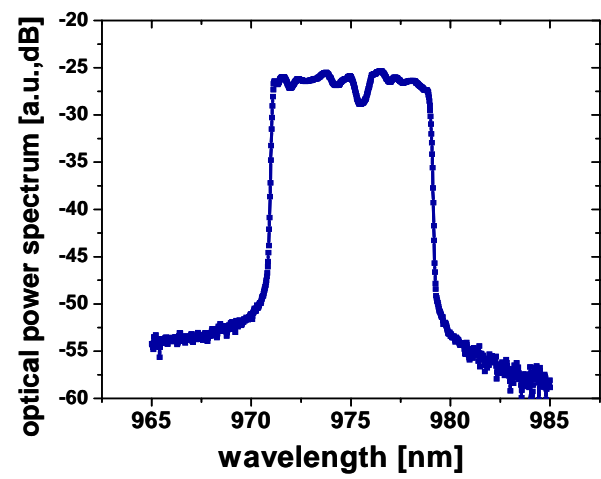
(a)   (b)

Figure 73. (a) Digital sampling oscilloscope trace and (b) optical spectrum of GFMLL

B-2. Fundamental Colliding Pulse Hybrid Mode-Locked Semiconductor Laser

A second harmonic CPMLL as a master oscillator in an X-CPA system is used as an injection source in passive optical cavity amplification. In case the correlation of two adjacent pulses from the second harmonic CPMLL is weak due to harmonic mode-locking, it is useful to use a fundamental CPMLL whose two adjacent pulses are correlated. A fundamental CPMLL as the injection source of a passive optical cavity amplifier was developed and Figure 74 illustrates the schematic diagram of the cavity setup. Because the cavity frequency was near 200MHz, the IBTSOA was driven by an amplified RF sinusoidal wave at near 200MHz. The amplified RF signal was combined with DC current by a bias tee. The average power from a fundamental CPMLL is ~5mW and energy per pulse is ~25pJ. Output characteristics of the fundamental CPMLL including the optical spectrum, autocorrelation, and digital sampling scope trace are shown in Figure 75. The FWHM of the autocorrelation in Figure 74 (d) is ~2ps after the bulk grating compressor.
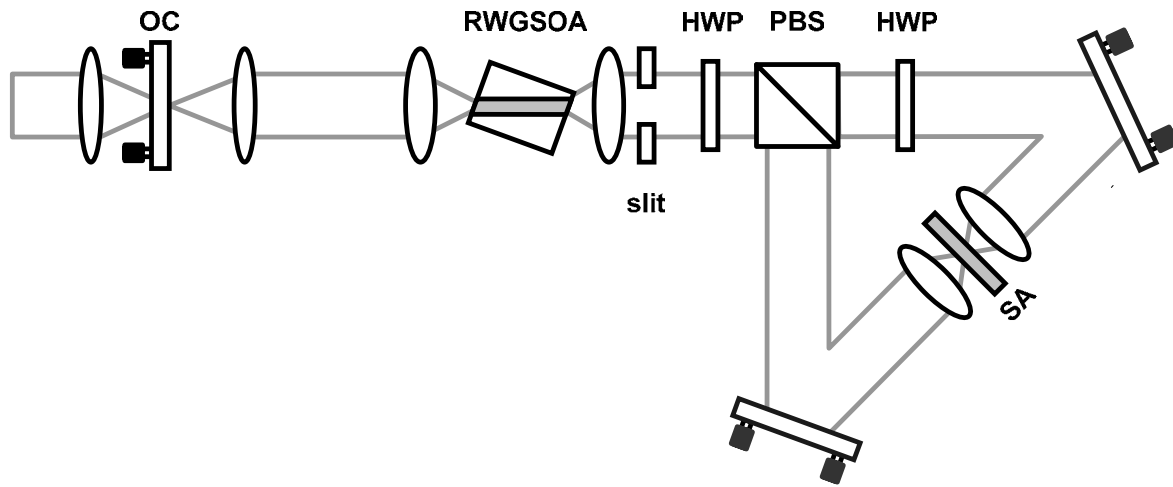
Figure 74. Schematic diagram of the fundamental colliding pulse hybrid mode-locked semiconductor laser, OC: output coupler, RWGSOA: ridge waveguide semiconductor optical amplifier, HWP: half wave plate, PBS: polarizing beam splitter, SA: multiple quantum well saturable absorber
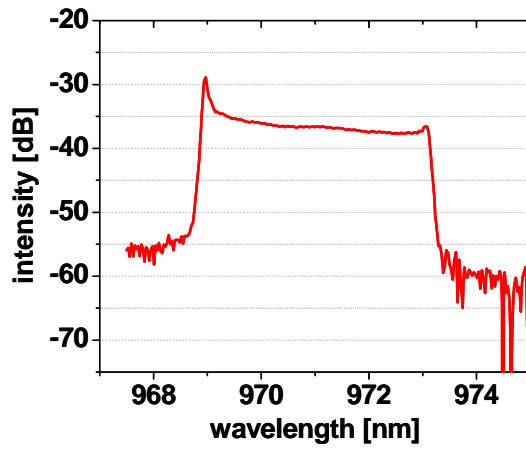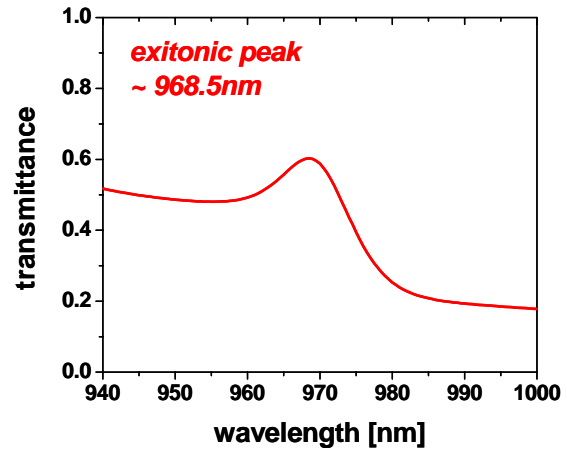
(a)   (b)
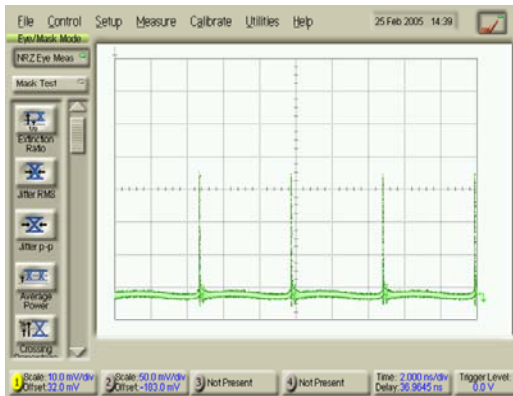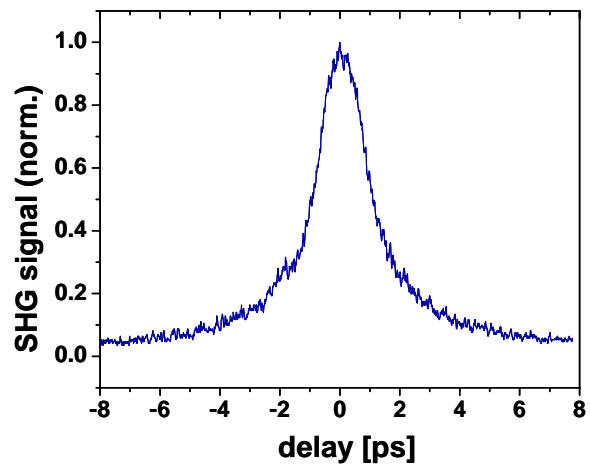
(c)   (d)

Figure 75. (a) Optical spectrum of the fundamental CPMLL and (b) excitonic absorption of

the saturable absorber used in the fundamental CPMLL, (c) Digital sampling oscilloscope

trace and (d) the autocorrelation trace of the optical pulse from the fundamental CPMLL

after pre-chirping was compensated by a bulk grating compressor

Appendix C: EQUIPMENT USED FOR MEASUREMENT

C-1. CHARACTERIZATION OF OPTICAL PULSE

Autocorrelation Trace:

Femtochrome Autocorrelator FR-103XL

Digital Sampling Oscilloscope Trace:

Agilent 86100B Infiniium DCA Wide-Bandwidth Oscilloscope 50GHz

Newfocus 1437-FS 20GHz Broadband Photodiode

Pasternack 26.5GHz RF cable

Streak Camera Image:

Hamamatsu Streak Camera C4334
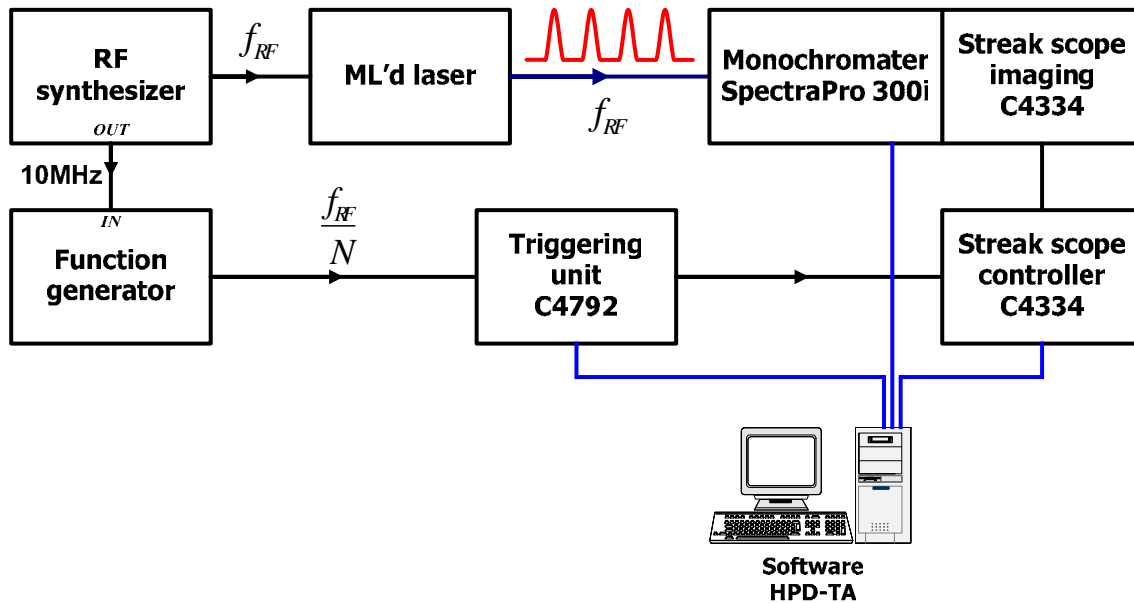
Figure 76. Schematic diagram of the pulse measurement setup using a streak camera

C-2. MEASUREMENT OF OPTICAL SPECTRUM:

ANDO Optical Spectrum Analyzer AQ6315

ANDO Optical Spectrum Analyzer AQ6317B

C-3. MEASUREMENT OF OPTICAL POWER:

Newport Power Meter Head 818SL Low Power Detector

Newport Power/Energy Meter 1825-C

Newport Multi Function Optical Meter 1835-C

LIST OF REFERENCES

CHAPTER 1

[1] X. Liu, D. Du, G. Mourou, "Laser ablation and micromachining with ultrashort laser pulses," IEEE Journal of Quantum Electronics, V33, I10 pp. 1706-1716 (1997)

[2] H. Lubatschowski, A. Heisterkamp, F. Will, A.I. Singh, J. Serbin, A. Ostendorf, O. Kermani, R. Heermann, H. Welling, W. Ertmer, "Medical applications for ultrafast laser pulses," RIKEN Review No. 50 pp. 113-118 (2003)

[3] M. Kanskar,T. Earles, T.J. Goodnough, E. Stiers, D. Botez, L.J. Mawst, "73% CW power conversion efficiency at 50 W from 970 nm diode laser bars," Electronics Letters, V41, I5, pp. 245-247 (2005)

[4] Knigge, G. Erbert, J. Jonsson, W. Pittroff, R. Staske, B. Sumpf, M. Weyers and G. Trankle, "Passively cooled 940nm laser bars with 73% wall-plug efficiency at 70W and 25C," Electronics Letters, V41, I5, pp. 250-251 (2005)

[5] S. Nakamura, S. Pearton, G. Fasol, "The Blue Laser Diode: The complete story," Springer-Verlag, 2nd Edition (2000)

[6] J. Faist, F. Capasso, D.L. Sivco, C. Sirtori, A.L. Hutchinson, A.Y.Cho, "Quantum Cascade Laser," Science, V264, I5158, pp. 553-556 (1994)

[7] P. J. Delfyett, L. T. Florez, N. Stoffel, T. Gmitter, N. C. Andeadakis, Y.Silberberg, J. P. Heritage, and G. A. Alphonse, "High-power ultrafast laser diodes," IEEE J. Quantum Electron., V28, pp. 2203–2219 (1992)

[8] K. A. Williams, I. H. White, R. V. Penty, and F. R. Laughton, "Gain switched dynamics of tapered waveguide bow-tie lasers: Experiment and theory," IEEE Photon. Technol. Lett., V9, pp. 167–169, (1997)

[9] K. A. Williams, J. Sarma, I. H. White, R. V. Penty, I. Middlemast, T. Ryan, F. R. Laughton, and J. S. Roberts, "Q-switched bow-tie lasers for high energy picosecond pulse generation," Electron. Lett., V 30, N 4, pp. 320–321 (1994)

[10] B. Zhu, I. H. White, K. A. Williams, F. R. Laughton, and R. V. Penty, "High peak power picosecond optical pulse generation from Q-switched bow-tie laser with a tapered traveling wave amplifier," IEEE Photon. Technol. Lett.,V8, pp. 503–505 (1996)

[11] S. Gee, G. Alphonese, J. Connolly, P. J. Delfyett, "High-power mode-locked external cavity semiconductor laser using inverse bow-tie semiconductor optical amplifiers," IEEE. J. Select. Topics Quantum Electron., V4, pp.209-215 (1998)

[12] A. Mar, R. Helkey, J. Bowers, D. Mehuys, and D. Welch, "Modelocked operation of a master oscillator power amplifier," IEEE Photon. Technol. Lett., V6, pp. 1067–1069 (1994)

[13] L. Goldberg, D. Mehuys, and D. Welch, "High power modelocked compound laser using a tapered semiconductor amplifier," IEEE Photon. Technol. Lett., V 6, pp. 1070–1072 (1994)

[14] S. Augst, A. Goyal, R. Aggarwal, T. Fan, and A. Sanchez, "Wavelength beam combining of ytterbium fiber lasers ," Opt. Lett. **28**, pp. 331-333 (2003)

[15] V. Daneu, A. Sanchez, T. Fan, H. Choi, G. Turner, and C. Cook, "Spectral beam combining of a broad-stripe diode laser array in an external cavity ," Opt. Lett. **25**, pp. 405-407 (2000)

[16]   B. Resan, P. J. Delfyett, "Dispersion-managed breathing-Mode semiconductor mode-locked ring laser: experimental characterization and numerical simulations," IEEE J. Quantum Electron., V40, pp.214-221, (2004)

[17]   A. Aschwanden, D. Lorenser, H. J. Unold, R. Paschotta, , E. Gini, U. Keller, "2.1W picosecond passively mode-locked external-cavity semiconductor laser," Opt. Lett., V30, pp. 272-274 (2005)

[18]   A. Garnache, S. Hoogland, A. C. Tropper, I. Sagnes, G. Saint-Girons, J. S. Roberts, "sub-500fs soliton-like pulse in a passively mode-locked broadband surface-emitting laser with 100mW average power," Appl. Phys. Lett., V80, pp. 3892-3894 (2002)

CHAPTER 2

[19]   S. O'Brien, D.F. Welch, R.A. Parke, D. Mehuys, K. Dzurko, R.J. Lang, R. Waarts, D. Scifres, "Operating characteristics of a high-power monolithically integratedflared amplifier master oscillator power amplifier," IEEE Journal of Quantum Electronics, V29, I6, pp. 2052-2057 (1993)

[20]   A. Liem, J. Limpert, H. Zellmer, and A. Tnnermann, "100-W single-frequency master-oscillator fiber power amplifier," Opt. Lett. **28**, pp. 1537-1539 (2003)

[21]   P. Becker, A. Olsson, J. Simpson, "Erbium doped fiber amplifier," Academic Press (1999)

[22]   T. Durhuus, C. Joergensen, B. Mikkelsen, R. J. S. Pedersen, K. E Stubkjaer, "All optical wavelength conversion by SOA's in a Mach-Zehnder configuration," IEEE Photonics Technology Letters, V6, N1, pp. 53-55 (1994)

[23]   M. Perry, D. Pennington, B. Stuart, G. Tietbohl, J. Britten, C. Brown, S. Herman, B. Golick, M. Kartz, J. Miller, H. Powell, M. Vergino, and V. Yanovsky, "Petawatt laser pulses," Opt. Lett. **24**, 160-162 (1999)

[24]   G. P. Agrawal, N. A. Olsson, "Self-Phase Modulation and Spectral Broadening of Optical Pulses in Semiconductor Laser Amplifiers", IEEE Journal of Quantum Electronics, V25, N11, pp. 2297-2306 (1989)

[25]   K. L. Hall, G. Lenz, E. P. Ippen, U. Koren, and G. Raybon, "Carrier heating and spectral hole burning in strained-layer quantum-well laser amplifiers at 1.5 µm," Applied Physics Letters, V 61, I21, pp. 2512-2514 (1992)

[26]   H.J.S. Dorren, X. Yang, D. Lenstra, H. de Waardt, G.D. Khoe, T. Simoyama, H. Ishikawa, H. Kawashima, T. Hasama, "Ultrafast refractive-index dynamics in a multiquantum-well semiconductor optical amplifier," IEEE Photon. Technol. Lett., V15, I6, pp. 792-794 (2003)

[27]   P. J. Delfyett, A. Dienes, J. P. Heritage, M. Y. Hong, Y. H. Chang, "Femtosecond hybrid mode-locked semiconductor laser and amplifier dynamics," Appl. Phys. B, 58, pp. 183-195 (1994)

[28]   J.R. Marciante, G.P. Agrawal, "Nonlinear Mechanisms of Filamentation in Broad-Area Semiconductor Lasers," IEEE Journal of Quantum Electronics. V**32,** N 4, pp. 590-596 (1996)

[29]   O. Hess, S.W. Koch, J.V. Moloney, "Filamentation and beam propagation in broad-area semiconductor lasers," IEEE Journal of Quantum Electronics, V31, I1, pp. 35-43 (1995)

[30]   W. Koechner, "Solid-State Laser Engineering," Chap. 4, Springer, 5th edition, (1999)

[31]   L.E. Nelson, D.J. Jones, K. Tamura, H.A. Haus, E.P. Ippen, "Ultrashort-pulse fiber ring lasers," Applied Physics B: Lasers and Optics, V65, I 2, pp. 277-294 (1997)

[32]   M.E. Fermann, A. Galvanauskas, G. Sucha, D. Harter, "Fiber-lasers for ultrafast optics," Applied Physics B: Lasers and Optics, V65, I2, pp. 259-275 (1997)

[33]   F.Ö. Ilday, J.R. Buckley, W.G. Clark, F.W. Wise, "Self-Similar Evolution of Parabolic Pulses in a Laser," Phys. Rev. Lett. **92**, 213902 (2004)

[34]   F. Röser, J. Rothhard, B. Ortac, A. Liem, O. Schmidt, T. Schreiber, J. Limpert, and A. Tünnermann, "131 W 220 fs fiber laser system," Opt. Lett. **30**, pp. 2754-2756 (2005)

[35]   J. Limpert, T. Schreiber, S. Nolte, H. Zellmer, and A. Tünnermann, "All fiber chirped-pulse amplification system based on compression in air-guiding photonic bandgap fiber," Opt. Express **11**, pp. 3332-3337 (2003)

[36]   C. H. Lee, P. J. Delfyett, "Limits on Amplification of Picosecond Pulses by Using Semiconductor Laser," IEEE Journal of Quantum Electronics, V27, N5, pp. 1110-1114 (1991)

[37]   J-C. Diels, W. Rudolph, "Ultrashort Laser Pulse Phenomena," Academic Press, Inc. (1996)

[38]   S. Lee, K. Kim and P. J. Delfyett, "Extreme chirped pulse modelocked diode laser ring oscillator using a theta cavity design," in Proc. IEEE LEOS Annual Meeting, paper WV4, 2005

CHAPTER 3

[39]   G. C. Gilbreath, W. S. Rabinoich, T. J. Meehan, R. Mahon, R. Burris, M. Ferraro, I. Sokolsky, J. A. Vasquez, C. S. Bovais, K. Cochrell, K. C. Goins, R. Rarbehenn, D. S. Katzer, K. Ilkossi-Anansasiou, M. J. Montes, "Large aperture multiple quantum well modulating retroreflector for free-space optical data transfer on unmanned aerial vehicles," Opt. Eng. vol. 40, pp. 1348-1356, 2000

[40]   G.A. Alphonse, N Morris, M.G. Harvey, D.B. Gilbert, J.C. Connolly, "New high-power single-mode superluminescent diode with low spectral modulation," CLEO '96. CTul3, pp. 107- 108 (1996)

[41]   J. Brennan and D. LaBrake, "Realization of >10-m-long chirped fiber Bragg gratings," Bragg Gratings, Photosensitivity, and Poling in Glass Waveguides (OSA, Washington. DC, 1999), pp. 128-130

[42]   K. O. Hills, G. Meltz, "Fiber Bragg grating technology fundamentals and overviews," J. Lightwave Technol., V15, pp. 1263-1276 (1997)

[43]   T. Erdogan, "Fiber grating spectra," Journal of Lightwave Technology, V15, I8, pp.1277-1294 (1997)

[44]   G.P. Agrawal, N.K. Dutta, "Semiconductor Lasers," Chapter 11, Van Nostrand, New York, 2nd edition (1993)

[45]   O. Martinez, "3000 times grating compressor with positive group velocity dispersion: Application to fiber compensation in 1.3-1.6 µm region," IEEE J. Quantum Electron, vol. 23, pp.59-64 (1987)

[46]   O. Svelto, "Principles of Lasers," Chapter 12, Plenum Press, New York and London, 4th edition (1998)

CHAPTER 5

[47]   Zh. I. Alferov, V. M. Andreev, S. A. Gureevich, R. F. Kazarinov, V. R. Larionov, M. N. Mizerov, E. L. Portnoi, "Semiconductor Laser with the Light Output Through the Diffraction Grating on the Surface of the Waveguide Layer", IEEE J. of Quantum Elect., **QE-11**, pp. 449-451 (1975)

[48]   J. Jiang, O. Smoski, C. Roychoudhuri, E. Portnoi, G. Venus, I. Gadjiev and J. McKillop, "Broad Tunability of Grating Surface Emitting Laser with External Cavity", Electron. Lett., **35**, pp.1847-1848 (1999)

[49]   V. Smolski, J. Jiang, C. Roychoudhuri, E. L. Portnoi, G. B. Venus, J. Bullington, "Tunable picosecond pulses from gain-switched grating coupled surface-emitting laser," in Novel In-Plane Semiconductor Lasers, Proc. of SPIE, **4651**, pp.59-62 (2002).

[50]   Y. Hu, A. Gubenko, G. Venus, I. Gadjiev, N. Il'inskaja, S. Nesterov, E. Portnoi, M. Dubov, I. Khrushev, "Gain switching of an external cavity grating-coupled surface emitting laser with wide tunability", Appl. Phys. Lett., **82**, pp. 4236-4237 (2003).

[51]   D. Mehuys, A. Hardy, D. F. Welch, R. G. Waarts and R. Parke, "Analysis of detuned second-order grating output couplers with an integrated superlattice reflector," IEEE Photon. Techn. Lett., **3**, pp. 342-344 (1991).

[52]   G. Evans, N. Carlson, J. Hammer, "Grating-outcoupled surface emitting semiconductor lasers" in "Surface emitting semiconductor lasers and arrays" edited by G. Evans, J. Hammer, Academic Press, Inc. (1993).

[53]   M. Uemukai, N. Matsumoto, T. Suhara, H. Nishihara, N. Eriksson, A. Larsson, "Monolithically Integrated InGaAs–AlGaAs Master Oscillator Power Amplifier with Grating Outcoupler", IEEE Photon. Techn. Lett., **10**, pp. 1097-1099 (1998).

[54]   M. Hagberg, N. Eriksson, T. Kjellberg, A. Larsson, "Dependence of output coupling efficiency on detuning in surface grating output couplers", Opt. Lett., **20**, pp. 180-183 (1995).

CHAPTER 6

[55]   V. Yanovsky, F. Wise, "Frequency doubling of 100-fs pulses with 50% efficiency by using a resonant enhancement cavity," Opt. Lett. **19**, 1952- (1994)

[56]   M. Pshenichnikov, W. de Boeij, D. Wiersma, "Generation of 13-fs, 5-MW pulses from a cavity-dumped Ti:sapphire laser," Opt. Lett. **19**, 572- (1994)

[57]   P. Zalicki and R. N. Zare, "Cavity ring-down spectroscopy for quantitative absorption measurements," J. Chem. Phys. **102**, 2708 (1995).

[58]   E. Potma, C. Evans, X. Xie, R. Jones, and J. Ye, "Picosecond-pulse amplification with an external passive optical cavity," Opt. Lett. **28**, 1835-1837 (2003)

[59]   R. Jones and J. Ye, "High-repetition-rate coherent femtosecond pulse amplification with an external passive optical cavity," Opt. Lett. **29**, 2812-2814 (2004)

[60]   Y. Vidne, M. Rosenbluh, T.W. Hansch, "Pulse picking by phase-coherent additive pulse generation in an external cavity," Opt. Lett. 23(23), 2396-2398 (2003)

[61]   A. Siegman, "Lasers," University Science Books (1986)

[62]   H. Kogelnik, E.P. Ippen, A. Dienes, C. Shank, "Astigmatically compensated cavities for CW dye lasers," IEEE. J. Quantum Elec. (1972)

[63]   "Fiber Optics Test and Measurement," edited by D. Derickson, Prentice Hall PTR (1998).

[64]   D.W. Rush, G.L. Burdge, P-T. Ho, "The linewidth of a mode-locked semiconductor laser caused by spontaneous emission: Experimental comparison to single-mode   operation," IEEE Journal of Quantum Electronics. Vol. QE-22, pp. 2088-2091. (1986).

[65]   T.W. Hansch, B. Couillaud, "Laser frequency stabilization by polarization spectroscopy of a reflecting reference cavity," Opt. Comm. V35, pp. 441-444 (1980)